The roles of *Tbx5* and *Tbx4* in the bilaterally symmetric initiation of the left and right limbs

Fatima Ann Sulaiman

Division of Developmental Biology

MRC National Institute for Medical Research

UCL

Submitted in 2011 for the degree of Doctor of Philosophy

ABSTRACT

Although there is no obvious communication between the left and right limb buds they develop to form bilaterally symmetrical structures of equal size (Summerbell & Wolpert, 1973). The underlying mechanisms that ensure symmetrical limb formation are unknown. Holt-Oram Syndrome (HOS) [OMIM 142900] is a congenital syndrome associated with mutations in *TBX5* that lead to heart and upper limb defects. Strikingly, over 70% of HOS patients have left-biased upper limb defects. Using two separate strategies, I show that hypomorphic levels of *Tbx5* in both the left and right forelimb buds produces forelimb defects that are consistently more severe in the left limb than the right. Using the *INV/INV* mutant background, in which the left-right axis is reversed, I show that the laterality of these defects is reversed in *Tbx5* hypomorphic mutants with situs inversus. Additionally, I also show that transgenic expression of equal levels of *Fgf10* in the forelimb buds of these *Tbx5* hypomorphs can partially rescue outgrowth defects but not the left-bias asymmetry of their presentation. Together, this data suggests that *Tbx5* has a role in ensuring symmetrical forelimb formation and that this is independent of its transcriptional regulation of *Fgf10*.

Tbx4, the paralogue of *Tbx5*, is expressed in the hindlimb. I have used a conditional deletion approach to delete *Tbx4* expression from the hindlimb area thus avoiding early embryonic lethality. I show that deletion of *Tbx4* leads to a loss of proximal hindlimb skeletal elements as well as mispatterning of the distal hindlimb. I also show that *Pitx1* partially contributes towards the establishment of the FGF signalling positive feedback loop during initiation of hindlimb bud outgrowth.

ACKNOWLEDGEMENTS

The completion of the PhD process is the accomplishment of the individual, but it is also the accomplishment of those who surround that individual. I would certainly not be at this stage without the help and support of the following people.

Firstly, I would like to thank Dr. Malcolm Logan, my PhD supervisor. To say that his guidance and advice, as well as his calming influence, has been invaluable is something of an understatement. Anna Kucharska is THE mouse authority. Sayings, both wise and hilarious, are just one of the numerous contributions from Peleg Hasson. Sorrel Bickley kindly listened to my no doubt tedious rants on a variety of topics. Satoko Nishimoto and Sue Miller are great experts on chick embryos. Natalie Butterfield and Veronique Duboc have provided great insight as well as immense technical advice.

I have to thank the Leafield Crew i.e. Holly Ironfield, Vicky Spivey and Bex Leyland. Chris Wardlaw is a legend. My parents, Shah Khalid Sulaiman and Raashda Ainuddin Sulaiman have been extremely patient and supportive throughout this process. And lastly, it should be mentioned that this work has largely been powered by the excellent baking of my younger sister, Kulsoom Ann Sulaiman.

I, Fatima Ann Sulaiman, confirm that the work presented in this thesis is my own and was performed in the laboratory of Dr. Malcolm Logan at the MRC-NIMR. I confirm that information and reagents that have been derived from other sources has been stated within this thesis. This work has been submitted in 2011 for the degree of Doctor of Philosophy.

LIST OF FIGURES

LIST OF TABLES

CHAPTER ONE:

INTRODUCTION

1.1 VERTEBRATE LIMB DEVELOPMENT

Initial studies in the chick have paved the way towards understanding the mechanisms that regulate the embryological development of the limb. In more recent years, genetic studies in the mouse and zebrafish have facilitated our understanding of the signalling pathways and genetic cues involved during the transformation of a morphologically uniform limb bud to a discrete appendage. While the processes underlying this morphological change are beginning to be more clearly understood, how these processes are regulated and fidelity is maintained to ensure the bilaterally symmetric formation of the left and right limbs has not yet been fully explored. In 1973, Summerbell and Wolpert published a study in which they measured the lengths of right and left late-stage chick wings and compared them to one another. They found that there was very little difference in the overall size and length of the left and right wings, a finding made more intriguing by the lack of evidence supporting any molecular crosstalk between the left and right developing limb buds (Summerbell and Wolpert., 1973). The mechanisms governing the bilaterally symmetric formation of the left and right limbs are as yet unknown.

Figure 1.1

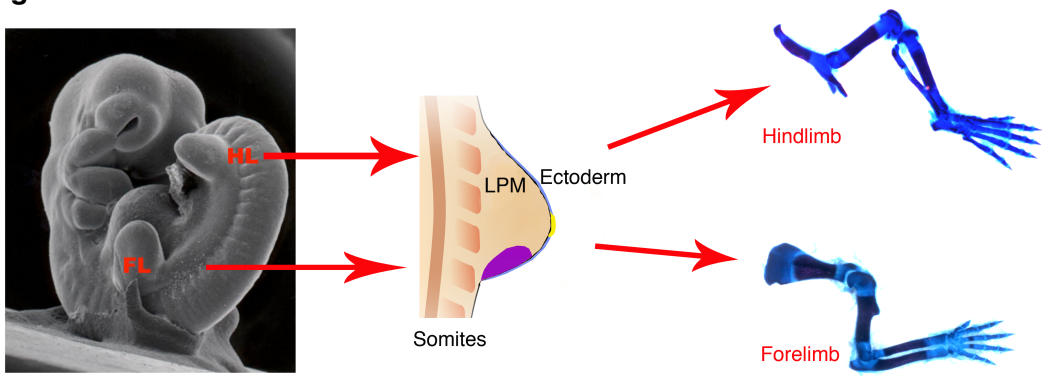

Figure 1.1 The establishment of three signalling centres in the limb bud enable the transformation of the bud from a morphogenetically uniform mass of cells to a highly specialized appendage. Zone of polarizing activity – purple, apical ectodermal ridge – yellow, dorso-ventral axis – blue. (Scanning electron microscope image of E10.5 mouse embryo provided by Dr. M Logan)

Nascent limb bud formation is triggered from the LPM in response to an axial cue. An FGF signalling positive feedback-loop between the limb mesenchyme and a ridge of ectoderm at the distal tip of the limb bud is then established. Three spatially distinct signalling centres are established in the early limb bud that ultimately produce the patterning signals that transform the initially morphogenetically uniform limb bud into morphologically distinct forelimbs and hindlimbs (Fig 1.1).

Limb bud formation is initiated by a series of cues from the LPM.

The role of the axial tissue in establishing the initiation of limb bud formation from the LPM was revealed in a series of embryological experiments in the chick embryo. By placing a barrier between the axial tissue and LPM, wing bud formation is completely blocked (Sweeny and Watterson., 1969; Stephens and McNulty., 1981). This suggests that the induction of the limb bud in the LPM requires a morphogenetic cue arising from the adjacent axial tissue, such as the intermediate mesoderm (IM) and the somites. There is some evidence to suggest that retinoic acid, a derivative of vitamin A (retinol), may play a role during the initiation of limb

bud formation. Experiments in the chick and zebrafish involving the use of antagonists to block either retinoid signalling at the level of the receptor or retinoic acid synthesis, have shown that in the absence of retinoid signalling a forelimb bud fails to form (Stratford et al., 1996; Grandel et al., 2002; Gibert et al., 2006). Data obtained from genetic studies in the mouse support the role of retinoid signalling during limb initiation. The RALDH enzymes convert retinaldehyde into retinoic acid. *Raldh2* is expressed in the developing heart, brain, limbs and other organs (Niederreither et al., 2002). It has been shown that the deletion of *Raldh2* from the developing embryo leads to a failure of forelimb bud initiation (Niederreither et al., 1999; Niederreither et al., 2002). *Raldh2* null embryos do not survive beyond E9.0, therefore further examination of this phenotype has not yet been possible.

More recent work has shown that expression of the transcription factors, *Tbx5* and *Tbx4*, is vital for forelimb and hindlimb bud initiation. *Tbx5* and *Tbx4* both belong to the T-box family of transcription factors, the founding member of which is the *brachyury* (T) gene (Kispert et al., 1993). *Tbx5* expression is restricted to the forelimb bud of mammalian and avian embryos, and *Tbx4* expression is restricted to the hindlimb bud (Gibson-Brown et al., 1996). *Tbx3* and *Tbx2* are paralogue transcription factors also expressed during limb development (Gibson-Brown et al., 1996; Rallis et al., 2005; Logan et al., 1998). Phylogenetic analysis of the conserved T-box DNA binding domains of these four genes has led to the conclusion that *Tbx5*, *Tbx4*, *Tbx3* and *Tbx2* originated from a single ancestral gene. Tandem duplication of the ancestral gene would have led to the formation of two separate genes, the ancestral *Tbx4*/*Tbx5* and *Tbx2*/*Tbx3* genes. A further duplication event led to the formation of the genes *Tbx4* and *Tbx2* on one chromosome and the formation of *Tbx5* and *Tbx3* on another (Fig 1.2) (Agulnik et al., 1996).

Figure 1.2

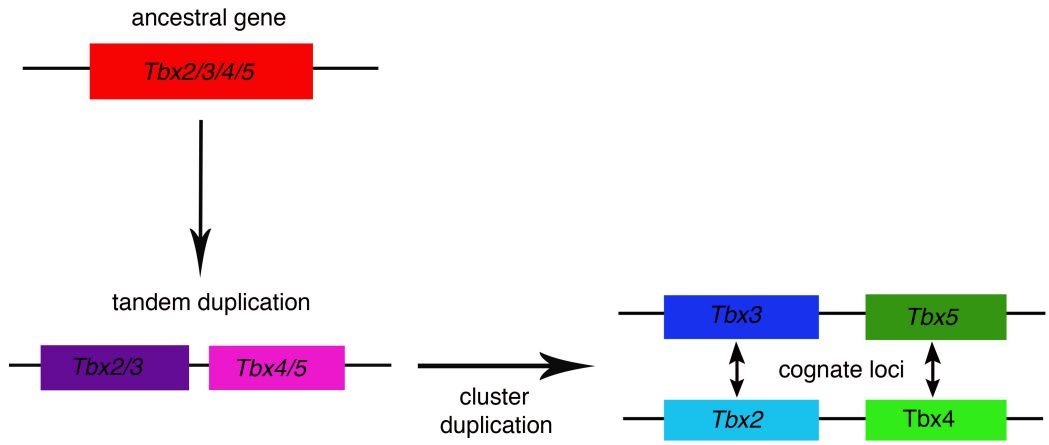

Figure 1.2 Schematic detailing the shared descent of *Tbx5* and *Tbx4* from an ancestral gene. Tandem duplication of the ancestral gene led to the formation of two duplicate genes. Further duplication of these genes led to the formation of the paralogues *Tbx3*/*Tbx2* and *Tbx4*/*Tbx5* (figure adapted from Agulnik et al., 1996).

Early work has shown that the knockdown of *Tbx5* in the chick leads to the disruption of wing formation. Similarly, the knockdown of *Tbx4* disrupts leg formation (Rodriguez-Esteban et al., 1999). These results infer a role for *Tbx5* and *Tbx4* during limb development although it is unclear from these studies what the nature of the role is. Genetic studies in the mouse have since identified the function of *Tbx5* during forelimb bud formation. *Tbx5* null mouse embryos display a complete lack of forelimb bud formation, in addition to severe heart defects that lead to early embryonic death at E10.5 (Agarwal et al., 2003). In another study it was shown that the conditional deletion of *Tbx5* from the forelimb-forming region of the LPM leads to a total loss of forelimb bud initiation and as a consequence the elements of the forelimb never form (Rallis et al., 2003). The results of these two studies indicate that *Tbx5* expression is crucial for the initiation of forelimb bud formation. A follow up study, using a tamoxifen-inducible cre line, sought to determine whether *Tbx5* is required post forelimb bud initiation for continued limb outgrowth. Interestingly, when

Tbx5 is deleted at later stages, forelimb outgrowth is not disturbed although tendon and other soft tissue formation is disrupted (Hasson et al., 2007; Hasson et al., 2010). This suggests that there are two phases of Tbx5 activity during forelimb bud formation, the first of which is required for forelimb bud initiation and the second for normal soft tissue formation.

Expression of *Tbx4* is restricted to the hindlimb-forming region. When *Tbx4* is misexpressed in the forelimb-forming regions of mutant embryos from which conditional *Tbx5* has been deleted, forelimb bud initiation is rescued (Minguillon et al., 2005). This demonstrates that *Tbx4* and *Tbx5* play equivalent roles in limb bud initiation and suggests that they act on the same transcriptional targets. When *Tbx4* is conditionally deleted prior to hindlimb bud initiation, however, a small hindlimb bud is formed (Naiche and Papaioannou., 2003). This study used a *β-actinCre* transgenic mouse line to conditionally delete *Tbx4*, which leads to early embryonic lethality due to a failure of chorioallantois formation. Therefore to study later hindlimb bud development, the authors cultured whole hindlimb bud explants of both mutant and control embryos (Naiche and Papaioannou., 2003). The control hindlimb bud continues outgrowth in culture up to 3 days post explantation, whereas the mutant hindlimb bud does not. This analysis would suggest that in contrast to *Tbx5*, *Tbx4* expression is not exclusively required for hindlimb bud initiation.

Limb bud outgrowth is directed by the paracrine FGF signalling pathway.

Continued outgrowth of the limb bud is crucial once the formation of the nascent limb bud has been initiated. The apical ectodermal ridge (AER) is a discrete region of the ectoderm located at the dorso-ventral junction at the distal tip of the limb bud. The importance of the AER in limb bud outgrowth has been shown through now classical embryological experiments carried out by Saunders. The AER

was removed from chick wing buds at different stages of development, ranging from early to late. It was observed that the distal most wing elements failed to form in the absence of the AER, demonstrating that the AER is required for continued limb outgrowth (Saunders., 1948; Summerbell., 1974). Subsequent studies identified a gene expressed in the AER known as *Fgf8*, a fibroblast growth factor (Ohuchi et al., 1994). In the absence of the AER, the application of Fgf8 to the wing bud will rescue limb outgrowth, indicating a significant role for *Fgf8* expression in limb formation (Niswander et al., 1993; Mahmood et al., 1995; Ohuchi et al., 1997).

During nascent limb bud formation, the AER is directly induced in the ectoderm by signals from the underlying mesenchyme. *Fgf10* has since been identified as the FGF ligand responsible for induction of the AER in the overlying ectoderm. Fgf10 applied to chick flank mesenchyme leads to the formation of an ectopic AER in which *Fgf8* expression can be detected (Ohuchi et al., 1997; Yonei-Tamura et al., 1999). The loss of *Fgf10* expression throughout the developing mouse embryo leads to the severe truncation of the forelimbs and hindlimbs, which are reduced to a rudimentary scapula and pelvis respectively (Min et al., 1998; Sekine et al., 1999). *Tbx5* expression can still be detected in the forelimb regions, whereas *Fgf8* and *Fgf4* cannot (Sekine et al., 1999; Agarwal et al., 2003). The unchanged expression of *Tbx5* in the absence of *Fgf10* implies that *Tbx5* is upstream of *Fgf10* expression during forelimb bud initiation, which is supported by the lack of *Fgf10* expression in *Tbx5* mutant embryos (Agarwal et al., 2003; Rallis et al., 2003).

Paracrine FGF signalling takes place between the limb bud mesenchyme and ectoderm, which is mediated by the expression of *FgfR2*. *FgfR2*$^{-/-}$ mutant embryos display a limb phenotype that is strikingly reminiscent of the *Fgf10*$^{-/-}$ null

mutant, in that the limbs have failed to undergo further outgrowth post initiation (Xu et al., 1998; Arman et al., 1999). Furthermore, *Fgf8* expression is lost from *FgfR2*$^{-/-}$ null limb buds whereas *Fgf10* expression is downregulated, supporting the hypothesis that *Fgf10* expression in the limb mesenchyme activates the transcription of *Fgf8* in the overlying ectoderm via *FgfR2* receptors in the limb bud. *Fgf8* is thought to upregulate the expression of *Fgf10* in the underlying mesenchyme therefore initiating the formation of the positive FGF signalling feedback-loop. This mechanism has been further dissected through the examination of the isoforms of *FgfR2*. There are two isoform splice variants of *FgfR2* expressed in the limb bud, *FgfR2c* in the mesenchyme and *FgfR2b* in the ectoderm. Through affinity assay analysis and global deletion experiments, it has been shown that *Fgf10* acts as the ligand for *FgfR2b* (De Moerlooze et al., 2000; Ohuchi et al., 2000). *FgfR2b*$^{-/-}$ mutants display a similar limb phenotype to those described in the *FgfR2*$^{-/-}$ and *Fgf10*$^{-/-}$ mutants, lending further support to the model of FGF signalling (De Moerlooze et al., 2000). Taken together, the data taken from the published literature suggests the following mechanism for AER induction and limb bud outgrowth. *Fgf10* expression in the limb bud mesenchyme induces the expression of *Fgf8* in the overlying ectoderm, via the ectodermal *FgfR2b* receptor. The Fgf8 ligand then reciprocates via the mesenchymal *FgfR2c* receptor to positively upregulate *Fgf10* expression in the underlying mesenchyme. This leads to the induction of the positive FGF signalling feedback-loop leading to the formation of the AER, which in turn drives limb bud outgrowth (Fig 1.3).

Figure 1.3.

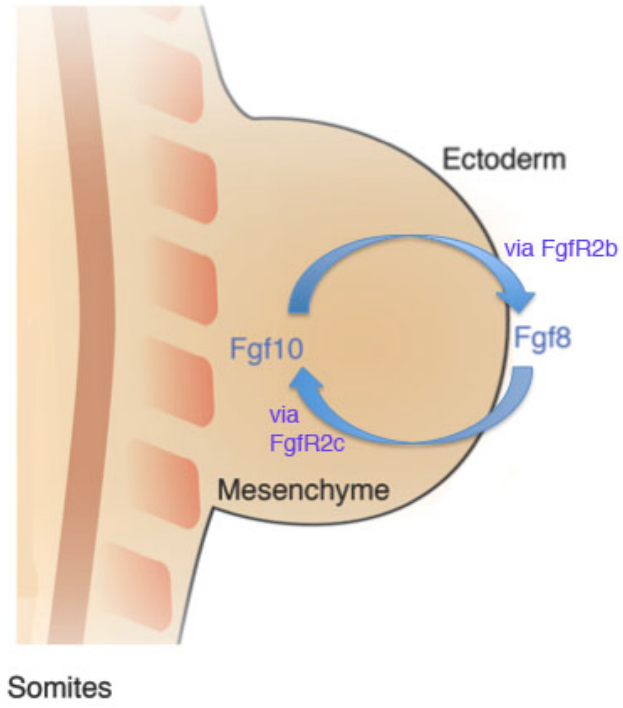

Figure 1.3. A paracrine positive feedback FGF loop drives limb bud outgrowth. *Fgf10*, expressed in the limb mesenchyme, initiates *Fgf8* expression in the overlying ectoderm via the ectodermal FgfR2b receptor. Fgf8 then signals via mesenchymal FgfR2c receptor to positively upregulate *Fgf10* expression in the underlying mesenchyme.

Signalling pathways established in discrete regions of the distal limb bud regulate limb patterning.

The zone of polarizing activity (ZPA) and the dorso-ventral axis pattern the vertebrate limb. The ZPA is comprised of mesenchymal cells located in the posterior region of the limb bud, and was first identified as a signalling centre in the limb in 1968. Graft experiments placing the posterior limb bud onto anterior chick wing buds resulted in a mirror duplication of the distal chick wing (Saunders and Gassling., 1968). Expression of a key morphogen *sonic hedgehog* (*Shh*) has since been identified as the primary factor expressed in the ZPA that is responsible for distal limb patterning. *Shh* belongs to a gene family related to the drosophila homolog, *Hh,* and is expressed in discrete regions throughout the developing embryo (Echelard et

al., 1993). The implantation of cells expressing *Shh* into the anterior region of the limb bud recapitulates the mirror duplication generated by a ZPA graft, thus identifying Shh as the key signal emanating from the ZPA to pattern the anterior-posterior axis of the limb (Riddle et al., 1993). Ectopic expression of *Shh* results in the expansion of the AER, which suggests that there is some positive interaction between the signalling pathways originating from the ZPA and AER. Indeed, subsequent work has provided evidence for a positive feedback-loop between Shh signalling from the ZPA and FGF signalling in the AER (Niswander et al., 1994, Bueno et al., 1996, Zuniga et al., 1999).

The pathway through which *Shh* activates gene transcription has been well documented. In brief, Shh inhibits Patched activity, allowing the Smoothened receptor to enable Gli to enter the nucleus and transcriptionally activate genes such as *Twist, Gli, Patched* (reviewed by Jenkins., 2009). Significantly, the Shh-Patched pathway is believed to specify cells in the distal limb tip according to digit identity and number. The loss of *Shh* expression throughout the developing embryo leads to various defects including holoprosenchephaly and limb truncations, but strikingly *Shh* null limbs present with a single digit, digit one (Chiang et al., 1996). Subsequent studies have provided evidence for a temporal based expansion model of digit specification and identity. Cells in the most anterior region of the limb bud are independent of Shh activity during cell specification thus leading to the distinct morphological characteristics of digit one. Digits two and three are targets of Shh paracrine activity, whereas digits four and five arise directly from the ZPA and experience autocrine signalling activity (Harfe and Tabin., 2004; reviewed in McGlinn and Tabin., 2006).

1.2 CONGENITAL DISORDERS AFFECTING LIMB DEVELOPMENT IN HUMANS

Congenital limb defects are amongst the most common disorders affecting humans. These disorders present as part of a variety of clinical features and can comprise of skeletal, nerve, vascular and muscular defects. Due to recent advances in genetic analysis, the cause of various congenital syndromes can now be attributed to mutations in multiple gene combinations or in single genes that are required for correct limb development.

Holt-Oram Syndrome patients present with upper limb defects that are consistently more severe in the left than the right.

Using published case studies I have tabulated the total instances of left-biased, right-biased and non-biased upper limb defects in a range of congenital human syndromes. This analysis isolates congenital syndromes in which asymmetrical upper limb defects present with a clear bias, allowing us to examine further the causative effect of the noted associated gene mutation. It should be noted that these individual case studies are subject to the diagnosis and judgment of the observing clinician, therefore there will be differing emphasis on specific clinical features.

Upper limb abnormalities within human congenital syndromes are varied, ranging from digital anomalies including triphalangeal thumbs to full aplasia of the limb. A common feature is that the limbs are affected bilaterally, with very rare cases of unilateral limb abnormalities noted. An OMIM search for unilateral limb defects turned up sporadic cases in syndromes where the defects are otherwise bilateral. Examples include Hemi-facial Microsomia with Radial Defects [OMIM 141400] and Townes-Brockes syndrome [OMIM 107480]. These syndromes all have reported

cases of unilateral limb defects but these are rare and have no discernable bias towards the right or left side.

Okihiro syndrome (OS) [OMIM 607323], or Duane Radial Ray Syndrome, is characterized by bilateral upper limb defects, which are commonly in the form of hypoplastic thumbs or the absence of thumbs. In severely affected patients, radial hypoplasia is a feature. I have identified asymmetrical limb defects in ~ 40% of the OS patients recorded in this report. Of these patients presenting with asymmetrical upper limb defects, the majority present with upper limb defects that are more severe in the left than the right (Aalfs Cora et al., 1996; MacDermot et al., 1987; Halal et al., 1984). OS is associated with mutations occurring in *SALL4*, a protein belonging to the SAL family of zinc finger transcription factors. Screening of patients with OS has revealed that the majority of mutations located within the *SALL4* region are heterozygous nonsense or frameshift mutations. These mutations are predicted to lead to the formation of premature stop codons within the sequence, resulting in the formation of a truncated protein that is then presumably degraded (Al-Baradie et al., 2002; Kohlhase et al., 2002). Other mutations identified include other single nucleotide polymorphisms, although the exact nature is unclear.

Lacrimo-auricular-dento-digital syndrome (LADD) [OMIM 149730] is characterized by defects in the lacrimal glands, inner ear, teeth and digits of the hand including the absence or bifurcation of the thumb. Half of the case studies analyzed in this report (47%) identify patients in which the left upper limb presents with more severe defects than the right (Francannet et al., 1994; Heinz et al., 1993; Levy et al., 1996). This presents a higher incidence rate than that tabulated in OS patients. Mutations in LADD have been linked to the components of the FGF signalling pathway, specifically the tyrosine kinase receptor, *FGFR2*, and the ligand

FGF10. The predominant mutations in *FGFR2* in LADD patients take place in the form of missense mutations that are thought to affect the tyrosine kinase activity of FGFR2 (Rohman et al., 2006). While still uninvestigated, it is believed that the majority of mutations cause a decrease in FGFR2 activity, thus perhaps leading to a decrease in FGF signalling. This is in contrast to another congenital syndrome, Apert Syndrome [OMIM 101200], in which patients present with severe syndactyly of the digits. Mutations within *FGFR2* in Apert Syndrome patients are believed to lead to the increased activity of FGFR2, resulting in a constant upregulation of FGF signalling (Wilkie et al., 1996; Lajeunie et al., 1999). Apert Syndrome patients are not reported to present with asymmetrical limb defects. In other case studies, mutations in *FGF10* have been reported in LADD patients. In one family a missense mutation in *FGF10* believed to result in a dominant-negative protein has been reported, whereas in other families missense and nonsense mutations predicted to lead to prematurely truncated proteins have been reported (Milunsky et al., 2006; Rohmann et al., 2006). These truncated proteins are thought to be either inactive or targeted for degradation. The majority of LADD patients, however, appear to be associated with mutations in *FGFR2* (Rohmann et al., 2006).

Holt-Oram syndrome (HOS) [OMIM 142900] is characterized by limb and heart defects. Strikingly, over 70% of HOS patients are reported to have consistently left-biased asymmetrical upper limb defects (Smith et al., 1979; Glauser et al., 1989; Newbury-Ecob et al., 1996). I have compared the incidence rates of HOS and other previously described congenital syndromes in the table below (Table 1). This table highlights the extremely high percentage of left-biased asymmetrical upper limb defects in HOS patients compared to other syndromes affecting the upper limb. This table identifies HOS as a rather unique condition in which left-biased asymmetrical upper limb defects are a key feature.

Table 1.

	Associated gene(s)	N (Cases)	Bilateral	Right bias	Left bias
Hemi-facial Microsomia with Radial Defects	UNKNOWN	21	19%	38%	43%
Townes-Brockes syndrome	*SALL1*	13	62%	15%	23%
Okihiro syndrome	*SALL4*	20	60%	10%	30%
Lacrimo-auricular-dento-digital syndrome	*FGF10, FGFR2, FGFR3*	19	37%	16%	47%
Holt-Oram syndrome	*TBX5*	99	27%	3%	70%

Table 1. A table of congenital syndromes and the frequency of noted asymmetrical bias in the presentation of various upper limb defects. Patients in which HOS has been diagnosed present with a significantly high number of left-biased asymmetrical upper limb defects, whereas patients suffering from syndromes such as LADD or OS present with either bilateral upper limb defects or non-biased asymmetrical upper limb defects.

A wide spectrum of upper limb defects can be identified in HOS patients. These range from triphalangeal thumbs (in which a third phalanx is added to the normally biphalangeal digit) and the loss of the thumb to radial aplasia of the upper limb. In the majority of cases the left upper limb is more severely affected than the right, for example a patient may have a triphalangeal thumb on the right hand and have lost the thumb on the left hand or in more severe cases, have three digits on the right hand and a severely truncated left upper limb (Newbury-Ecob et al., 1996). The association of HOS with mutations in *TBX5* has been well documented, with various point mutations accounting for various specific heart and limb defects in patients (Li et al., 1997; Basson et al., 1997; Yang et al., 2000; Akrami et al., 2001). A high majority of the documented point mutations in *TBX5* lead to the formation of

a premature stop codon within the sequence (Basson et al., 1999). These are then predicted to lead to the formation of truncated proteins that may be unable to fold properly or are targeted for degradation. HOS patients are heterozygous carriers of mutations in *TBX5* i.e. the patient carries a single functional copy of *TBX5*. *TBX5* expression is thought to be bi-allelic, i.e. both copies are required for gene expression, the loss of one functional copy of *TBX5* leads to haploinsufficiency resulting in the upper limb defects observed in patients (Basson et al., 1999; Boogerd et al., 2010).

Mutations in *TBX4* are associated with Small-Patella Syndrome.

One of the more common lower limb defects presenting in humans is clubfoot. It is characterized by an inward turning of the foot and can include skeletal and soft tissue defects, which in many cases is resolvable through surgery. In 2008 a case study of a 5-generation family describing right-biased asymmetrical lower limb defects, such as clubfoot, hypoplastic patella, tibial hemimelia and in one case right sided polydactyly, was published. Analysis of family members led to the identification of a point mutation in the homeodomain region of the gene *PITX1*, a paired-like homeodomain transcription factor active during embryonic hindlimb development (Lanctot et al., 1999). This is predicted to result in the reduced ability of PITX1 to bind to target DNA sequences and enable transcriptional activation of downstream targets (Gurnett et al., 2008). These defects present with increased severity in the right lower limb, which is consistent with defects displayed by mice in which *Pitx1* has been deleted (Lanctot et al., 1999).

A known target of *Pitx1* activity is *Tbx4*, the paralogue of *Tbx5,* which is expressed in the hindlimb region during development (Logan and Tabin., 1999). Interestingly, another case study has reported findings in which patients present

with lower limb defects, including clubfoot and a shortened calcaneus, due to a recurring microduplication in the chromosomal region encoding for *TBX4* (Alvarado et al., 2010). This is intriguing as mutations in *TBX4* are typically associated with Small-Patella Syndrome (SPS) [OMIM 147891], the clinical features of which do not usually present with clubfoot. SPS patients present with relatively mild lower limb defects, such as the bilateral loss of the patella, a widened space between the first and second toes, and minor pelvic defects (Bongers et al., 2001; Scott and Taor., 1979; Burckhardt., 1988). In a case study by Bongers et al, six separate mutations were identified within the *TBX4* coding region in a cohort of SPS patients. These included nonsense, missense, frame-shift and splice-site mutations. The majority of mutations are predicted to form truncated proteins that are presumably non-functional (Bongers et al., 2004). However one missense mutation, identified in a family with SPS patients, has been predicted to lead to an amino acid substitution within the T-Box DNA binding domain. This is thought to impair the ability of the mutant TBX4 protein to bind to target DNA sequences, but it is not clear whether this protein would be non-functional or a dominant-negative (Bongers et al., 2004). All of the reported mutations are heterozygous and are also most likely to lead to loss of function proteins. This would presumably lead to SPS patients having one functional copy of *TBX4* as well as one non-functional copy. This would imply that the majority of SPS patients are haploinsufficient for *TBX4*.

The loss of *Tbx5* expression from the forelimb areas of mouse embryos leads to the total loss of forelimb bud initiation and formation, whereas in contrast the loss of *Tbx4* expression from the hindlimb regions leads to the initiation of a small hindlimb bud (Agarwal et al., 2003; Rallis et al., 2003; Naiche and Papaioannou., 2003). This difference in mutant mouse phenotype suggests that the role of *Tbx4* in the hindlimb is partially redundant with other factors that contribute

towards hindlimb formation. This explanation may account for the sharp contrast in the relative severity of limb defects in HOS and SPS human patients. The lower limb phenotypes reported in SPS patients are relatively mild, which may be due to compensation by another transcription factor in the event of lowered levels of TBX4 activity in SPS patients.

1.3 LEFT-RIGHT AXIS FORMATION AND LIMB DEVELOPMENT

Various genetic and embryological studies in the mouse, chick and zebrafish have greatly advanced our understanding of the genetic pathways underlying limb formation and development. However, the bilaterally symmetric formation of the left and right limbs is little understood. Part of the focus of my work has been to understand the mechanisms leading to the left-biased asymmetrical upper limb defects in HOS patients, which deviate from the bilaterally symmetric body plan. Due to this, I have briefly reviewed the literature detailing the establishment of the left-right axis, as well as various mouse models in which asymmetric limb defects form a part of the overall phenotype.

The left-right pathway is established due to a series of events at the node during early embryogenesis.

Bilateral symmetry of organs such as the limbs, eyes, and ears is a conserved feature across many organisms, as is the asymmetrical presentation of interior organs. The establishment of the left-right axis is a key embryological event and the asymmetrical patterning of visceral organs is known to manifest as a result.

During early embryogenesis the embryo originates as a ‘cup’ that then, through a series of signalling cascades, develops the anterior-posterior and left-right axis through which the morphology of the embryo is determined. The node arises during gastrulation as a structural recess in the midline of the flat embryo. The

ventral surface of this structure contains several monocilia, referred to as nodal monocilia. It is through events taking place at this structure that the left-right axis and thus left-right patterning is determined. The nodal monocilia were originally thought to be immotile, however through fluorescent imaging and bead experiments it has since been shown that the cilia rotate leftwards in a clockwise motion, generating the left-ward movement of fluid over the node ('nodal flow') (Nonaka et al., 1998; Takeda et al., 1999). It is hypothesized that the generation of nodal flow leads to the left-biased expression of the genes *Nodal*, *lefty1/2* and *Pitx2*, although how this occurs is still subject to much debate. It has been proposed that the leftward direction of the nodal flow serves to produce a morphogenetic gradient, which would then lead to the left-biased expression of *Nodal*. The identity of the morphogen is unknown, although candidates include Shh, FGF ligands, and retinoic acid. A study by Tanaka et al in 2005 proposed that the leftward nodal flow served to transport vesicular nodal parcels containing factors such as Shh and retinoic acid to the left side of the embryo. FGF signalling was then required to release these factors from the particles (Tanaka et al., 2005). Another model proposed by Tabin and Vogan suggests that nodal flow initiates the left-biased expression of *Nodal* through a mechanosensory mechanism. The two cilia model relies on the evidence for two types of nodal cilia, motile and immotile, located on the ventral surface of the node. The motile cilia rotates clockwise leftward to generate the flow of fluid over the node, the pressure of which is then sensed by the immotile cilia (Tabin and Vogan., 2003). This triggers a calcium-dependent signal transduction event, which then leads to the activation of a signalling factor on the left side of the midline. Evidence in support of both models comes from investigations examining the nodal monocila in both *iv* and *inv* mutant embryos. *iv* mutants present with randomized situs laterality, whereas *inv* mutants are purported to present with consistent situs

inversus, the inversion of the presentation of the visceral organs (Hummel and Chapman., 1959; Yokoyama et al., 1993). The monocilia that are present in the nodes of *iv* mutants are immotile, resulting in a lack of nodal flow, whereas the monocilia in the nodes of *inv* mutants still rotate in a leftward motion although slowly. In both of these embryos the time and speed of nodal flow is disrupted, thus leading to the laterality defects manifested later on in development (Hummel and Chapman., 1959; Okada et al., 1999).

The culmination of these events is the left-biased expression of genes such as *Nodal*, *Pitx2* and *Lefty1/2* (Varlet et al., 1997; Norris and Robertson., 1999). Interestingly, a study by Meyers and Martin suggests that *Fgf8* expression in the left side of the mouse embryo may induce the expression of *Nodal* in the mesoderm. Conversely, in the chick, it has been proposed that Fgf8 activity in the right mesoderm acts to repress *Nodal* and *Pitx2* expression on the right side, thus restricting the expression of *Nodal*, *lefty1/2*, and *Pitx2* to the left side (Meyers and Martin., 1999; Boettger et al., 1999). Indeed, the application of Fgf8 to the left side of the chick embryo results in randomized situs and heart looping (Boettger et al., 1999).

Nodal is a member of the TGF-β family, which is expressed unilaterally in the left LPM of the early embryo (~E8.0). It acts through signal transduction to initiate and regulate the Smad pathway through which downstream targets are expressed (Zhou et al., 1993). The actions of *Nodal* in the left LPM lead to the expression of the *lefty1* and *lefty2* genes, also members of the TGF-β family. It is thought that *lefty2* acts to antagonize Nodal signalling in the left LPM resulting in the transient left sided expression of *Nodal* (Meno et al., 1996; Meno et al., 1999). In addition to this, *lefty1* is also thought to act as a midline barrier, preventing bilateral expression of

left sided genes although the mechanism for this is still unknown (Yamamoto et al., 2003).

The tightly regulated transient expression of *Nodal* in the left LPM serves to act as a left determinant, as loss of *Nodal* expression leads to the right-sided isomerism of the visceral organs whereas bilateral expression of *Nodal* leads to left-sided isomerism (Collignon et al., 1996). It is through the actions of *Nodal* during early embryogenesis that the situs specific morphology of the embryo is determined. *Pitx2* is expressed in the left LPM through the actions of Nodal, however this expression is maintained through later stages of embryonic development and is thus the only left-sided gene to persist in the LPM (Logan et al., 1998; Piedre et al., 1998). It is believed that *Pitx2* expression is required during the morphogenesis of various internal structures as disruption of *Pitx2* leads to morphogenetic defects such as the failure of the ventral body wall to close and heart defects (Kitamura et al., 1999). Through these various mechanisms, situs specific morphogenetic features are established in the developing embryo.

Asymmetrical pelvic vestiges are found in various stickleback populations.

While exterior bilateral limb symmetry is a conserved feature amongst many organisms, there are reported studies of directional limb asymmetry occurring naturally in distinct populations through evolutionary mechanisms. The three-spine stickleback, *Gasterosteus aculeatus*, is known for having robust pelvic armour that is thought to provide protection against saltwater predators. However, it has been found that many stickleback fish residing in isolated freshwater populations present with reduced pelvic rudiments, which may have evolved due to a lack of predators. Of these organisms, a strikingly high number present with right-biased vestigial pelvic rudiments, i.e. the right pelvic vestige is smaller than the left (Shapiro et al.,

2004; Cole et al., 2003). Examination of 27 isolated freshwater populations shows that while the majority of stickleback specimens display right-biased asymmetrical pelvic vestiges, a number also present with left-biased pelvic reduction as well as non-directional pelvic reduction (Bell et al., 2007). The pelvic reduction observed in these organisms has since been attributed to mutations in the cis-regulatory sequences upstream of *Pitx1*, a paired homeodomain-like transcription factor expressed in the hindlimb buds of mammalian and avian organisms (Chan et al., 2010; Shapiro et al., 2004; Lanctot et al., 1999; Logan and Tabin., 1999). Stickleback fish with full pelvic armour express *Pitx1* in the analogous hindlimb region while those presenting with right-biased asymmetric pelvic vestiges have lost *Pitx1* expression in the same area (Shapiro et al., 2004). This phenotype has been compared to the hindlimb phenotype in the *Pitx1*$^{-/-}$ mutant mouse, where the loss of *Pitx1* leads to a greater reduction of the right hindlimb over the left (Lanctot et al., 1999). Various studies have attributed the right-biased reduction of the pelvic armour in the three-spine stickleback to the partial compensatory effect of *Pitx2*. The left sided expression of *Pitx2* is conserved throughout a number of organisms and is required as part of the left-right pathway. Loss of *Pitx1* and *Pitx2* expression in the hindlimb-forming regions of the mouse embryo is purported to lead to bilateral hindlimb defects, thus removing any asymmetric presentation of the phenotype (Marcil et al., 2003). Although there is no evidence for *Pitx2* expression in the hindlimb bud regions of the stickleback embryo, it is thought that *Pitx2* may have a similar compensatory effect in the absence of correct *Pitx1* expression (Shapiro et al., 2004; Bell., 2007). However, it is still unclear which factors compensate for the loss of *Pitx1* expression in those specimens presenting with left-biased or non-directional pelvic reduction.

Intriguingly, the right-biased pelvic reduction observed in the stickleback freshwater populations is not restricted to teleost organisms. Mammalian sirenian organisms such as the manatee, *Trichechus manatus latirostis*, also present with right-biased vestigial pelvic elements. Aquatic mammals such as the manatee and dugong do not have hindlimbs and rely on their flipper-like forelimbs and large tail to propel them through the water. However, examination of manatee specimens shows that a significantly large proportion of animals present with smaller pelvic vestiges on the right side (Shapiro et al., 2006). Sirenian mammals, such as the manatee, are believed to have descended from quadruped ancestors capable of living both on land and in water (Domning., 2001) and may have lost the hindlimb elements through a similar loss of *Pitx1* expression. These studies show instances of asymmetry presenting in vertebrate organs, which are normally bilaterally symmetric, where the directional asymmetry is revealed through the loss or reduction of specific features via the loss of gene expression.

Mouse mutants presenting with asymmetric limb defects.

Directional asymmetry can be observed in naturally occurring vertebrate populations through the loss or reduction of gene expression. In some mouse models where limb development has been disrupted asymmetric defects are detectable although this is a rare event.

The BMP knockout mutant is an example of a genetic mouse model of limb asymmetry. Dunn et al reported the generation of a null allele for *Bmp4* (*Bmp4*^{tm1}) in 1997. Although homozygous mutants die around the gastrulation stage, heterozygous *Bmp4*$^{tm1/+}$ embryos present with a duplicated digit 1 in the hindlimb with 12% of all mutants showing a right-sided bias. Additionally, the double heterozygous *BMP4*$^{+/-}$*; BMP7*$^{+/-}$ mutant displays an increased prevalence of hindlimb

asymmetry with 28% of mutants showing right sided bias compared to 11% showing a left sided bias. However, in these mutants the penetrance of the overall phenotype is only 50% (Dunn et al., 1997; Katagiri et al., 1998). While presenting with an interesting phenotype, the prevalence of directional limb asymmetry is low compared to the *R-spondin2* null mouse model. *R-spondin2* is from the RSPO family of secreted proteins and is required to activate β-catenin signalling, which is crucial for development of the apical ectodermal ridge (AER). These mutants show syndactyly of the limbs with the left hindlimb more affected than the right hindlimb (n=91.7%, n=12) (Nam et al., 2007). There is no apparent asymmetry in the forelimbs, which display only an absence of claws. *R-spondin2* has been shown to be required for the activation of β-catenin signalling which has been implicated in activating and maintaining Wnt signalling via *Lef1* and *Tcf2* in mice.

The *footless* mouse model arose as a result of a transgenic insertion into *R-spondin2*, which is predicted to result in hypomorphic levels of R-spondin2 activity. Phenotypic features include kidney malformations, cleft palate and specifically, asymmetric limb malformations. Both the forelimbs and the hindlimbs are affected, with the right forelimb more affected than the left and the left hindlimb more affected than the right (Bell et al., 2003). In all the mouse models discussed, the directional bias of the limb malformations suggests that a unilaterally expressed factor or gene is partially compensating. *Pitx1* is involved in hindlimb morphogenesis and is believed to play a role in hindlimb specification (DeLaurier et al., 2006; Lanctot et al., 1999). The *Pitx1*$^{-/-}$ null mutant presents with hindlimb defects, often preferentially in the right hindlimb. It has been suggested that the left-sided expression of *Pitx2* partially compensates for the loss of *Pitx1*. The loss of both *Pitx1* and *Pitx2* expression in the *Pitx1*$^{-/-}$; *Pitx2*$^{-/-}$ double knockout mutant appears to affect both

hindlimbs bilaterally, suggesting that expression of *Pitx2* in the left lateral plate mesoderm is compensating for lack of *Pitx1* (Marcil et al., 2003).

Prior to these genetic mouse models of directional limb asymmetry, the maternal administration of teratogenic agents was used to examine the disruption of limb outgrowth. It has been shown that drugs such as cadmium and acetazolamide can induce right sided forelimb abnormalities in the mouse. In order to explore whether there are differences between the left and right limb-forming region in the developing mouse embryo, dams on the *iv* background were injected with acetazolamide. Situs solitus embryos had right-sided forelimb defects, whilst situs inversus embryos had left sided forelimb defects (Brown et al., 1989). Genetic studies supporting this finding have since been carried out in the mouse. The *legless* mouse strain arose due to a transgenic insertion by McNeish et al 1988 resulting in limb, facial and visceral organ phenotypic defects. The forelimb is quite severely affected with the anterior digits missing, including the loss of the radial elements in some cases. These defects are unilateral with a bias towards the right side (McNeish et al., 1988). Fifty percent of mutant mice were found to display situs inversus, which is the reversal of the placement of the internal visceral organs. Situs inversus develops as a result of a reversal of the left-right pathway thus left-sided genes are expressed on the right side. The study found that in those mice which display situs inversus, the right sided forelimb defect is reversed i.e. the anterior distal defect is now present on the left side (Schreiner et al., 1993). These reported findings are supported by a previous study carried out by Kocher-Becker et al in 1991. The *py* mouse strain displays polydactyly (*py*) in the right hindlimb and in the left forelimb. By crossing this mutant background to the *iv* mouse strain in which 50% of mutants develop situs inversus, it was found that the observed polydactyly is reversed in *py/py*; *iv/iv* double mutant mice (Kocher-Becker et al., 1991).

1.4 AIMS OF THE STUDY

Much progress has been made towards understanding the developmental pathways that underlie the transformation of the limb bud from a morphogenetically uniform mass of cells to bilaterally symmetric pairs of highly specialized appendages. There are still wide gaps in our understanding of key processes, two of which I seek to address.

Little is known about the bilaterally symmetric formation of the left and right limb or the underlying mechanisms. Through analytical studies in human syndromes and stickleback populations, it is clear that the reduction or loss of certain genes can lead to directional biased asymmetrical limb defects. I propose to recapitulate the striking left-biased asymmetrical upper limb defects observed in HOS patients by disrupting Tbx5 activity in the mouse. I will then use these mouse models to study the underlying mechanisms leading to asymmetric forelimb formation.

Tbx4 is a paralogue of *Tbx5*, expressed in the hindlimb. While the role of *Tbx5* during the induction of the forelimb bud from the LPM is clear, it is still uncertain whether *Tbx4* has the same role during hindlimb bud initiation. Through the usage of the appropriate cre transgenic line, I will conditionally delete *Tbx4* expression specifically in the hindlimb-forming region of the developing mouse embryo. I will then characterize and study the resulting phenotype at all stages, early and late, of embryonic development to ascertain the role of *Tbx4* in hindlimb development.

CHAPTER TWO:

METHODS AND MATERIALS

Generation of mutant mouse embryos

All of the mouse lines used throughout this work were maintained on mixed genetic backgrounds that include C57/BL6, Parkes, and BALB/c.

Breedings were set up to generate the following transgenic mouse lines:

$Tbx5^{lox/+}$; Prx1Cre

$Tbx5^{lox/+}$; Prx1Cre(98)

$Tbx5^{lox/+}$; Prx1Cre; Prx1-Tbx

These lines were then crossed to mice that were homozygous for the conditional *Tbx5* allele (*$Tbx5^{lox/lox}$*) to generate the following mutant embryos:

$Tbx5^{lox/lox}$; Prx1Cre

$Tbx5^{lox/lox}$; Prx1Cre(98)

$Tbx5^{lox/lox}$; Prx1Cre; Prx1-Tbx

The transgenic mouse line heterozygous for the *INV* mutant allele was crossed into the background of the *$Tbx5^{lox/+}$; Prx1Cre; Prx1-Tbx* mouse line to generate *$Tbx5^{lox/+}$; Prx1Cre; Prx1-Tbx;INV/+* transgenic mice. These mice were then crossed into the *INV/+* background again in order to generate *$Tbx5^{lox/lox}$; Prx1Cre; Prx1-Tbx; INV/INV* mutant embryos.

$Tbx5^{lox/lox}$; Prx1Cre; Prx1-Tbx; Z/EGFgf10 mutant embryos were generated through crossing *$Tbx5^{lox/+}$; Prx1Cre; Prx1-Tbx* mice with mice homozygous for the conditional *Tbx5* allele and hemizygous for the *Z/EGFgf10* allele (*$Tbx5^{lox/lox}$; Z/EGFgf10*). Breedings were set up to generate *$Fgf10^{-/+}$; Z/EGFgf10* and *$Fgf10^{-/+}$; Prx1Cre* transgenic mice. These were then crossed together to generate *$Fgf10^{-/-}$; Prx1Cre; Z/EGFgf10* mutant embryos.

The *RetRV5Cre* hemizygous transgenic line was crossed into the homozygous conditional *Tbx4* background to produce *$Tbx4^{lox/+;}$ RetRV5Cre*

transgenic mice. These were then crossed again into the homozygous conditional *Tbx4* background so that

Tbx4$^{lox/lox}$*; RetRV5Cre* mutant embryos were generated.

The *Tbx4*$^{lox/+}$*; RetRV5Cre* transgenic line was crossed into the *Pitx1*$^{-/+}$ heterozygous background to generate *Pitx1*$^{-/-}$*; Tbx4*$^{lox/lox}$*; RetRV5Cre* mutant embryos. The homozygous conditional *Tbx4* mouse line was bred onto the homozygous conditional *Tbx5* mouse background such that *Tbx4*$^{lox/lox}$*; Tbx5*$^{lox/lox}$ mice were produced. These were then crossed into the *HoxB6Cre* hemizygous transgenic background through a series of breedings to generate *Tbx4*$^{lox/lox}$*; Tbx5*$^{lox/lox}$*; HoxB6Cre* mutant embryos.

The cre transgenic lines (*HoxB6Cre*, *RetRV5Cre*, *Prx1Cre(98)*) were crossed with homozygous *Rosa26RlacZ/Rosa26RlacZ* reporter mice to produce *Rosa26RlacZ/+; Cre* embryos for the characterisation of the relevant cre transgenic line.

In all crosses mice were staged according to Kaufman. Noon on the day of vaginal plug observation was taken to be 0.5 embryonic days of development.

Tail and embryo sac DNA extraction and genotyping

Embryo sacs were digested overnight at 55^{o}C in 200 μl of lysis buffer (10mM Tris 7.5, 10mM EDTA, 100mM NaCl, 0.5% Sarkosyl, 0.1mg/ml Proteinase K). 1 μl of this was then used for the genotyping PCR.

The PCR reaction mix used for genotyping is 10 μl of 5x PCR buffer (250ml 1M KCL, 50 μl 1M Tris HCL ph8.4, 12.5 μl 1M $MgCl_2$, 10 μl 100mM dATP, 10 μl 100mM dTTP, 10 μl 100mM dGTP, 10μl 100mM dCTP, 85 ml BSA 10mg/ml, 562.5 ml distilled H20), 1 μl each of the forward and reverse primers, 0.2 μl of Taq polymerase (Sigma), 1 μl of the template DNA and 36.8 μl of H_20.

Table 2 shows the primer sequences for each mouse strain. Table 3 shows the PCR cycle programs used for each mouse strain. All PCR reactions were run out on 1% agarose gels, the exceptions being *Tbx5*$^{lox/lox}$ and *Tbx4*$^{lox/lox}$, which were run out on 3% agarose gels.

Table 2.

Mouse strain	**Primers 5' - 3'**
All Cre transgenic lines	Fwd ATC CGA AAA GAA AAC GTT GA
	Rev ATC CAG GTT ACG GAT ATA GT
INV/INV	Fwd INV GTG ATG TGC TGG AAG ATG GAA ATT G
	Rev INV TGA GTT GTG TGT GGA GGA ATC TCT T
	Fwd Tyrosine CTG TCC AGT GCA CCA TCT GGA CCT C
	Rev Tyrosine GAT TAC GTA ATA GTG GTC CCT CAG G
Tbx5$^{lox/lox}$	Fwd GCA GCG CAG TCC TCA CCA G
	Fwd AGC TGC CCT GGG TAT GCC TTA T
	Rev AAA TTC CAA CCC CTT CCA CAG AT
Tbx4$^{lox/lox}$	Fwd GAG GAT GTT CCC CAG CTA C
	Rev CAG TCT GAG AGG GTC AGA CTC
	Rev TCA TCT AGG CTT CAC AGC C
Pitx1$^{-/-}$	Fwd CAA CAT TCC AGG CGA CTA CAT
	Fwd CTA CAT GGC TCT TAC CCC ACA
	Rev GAA ACG CCG AGT TAA CGC CAT C
	Rev GCG ATC TCC TCT CTC ATG CT
Prx1-Tbx or Prx1-M4C	Fwd CTA AGC CAG ATG TCA GCC CCC
	Rev CAG TAG CCT CAT CAT CAC TAG ATG
Z/EGFgf10	Fwd TGC AGT GCT TCA GCC GCT AC
	Rev CCA GCA GGA CCA TGT GAT CG
Fgf10$^{-/-}$	Fwd CTT CCA GTA TGT TCC TTC TGA TGA GAC
	Fwd ACG ACG GGC GTT CCT TGC GCA GCT GTG
	Rev GTA CGG ACA GTC TTC TTC TTG GTC CC
	Rev TCA GAA GAA CTC GTC AAG AAG GCG ATA

Table 2. List of primers used to genotype various mouse strains.

Table 3.

Genotype	Step	temp	min	sec	cycle
Cre or $Fgf10^{-/-}$	1	94	2		
	2	94		30	
	3	54		30	
	4	72	1	30	
	GOTO 2				30
INV/INV	1	94	5		
	2	85	5		
	3	94		30	
	4	65		30	
	5	72	1		
	GOTO 3				30
	7	72	10		
	8	4	hold		
$Tbx5^{lox/lox}$	1	94	5		
	2	85	5		
	3	94		30	
	4	65		30	
	5	72	1		
	GOTO 3				30
	7	72	10		
	8	4	hold		
$Tbx4^{lox/lox}$	1	94	2		
	2	94		15	
	3	60		30	
	4	72		40	
	GOTO 2				29
$Pitx1^{-/-}$	1	95	5		
	2	95		30	
	3	60		30	
	4	72		57	
	GOTO 2				35
	6	72		5	
Prx1-Tbx or Prx1-M4C	1	94	2		
	2	94		30	
	3	65		30	
	4	72	1	30	
	GOTO 2				30
Z/EGFgf10	1	94	2		
	2	94		30	
	3	60		30	
	4	72	1		
	GOTO 2				30

Table 3. List of PCR reaction steps used during the genotyping procedures.

Whole mount in situ hybridisation

Whole mount in situ hybridisation was performed as previously described (Riddle et al., 1993). The following probes were used that have been previously described: *mFgf10* (Sala et al., 2006), *mSall4* (Harvey et al., unpublished), *mFgf8* (Mahmood et al., 1995), *mCol2a* (Metsaranta et al., 1991), *mPitx1* (Logan et al., 1999).

Probe plasmids were digested using 1 unit of enzyme (10 units/ ml) per 5 μl of plasmid DNA. The reaction mix was incubated at 37°C for one hour. 2 μl of this reaction mix was run out on a 1% agarose gel to check digestion of the plasmid. Linearised DNA was then extracted by adding 180 μl of 1mM Tris-HCL ph 7.5 and 200 μl of 49:49:1 phenol:chloroform:isoamyl alcohol to the reaction mix. This was vortexed and centrifuged for 5 minutes at 14,000 rpm. The clear upper aqueous liquid was removed and transferred to a new tube and the linearised DNA was precipitated by adding 20 μl of 4M LiCl (0.1 of the volume) and 500 μl of 100% ethanol alcohol (2.5 of the volume). This was vortexed for 45 seconds and then incubated overnight at -20°C. This was then centrifuged for 10 minutes at 14,000 rpm. The resulting pellet was washed with 500 μl of 70% ethanol alcohol (centrifuged for 1 minute at 14,000 rpm) and left to dry. The linearised DNA was re-suspended in 10 μl of 1mM Tris-HCL pH 7.5.

All digoxygenin probes were produced according to the manufacturer's protocol (Roche). All transcription mixes were incubated at 37°C for 2 hours. Transcription was checked by running 1 μl of the reaction mix on a 1% agarose gel. To purify the probe, 1 μl of DNAse (Roche) was added and the mixture was incubated for 15 minutes at 37°C. 100 μl of TE-8 (10mM Tris-HCL ph 7.5 and 0.1mM EDTA ph 8.0), 10 μl of 4M LiCl, and 300 μl of 100% ethanol alcohol was

added to the mixture and incubated overnight at -20°C. The mix was then centrifuged for 10 minutes at 14,000 rpm. The resulting pellet was washed with 300 μl of 70% ethanol for 1 minute at 14,000 rpm. The pellet was left to air dry and was subsequently re-suspended in 50 μl of TE-8 and 50 μl of hybridisation buffer.

Skeletal Preparation of embryos

E14.5 and older embryos were skinned and eviscerated in 100% ethanol. The skeletons were dehydrated in acetone overnight at room temperature. Skeletons were then incubated in a solution containing 5ml alcian blue (0.3% w/v alcian blue in 70% ethanol), 5ml alizarin red (0.1% w/v alizarin red S in 95% ethanol), 2.5 ml of glacial acetic acid and 37.5ml of 70% ethanol overnight at 37°C. Skeletons were then washed for 30 minutes in 95% ethanol at room temperature. The skeletons were cleared in 1% potassium hydroxide over a period varying from 1 week to 2 weeks depending on the embryonic stage. They were then gradually cleared in glycerol and photographed.

Wholemount and section LacZ embryo staining

Embryos staged up to E10.5 were fixed in 1% formaldehyde, 0.2% gluteraldehyde, 2mM $MgCl_2$, 5mM EGTA, 0.02% Igepal in phosphate buffered saline (PBS) were 15 minutes at 4°C. They were then washed 3 times in PBS/0.02% Igepal for 10 minutes each. Embryos were stained for 30 minutes to overnight at 37°C in 5mM $K_3Fe(CN)_6$, 5mM $K_4Fe(CN)_6$, 2mM $MgCl_2$, 0.01% NaDeoxycholate, 0.02% Igepal, 1 mg/ml X-gal in PBS. Stained embryos were then washed 3 times in PBS/0.02% Igepal for 10 minutes each and fixed in 4% paraformaldehyde in PBS.

For section stains, embryos were fixed and genotyped as above. Embryos were then suspended in 30% sucrose in PBS overnight at room temperature and then gradually introduced to O.C.T compound (Prolabo). Embryos were frozen and

embedded in O.C.T and then sectioned using the cryostat. The sections were washed in PBS/0.02% Igepal for 10 minutes at room temperature and then incubated in stain solution overnight at 37°C in a humidified chamber. Sections were washed 3 times in PBS/0.02% Igepal for 10 minutes each and then fixed in 4% paraformaldehyde in PBS. The sections were sealed using mounting medium supplied by Dako.

Quantitative PCR

RNA was extracted from the forelimb and hindlimb buds of embryos according to the manufacturers instructions using the RNeasy mini kit (Qiagen). cDNA was synthesised in the following reaction mix: 20μl (4mg) RNA, 23μl H_2O, 1μl random primers (Invitrogen), 1μl 10mM dNTPs (Invitrogen). This was incubated at 65°C for 5 minutes, then removed and placed on ice. 12μl 5x transcription buffer (Invitrogen), 1μl RNAsin1 (Promega), 2μl Superscript Reverse Transcriptase II (Invitrogen) were then added to the reaction mix, which was incubated at 50°C for an hour, then 70°C for 15 minutes.

Primer sets were generated using the PrimerBlast application available online (http://www.ncbi.nlm.nih.gov/tools/primer-blast) (Table 4). All primers were generated to produce 100-150bp amplicons that span an exon-exon junction in each gene.

Table 4.

Gene	Primers 5'-3'	
	Forward	**Reverse**
Tbx4	GAA GCG TAG AGA CAG TGC CC	GAG GGG GAG AAC GGA AAT AG
Tbx5	GGC CTT AAT CCC AAA ACG AA	CGG ACC ATT TGT TAT CAG CAA
GapDH	TGT CAG CAA TGC ATC CTG CA	CCG TTC AGC TCT GGG ATG AC
Cre	GAA CGA AAA CGC TGG TTA GC	CCC GGC AAA ACA GGT AGT TA
Fgf10	TCC GTA CAG TGT CCT GGA GAT	TTG AGC CAT AGA GTT TCC CC
Prx1-5N5T4C	GAG ACA GCT TTT ATC GCT GTG	CAT CGC TGC CCC GGA ATC CCT

Table 4. Primers used for quantitative analysis.

For quantification of genomic DNA, hindlimb buds were harvested from *Tbx4*$^{lox/lox}$*; RetRV5Cre* and *Tbx5*$^{lox/lox}$*; Tbx4*$^{lox/lox}$*; HoxB6Cre* mutant embryos, as well as control embryos. Ectoderm was removed from the hindlimb buds as described in Bruce et al 2010. Hindlimbs were incubated in 1unit/ml Dispase II (Gibco), 10% Foetal Bovine Serum (Sigma) in Puck's Saline A (5.4mM KCL, 140mM NaCl, 4.2mM $NaHCO_3$, 6.1mM glucose) for one hour at 37^{o}C (Bruce et al., 2010). The remaining mesenchyme was digested for 2 hours at 55^{o}C in 200 ml of lysis buffer. Genomic DNA was then extracted using phenol:chloroform:isoamyl and precipitated as described above. The primers used for quantification of *Tbx5*$^{lox/lox}$ were previously described in Hasson et al 2007. Reactions were normalised against mouse cardiac actin (mCA), described in Hasson et al 2007. The primers for conditional Tbx5 are exon3 Fwd 5′-GGCATGGAAGGAATCAAGGT-3',

int 3-4 Rev 5′-ATTCCCTCCAATGACTGTCC-3′ . The primers for mCA are

Fwd 5′-CCCCCTGGCTGATCCTCTAC-3′ and

Rev 5′TGGTCGCCTTAGCACCAT-3 (Hasson et al., 2007). Primers were designed flanking the LoxP site located in the intronic region 3' downstream of exon 4 in *Tbx4*$^{lox/lox}$ using the Primer Blast application. Forward primers used were 5'-CCTGCTCCTCCAGCAAGGAGT-3' and reverse primers were 5'-AGGGGGCTGACATCTGGCTT-3'. SyBr Green Master Mix (Applied Biosystems) was used for all quantitative PCR reactions. Results were quantified using the ratio

of DCT (cross over threshold) and normalised against mouse glyceraldehyde 3-phosphate dehydrogenase [GapDH] (for cDNA reactions) and mouse cardiac actin [mCA] (for genomic DNA reactions).

Quantitative Analysis

All analysis of quantitative PCR results were performed in the following manner.

For all samples, the ΔCT was obtained using this formula

$$CT_{\text{gene of interest}} - CT_{\text{normalising control}} = \Delta CT$$

ΔΔCT for all samples was obtained using this formula

$$\Delta CT_{\text{sample}} - \Delta CT_{\text{relative sample}} = \Delta\Delta CT$$

For all samples the following was used to extract the values presented in this work.

$$2^{-(\Delta\Delta CT)}$$

The two-tailed Student's *t*-test was used for statistical analysis of all quantitative PCR reactions.

Western blot analysis

The forelimb buds of mouse embryos were harvested and homogenised in 80 μl of RIPA buffer (5ml 10% Triton in H20, 0.5g sodium deoxycholate, 250 μl 20% SDS (Biorad), 1.5 ml 5M NaCl, 2.5ml 1M Tris ph 7.2, 41ml H20). Protein quantification was carried out according to the manufacturer's instructions using the Microplate BCA protein assay kit (Pierce).

Samples were run on a readymade NuPage BIS-Tris 4%-12% gel (Invitrogen), according to the manufacturer's instructions. Protein bands were then transferred onto a nitrocellulose membrane (Invitrogen) according to the manufacturer's instructions. The membrane was washed for 10 minutes in PBS/0.5% Tween-20 and blocked for 1 hour at room temperature in 5% milk

powder/PBS/0.5% Tween-20 (milk powder supplied by Marvel). The membrane was incubated in polyclonal Tbx5 antibody solution (1/200 in PBS/0.5% Tween-20) for an hour at room temperature. The membrane was then incubated in the secondary anti-HRP solution (1/10,000 in PBS/0.5% Tween-20). Protein bands were then developed onto film according to the manufacturer's instructions using the Immobilon Western Chemiluminescent HRP substrate (Millipore). The membrane was the placed into stripping buffer (100mM β-mercaptoethanol, 2% SDS and PBS) rocking gently for 30 minutes at room temperature. The membrane was washed 5 times at 10 minutes each in PBS/0.5% Tween-20, and then blocked again using 5% milk powder/PBS/0.5% Tween-20. The membrane was then incubated in polyclonal Actin antibody solution (1/7500 in PBS/0.5% Tween-20) for an hour at room temperature. This was repeated for another hour using the secondary anti-HRP solution (1/10,000 in PBS/0.5% Tween-20). Bands were then developed onto film as above. Actin was used as a loading control.

CHAPTER THREE:

GENERATION AND CHARACTERIZATION OF MOUSE MUTANTS MODELING THE UPPER LIMB PHENOTYPE OF HOS PATIENTS

Introduction

HOS is associated with mutations in *TBX5*, a T-box transcription factor expressed in the forelimb and heart. The clinical features of HOS include heart defects and a spectrum of upper limb defects ranging in severity from total aplasia of the radial elements to relatively mild defects such as the triphalangeal thumb, in which the normal biphalangeal digit presents with an extra third phalanx. A key clinical feature of these patients is that however severe the phenotypic presentation of upper limb defects, the left upper limb is consistently more severely affected than the right (Newbury-Ecob et al., 1996). Analysis of HOS patients has shown that mutations leading to the formation of a premature stop codon in the coding sequence for *TBX5* comprise the majority of *TBX5* mutations in patients. Some of these nonsense mutations are predicted to form very short truncated proteins that may fail to fold or are rapidly degraded. Other mutations would be predicted to produce longer protein products lacking the C-terminal activation domain that may disrupt the ability to bind to target DNA (Boogerd et al., 2010). There is no evidence suggesting that any of the *TBX5* mutations found in HOS patients lead to dominant-negative acting protein products. HOS patients are heterozygous for mutations in *TBX5* therefore it appears that both copies of *TBX5* are required for normal upper limb and heart development. This suggests that the defects that present in HOS patients arise through haploinsufficiency for *TBX5*.

Attempts to recapitulate the upper limb defects associated with HOS in the mouse have previously met with little success. Conditional heterozygous deletion of *Tbx5* using the limb-restricted *Prx1Cre* transgenic deleter line (*Tbx5*$^{lox/+}$*; Prx1Cre*) does not lead to any obvious forelimb phenotype, while homozygous conditional deletion of *Tbx5* (*Tbx5*$^{lox/lox}$*; Prx1Cre*) leads to a total loss of forelimb bud initiation and subsequent formation (Rallis et al., 2003). It has been reported that

heterozygous null *Tbx5* mutants (*Tbx5*$^{-/+}$) bred onto the pure C57BL/6 mouse strain present with very subtle forelimb digit defects (Bruneau et al., 2001). As neither conditional nor heterozygous *Tbx5* mutants present with the extensive upper limb defects found in HOS patients, I have developed two alternative strategies to model in the mouse the left-biased asymmetrical upper limb defects of HOS patients.

Tbx5 is a transcription factor known to be required for the initiation of forelimb bud formation, as previous studies have shown that the conditional deletion of *Tbx5* from the forelimb-forming area using the *Prx1Cre* transgenic line leads to a bilateral failure of right and left forelimb bud initiation from the LPM (Rallis et al., 2003; Agarwal et al., 2003). In a small number of cases, however, a small remnant of limb tissue was present on the right side of mutant embryos. It was suggested that this was due to a failure in delivery of cre recombinase to every cell in the forelimb-forming region of the left and right LPM, resulting in a few cells escaping deletion of the *Tbx5* conditional allele. In all cases, the limb tissue remnant was observed on the right side i.e. the left side was always more affected than the right. This is particularly interesting as HOS patients present with upper limb defects that are characteristically more severe in the left limb than the right.

To investigate the origins of the left bias to the severity of defects that develop in HOS patients, I have produced two different genetic strategies to disrupt *Tbx5* expression in the left and right forelimb area. The first strategy uses a mosaic cre deleter line, the *Prx1Cre(98),* to delete conditional *Tbx5* from cells in the right and left forelimb-forming LPM. This leads to the formation of forelimbs presenting with defects that vary in severity, but are consistently more severe in the left forelimb than the right. The second approach utilizes a gene deletion-gene replacement strategy in which conditional *Tbx5* is deleted using the *Prx1Cre* deleter line and

hypomorphic levels of a novel *Prx1-Tbx* transgene are expressed in the forelimb regions of the same embryo. This results in mutant embryos in which the presentation of forelimb defects is more severe in the left forelimb than the right. Both mouse models successfully recapitulate the types of upper limb abnormalities observed in HOS patients and in particular significance for my study, the left bias in the severity of the upper limb defects.

3.1 MOSAIC DELETION OF *Tbx5* LEADS TO LEFT-BIASED ASYMMETRICAL FORELIMB DEFECTS.

Analysis of the spatio-temporal activity of cre recombinase in the forelimb-forming region of the LPM in the *Prx1Cre(98)* cre deleter transgenic mouse line.

The published *Prx1Cre* cre deleter transgenic mouse line was generated through the random integration of a transgene construct into the mouse genome. In this transgenic construct, *cre recombinase* is under the control of a regulatory sequence from the *paired-related homeobox gene-1* (*Prx1*) gene, which is normally expressed in mouse limb buds (Logan et al., 2002). Under control of the *Prx1* regulatory element, cre recombinase activity is detectable in the forelimb-forming regions of the LPM (Logan et al., 2002). When this line is used in combination with the conditional allele for *Tbx5*, *Tbx5* expression is lost from the forelimb-forming region of the LPM. This leads to a failure of forelimb bud initiation resulting in a failure of the forelimb elements to form (black arrow, Fig 3.1 A). The original *Prx1Cre* transgenic construct was also used to produce a novel transgenic mouse line, the *Prx1Cre(98)*. In contrast to the original *Prx1Cre* line, when the *Prx1Cre(98)* cre deleter transgenic line is used in combination with conditional *Tbx5*

(*Tbx5*$^{lox/lox}$*; Prx1Cre(98)*) a forelimb is formed (black arrow, Fig 3.1 B). Interestingly, *Tbx5*$^{lox/lox}$*; Prx1Cre(98)* mutant embryos present with forelimb defects that are more severe in the left forelimb than the right (see Fig 3.3).

To explain the difference in phenotype I obtained using these two lines, I characterized the spatial and temporal activity of cre recombinase in the *Prx1Cre(98)* transgenic line and compared it to the original *Prx1Cre* transgenic line. For this analysis I have chosen to use the *Rosa26RlacZ* reporter line. In the *Rosa26RlacZ* reporter line, cre mediated recombination of a stop cassette within the transgenic construct leads to the expression of β-galactosidase. This is detectable through the application of X-gal, an artificial substrate for the enzyme. The resulting cleavage product, 5-bromo-4-chloro-3-hydroxyindole, is oxidized to form an insoluble blue product thus marking cells in which cre recombinase is active.

The first morphological features of the forelimb bud arising from the LPM are evident in 16 somite stage mouse embryos. At this stage in *Rosa26RLacZ/+;Prx1Cre* embryos, cre activity is detectable throughout the forelimb-forming region of the LPM, which spans from the 5th to the 10th somite (marked by black asterisks, Fig 3.1 C). Cre activity is also detectable in regions of the LPM extending rostral and caudal to the forelimb-forming region (Fig 3.1 C). In contrast, cre recombinase activity is not detectable in the equivalent region of the LPM in *Rosa26RlacZ/+; Prx1Cre(98)* embryos at the same stage (marked by black asterisks, Fig 3.1 D). The nascent forelimb bud is an obvious protrusion from the LPM in 22 somite stage embryos. At this stage in *Rosa26RLacZ/+;Prx1Cre* embryos, cre activity is detectable throughout the nascent forelimb bud (marked by black asterisks, Fig 3.1 E). Cre activity is also detectable in the LPM rostral, caudal and medial to the forelimb bud (Fig 3.1 E). At this stage, LacZ-positive cells are first

detectable in the nascent forelimb buds of *Rosa26RLacZ/+;Prx1Cre(98)* embryos. Cre activity is not detectable in cells of the LPM extending past the length of the nascent forelimb bud (Fig 3.1 F). By E10.5, the forelimb buds are prominent outgrowths in wild-type mouse embryos. Cre activity is detectable throughout the forelimb buds of *Rosa26RLacZ/+;Prx1Cre* embryos (black arrowhead, Fig 3.1 G). Additionally, LacZ-positive cells are detectable rostral and caudal to the forelimb bud. In E10.5 *Rosa26RLacZ/+;Prx1Cre(98)* embryos, cre activity is detectable in a 'salt and pepper' mosaic manner throughout most of the forelimb bud (outlined by the dashed line) but is apparently excluded from distal regions of the forelimb (black arrowhead, Fig 3.1 H). My wholemount analysis of the spatial and temporal activity in the *Prx1Cre(98)* cre deleter transgenic line indicates that cre activity is delayed compared to activity in the *Prx1Cre* line and that it is not detectable in every cell of the forelimb buds.

Figure 3.1

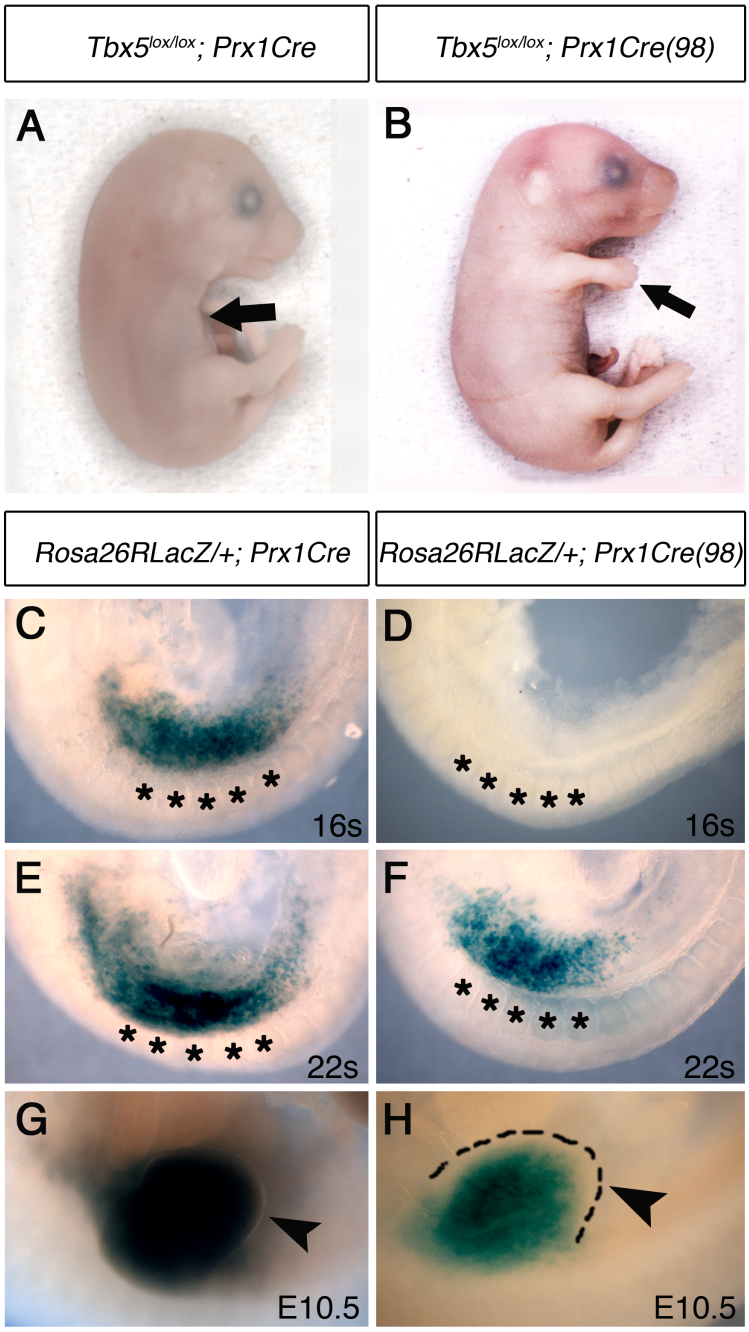

Figure 3.1 Cre activity occurs after forelimb bud initiation in the *Prx1Cre(98)* transgenic deleter line.

All panels (**A-H**) are lateral views of right-sided embryos. **A** E17.5 *Tbx5$^{lox/lox}$; Prx1Cre* mutant embryo in which all the elements of the forelimb have failed to form (black arrow). **B** E17.5 *Tbx5$^{lox/lox}$; Prx1Cre(98)* embryo in which an abnormal forelimb has formed (black arrow). **C** 16 somite stage *Rosa26RlacZ/+; Prx1Cre* embryo. Blue stain corresponding to LacZ activity induced by cre recombinase is detectable

throughout the forelimb-forming region (the span of which is marked by black asterisks in the adjacent somites). **D** 16 somite stage *Rosa26RlacZ/+; Prx1Cre(98)* embryo in which there is no blue stain detectable in the forelimb-forming region (marked by black asterisks in the adjacent somites). **E** 22 somite stage *Rosa26RlacZ/+; Prx1Cre* embryo in which blue stain is detectable throughout nascent forelimb bud (marked by black asterisks in the adjacent somites), as well as rostral, caudal and medial to the forelimb-forming region. **F** 22 somite stage *Rosa26RlacZ/+; Prx1Cre(98)* embryo. Blue stain is detectable in a 'salt and pepper' mosaic manner in the nascent forelimb bud (marked by black asterisks in the adjacent somites). **G** E10.5 *Rosa26RlacZ/+; Prx1Cre* mutant embryo. Blue stain is detectable throughout the forelimb bud (black arrowhead). **H** E10.5 *Rosa26RlacZ/+; Prx1Cre(98)* embryo. Blue stain is detectable in a mosaic manner in the forelimb bud (outlined by the dashed line). Blue stain is not detectable in the distal most region of the forelimb bud (black arrowhead).

To examine cre activity in the forelimb buds of *Prx1Cre(98)* transgenic embryos at a higher resolution, I analyzed transverse cryosections of the forelimb buds of E9.0, E9.5 and E10.5 embryos. Within the forelimb-forming region of E9.0 *Rosa26RlacZ/+;Prx1Cre(98)* embryos, a small number of isolated LacZ-positive cells are detectable (Fig 3.2 A). In E9.5 *Rosa26RlacZ/+;Prx1Cre(98)* embryos, the number of LacZ-positive cells has increased (black arrowhead, Fig 3.2 B). A similar proportion of LacZ-positive cells are detectable within the forelimb bud mesenchyme of E10.5 *Rosa26RlacZ/+;Prx1Cre(98)* embryos, suggesting that cre activity has not been initiated in a new subset of cells at this stage. Cre activity is not detectable in the forelimb bud ectoderm (black arrowhead, Fig 3.2 C).

My analysis of the spatio-temporal activity of cre recombinase in the *Prx1Cre(98)* transgenic line demonstrates two key differences in comparison to the original *Prx1Cre* line. Initially, there is a relative delay in the onset of cre activity in the *Prx1Cre(98)* line and once cre activity takes place in the nascent forelimb bud it does so in a mosaic manner. From this analysis, I therefore predict that use of the *Prx1Cre(98)* line in combination with the conditional *Tbx5* allele leads to the mosaic

deletion of *Tbx5* from the cells of the early forelimb bud. This leads to the formation of forelimbs displaying extensive defects. Significantly, these mutants present with forelimb defects that occur with greater frequency in the left forelimb compared to the right.

While demonstrating that the *Tbx5$^{lox/lox}$; Prx1Cre(98)* mutant embryo recapitulates the left-biased asymmetrical upper limb defects found in HOS patients, it was important to confirm that cre recombinase is expressed symmetrically in both the left and right forelimb buds. My analysis of *Rosa26RlacZ/+; Prx1Cre(98)* embryos in wholemount did not reveal any apparent asymmetric distribution of LacZ-positive cells between the left and right forelimb buds. Furthermore my analysis of cre recombinase activity at a higher resolution in sectioned embryos does not reveal any obvious asymmetry in either the onset or spatial distribution of the number of cells positive for cre activity (not shown). I decided to use RT QT PCR to analyze the transcript levels of *cre recombinase* to determine whether it is expressed asymmetrically between the left and right forelimb buds of *Prx1Cre(98)* embryos.

I designed forward and reverse primers against the ORF of *cre recombinase* such that an amplicon of 129bp is generated. I extracted RNA from the right and left transgenic forelimb buds of E9.5 and E10.5 embryos, as LacZ positive cells are clearly visible at these stages (N=10). I then synthesized cDNA for QT PCR analysis. The raw data was analysed as described in the Methods and Materials. In E9.5 forelimb buds, the difference in cre recombinase transcript level in the right and left forelimb buds is less than 0.5 fold (Fig 3.2 D). Statistical analysis using the two-tailed Student's *t*-test renders this an insignificant difference in transcript level ($p >$

0.05, p = 0.3). As expected, this difference is not increased in E10.5 left and right forelimb buds and is not significant (Fig 3.2 D) ($p > 0.05$, p = 0.34).

Figure 3.2

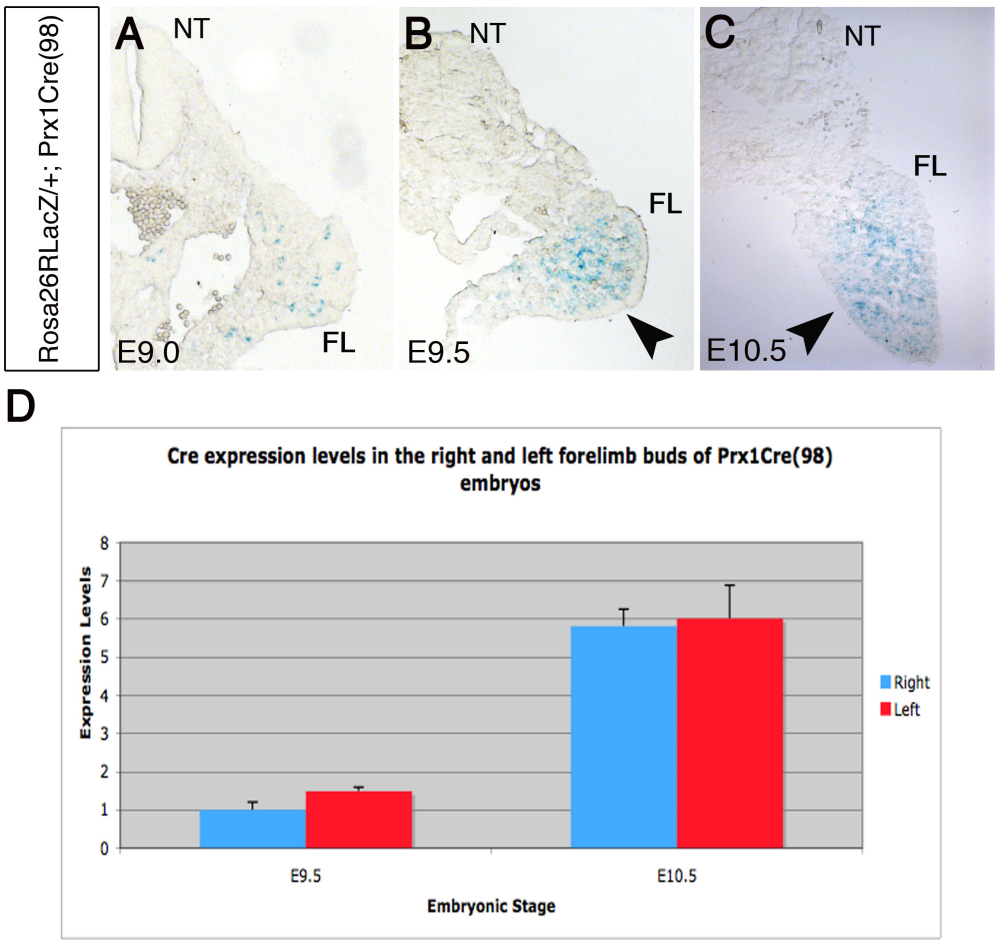

Figure 3.2 Cre activity is detectable in a small number of cells in the left and right limb bud and is expressed symmetrically in *Rosa26RlacZ/+; Prx1Cre(98)* embryos.

Panels **A-C** show transverse cryosections of the right forelimb bud of *Rosa26RlacZ/+; Prx1Cre(98)* embryos. **A** E9.0 *Rosa26RlacZ/+; Prx1Cre(98)* embryo. Blue stain is detectable in isolated cells within the forelimb mesenchyme. **B** E9.5 *Rosa26RlacZ/+; Prx1Cre(98)* embryo. Blue stain is detectable in a mosaic manner in the forelimb mesenchyme (black arrowhead). **C** E10.5 *Rosa26RlacZ/+; Prx1Cre(98)* embryo. Blue stain is evident throughout most of the forelimb mesenchyme, but is not detectable in the ectoderm (black arrowhead). **D** Graph showing the relative expression levels of cre recombinase in the left and right forelimb buds of E9.5 and E10.5 *Prx1Cre(98)* transgenic embryos.

There is no significant difference in cre recombinase transcript levels between the left and right forelimb buds at any stage. ('y' axis – cre recombinase expression levels, 'x' – embryonic stage.) NT-Neural tube, FL – Forelimb

Mosaic deletion of conditional *Tbx5* from the forelimbs of *Tbx5$^{lox/lox}$; Prx1Cre(98)* mutants leads to left-biased asymmetrical forelimb defects.

My analysis of the spatio-temporal activity of cre recombinase in the *Prx1Cre(98)* transgenic line indicates that the conditional allele for *Tbx5* is deleted mosaically from the left and right nascent forelimb buds of *Tbx5$^{lox/lox}$; Prx1Cre(98)* mutant embryos. This results in the formation of abnormal forelimbs in which the defects are more severe in the left forelimb than the right. To confirm that the left-sided bias to the forelimb defects is present in every mutant, I have analyzed the skeletal forelimb elements using alcian blue to mark the cartilage and alizarin red to mark the bone. I have subsequently tabulated forelimb defects in a total of 18 E17.5 mutants. I have chosen to present the left and right forelimbs of 5 mutant embryos in a representational series (see Fig 3.3). This shows the full range and extent of forelimb defects that have resulted from the mosaic deletion of *Tbx5*.

In recapitulating the left-biased asymmetrical upper limb defects of HOS patients, I have also recapitulated certain upper limb defects that are characteristic features of HOS patients in the *Tbx5$^{lox/lox}$; Prx1Cre(98)* mutant. The range and scale in the severity of upper limb defects in HOS patients varies greatly. Defects such as the addition of a third phalanx to the normally biphalangeal thumb (triphalangeal thumb), the bifurcation of the digits, and the loss of the thumb present as part of the less severe clinical phenotype in HOS patients whereas defects such as the aplasia of the humerus are regarded as more severe. *Tbx5$^{lox/lox}$; Prx1Cre(98)* mutant embryos present with all of these defects, therefore I have tabulated the frequency

of their occurrence. In my skeletal analysis of *Tbx5$^{lox/lox}$; Prx1Cre(98)* mutant embryos, I have not included the scapula in this study.

Left and right forelimbs in an E17.5 control embryo are bilaterally symmetric in the overall length, morphology and size of individual skeletal elements (Fig 3.3 A). In contrast, *Tbx5$^{lox/lox}$; Prx1Cre(98)* mutant forelimbs have an extensive but stereotypic range of forelimb defects (Fig 3.3 B). These include the formation of triphalangeal digit 1 (the addition of a third phalanx to the normally biphalangeal digit 1) and the total loss of digit 1, both of which are a common clinical feature observed in HOS patients. Other abnormalities include shortened humerii and bifurcated digits. Example 1 of Fig 3.3 shows a pair of mutant right and left forelimbs. The left forelimb has lost digit one and the humerus is severely truncated. The right forelimb presents with similar defects, although the humerus is of a larger size (Fig 3.3 B1). In example 2 the left-biased asymmetrical forelimb differences are clearer. The humerus of the left forelimb is severely truncated, compared to the humerus in the right forelimb. Additionally, the left forelimb presents with a fused pair of digits in the autopod. In contrast the right forelimb has a less severe humerus truncation and the digits of the autopod have apparently retained their features (Fig 3.3 B2). The pair of mutant left and right forelimbs in example 3 present with defects similar in extent and asymmetrical presentation to those in example 2. Additionally, however, the head of the humerus is now lost from the left mutant forelimb (Fig 3.3 B3). The left and right mutant forelimbs in example 4 are apparently symmetrical in humerus length, however the left forelimb presents with a partially bifurcated digit. Digit one in the autopod of the right forelimb is transformed from a biphalangeal to a triphalangeal identity (Fig 3.3 B4). The pair of mutant forelimbs in example 5 present with similar defects between the left and right forelimb, however the left limb presents with a triphalangeal digit 1 (Fig 3.3 B1). My tabulation of these forelimb

defects in 18 separate mutant embryos indicates that the stereotypic forelimb defects occur with greater frequency in the left forelimb than the right. Defects such as the loss of digit one, partially bifurcated digits, bifurcated digits are detectable more often in the left forelimb than the right. In addition, in many mutants the left humerus is reduced in length compared to the right (Table 5).

Figure 3.3

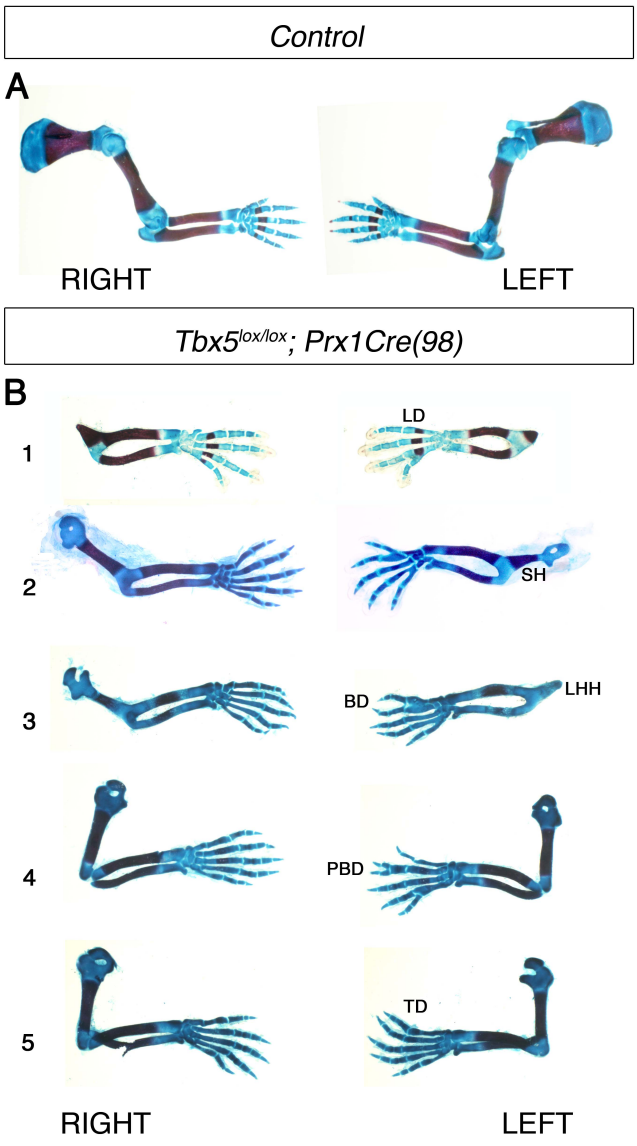

Figure 3.3 Conditional deletion of *Tbx5* with the *Prx1Cre(98)* transgenic deleter results in left-biased asymmetrical forelimb defects.

A Dorsal view of the left and right forelimbs of an E17.5 control embryo. **B** Dorsal views of 5 pairs of the left and right forelimbs of 5 E17.5 *Tbx5$^{lox/lox}$; Prx1Cre(98)* mutant embryos. B1- LD shows the loss of digit one from the autopod of the left forelimb. B2 – SH shows the comparatively reduced length of the left humerus. B3 – BD and LHH show the bifurcated digit and loss of the humerus head respectively in the left forelimb. B4 – PBD shows the partially bifurcated digit in the left forelimb. B5 – TD shows the triphalangeal transformation of digit one.

LD – Loss of digit 1, SH – Shortened humerus, LHH – Loss of humerus head, BD – Bifurcated digit, PBD – partially bifurcated digit, TD – Triphalangeal digit one

Table 5.

	RIGHT						
	loss digit 1	TD	BD	partial BD	short h	lost HH	hole inHH
1		*	*				
2							
3							*
4							*
5		*					*
6		*					
7		*					*
8		*					*
9		*					*
10		*					*
11	*				*	*	
12				*			*
13							*
14							
15		*					
16							*
17		*					*
18							*

	LEFT					
loss digit 1	TD	BD	partial BD	short h	lost HH	hole in HH
				*		*
	*			*		*
			*	*		*
		*		*		*
	*					*
	*			*		
		*		*	*	
		*	*			*
	*					*
	*					*
*			*	*	*	
			*	*		
						*
	*	*				*
	*			*		*
*			*	*	*	
	*					*
*			*	*		

Table 5. Graph of total tabulated defects in the left and right forelimbs of 18 *Tbx5$^{lox/lox}$; Prx1Cre(98)* mutant embryos.

The gestation period in *mus musculus* typically lasts from 18-20 days, therefore by E17.5 embryonic limb formation is largely complete. Left-biased asymmetrical forelimb defects are obvious at this stage in *Tbx5$^{lox/lox}$; Prx1Cre(98)* mutant embryos. My analysis of the spatio-temporal activity of cre recombinase indicates that when the *Prx1Cre(98)* transgenic deleter line is used in combination with the conditional *Tbx5* line, *Tbx5* is deleted mosaically during forelimb bud initiation. It is therefore a strong possibility that the observed left-biased asymmetrical forelimb differences are detectable during early forelimb bud formation. To address when these asymmetrical differences become apparent, I examined *Tbx5$^{lox/lox}$; Prx1Cre(98)* mutant forelimb buds at an early stage of forelimb development.

In wild type embryos, the onset of *Tbx5* expression in the forelimb-forming region occurs prior to the initiation of the forelimb bud from the LPM. During forelimb bud initiation, Tbx5 activity in the mesenchyme directly leads to the expression of *Fgf10*. *Fgf10* then signals via *FgfR2* to initiate the transcription of *Fgf8* in the

overlying ectoderm. *Sall4*, a purported target of *Tbx5*, is thought to be upstream of mesenchymal *FgfR2* expression (Harvey et al., 2005, Koshiba-Takeuchi et al., 2006). The genetic cascade downstream of *Tbx5* serves to enable forelimb bud outgrowth, thus *Fgf10*, *Fgf8* and *Sall4* can serve as excellent molecular markers of early forelimb bud outgrowth. A minimum of 4 mutant embryos were analysed for each probe.

In E10.5 control embryos, the forelimb bud is a prominent outgrowth of the LPM, and there is no obvious difference in the size of the left and right limb buds. *Fgf10* and *Sall4* in the limb bud mesoderm and *Fgf8* expression in the overlying ectoderm appear equivalently expressed in the left and right forelimb buds (Fig 3.4 A, C, E). In same stage *Tbx5*$^{lox/lox}$*; Prx1Cre(98)* embryos both mutant limb buds are reduced in comparison to the control limb buds, however the left mutant limb bud is smaller in size than the right mutant limb bud (black arrowheads Fig 3.4 B, D, F). Although the left limb bud is smaller than the right, there is no discernable difference in the expression patterns of *Fgf10* and *Sall4* in the left and right forelimb buds (black arrowheads, Fig 3.4 B, F). *Fgf8* expression in the left bud ectoderm is disturbed as indicated by intermittent AER expression, in contrast to the expression of *Fgf8* in the right limb bud which is unchanged (black arrowhead, Fig 3.4 D). The disruption of *Fgf8* suggests that there is a partial breakdown in signal transduction between the mesenchyme and the ectoderm in the left limb bud. In all of the mutant embryos analyzed (n=12), the left limb bud is consistently smaller than the right. It is unclear from this analysis whether the difference in gene expression between the left and right limb bud is related to the smaller size of the left limb bud or is in fact the cause of the difference in size.

Through my analysis, I have demonstrated that the mosaic deletion of *Tbx5* expression during forelimb bud initiation leads to the formation of abnormal left and right forelimbs. Significantly, these mutant embryos present with more defects in the left forelimb than the right at both the early and late stages of forelimb development therefore recapitulating the left-biased asymmetrical upper limb defects observed in HOS patients. Thus, using a conditional deletion strategy, I have shown that the bilaterally symmetric mosaic deletion of *Tbx5* from the left and right forelimb regions of the LPM leads to left-biased asymmetrical forelimb defects.

Figure 3.4

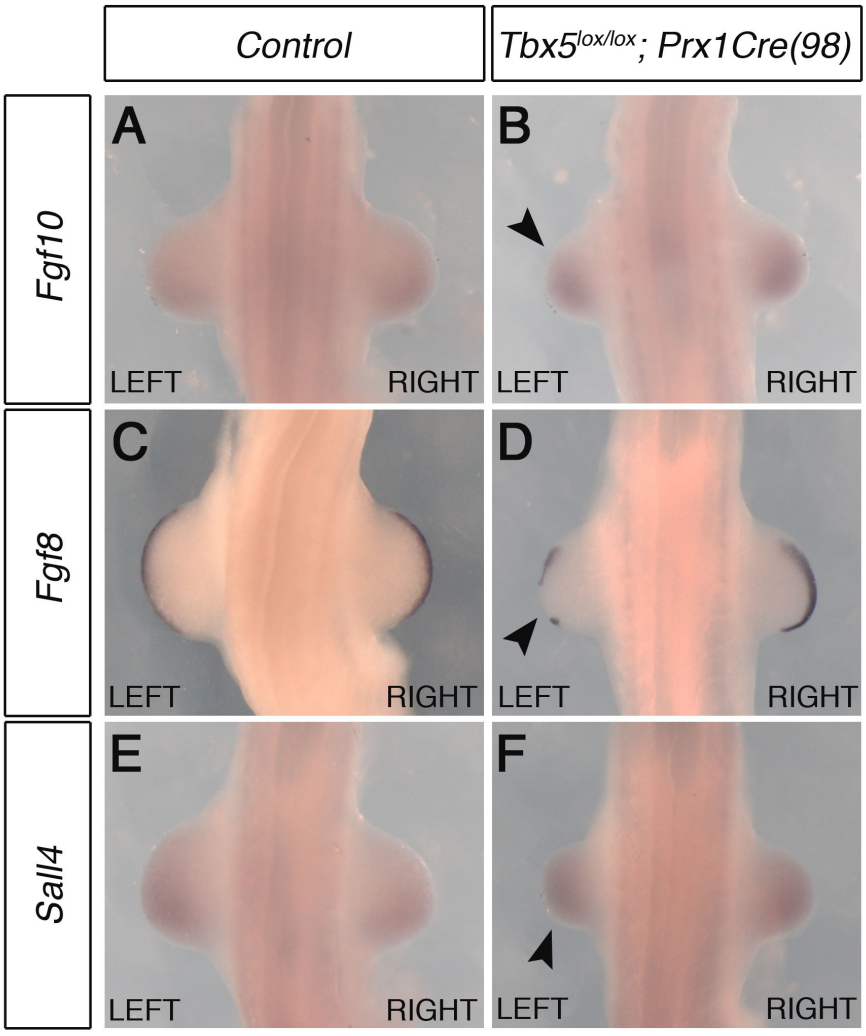

Figure 3.4 The left forelimb bud is reduced in the overall size compared to the right in *Tbx5$^{lox/lox}$; Prx1Cre(98)* mutants.

All panels (**A-F**) show dorsal views of E10.5 embryos, processed by whole mount in situ hybridisation. The left and right forelimbs are labelled in each panel. **A** *Fgf10* expression in a control embryo. **B** *Fgf10* expression in a *Tbx5$^{lox/lox}$; Prx1Cre(98)* mutant embryo. The left forelimb bud is reduced in size compared to the right (black arrowhead). **C** *Fgf8* expression in a control embryo. **D** *Fgf8* expression in a *Tbx5$^{lox/lox}$; Prx1Cre(98)* mutant embryo. *Fgf8* is disrupted in the left forelimb ectoderm (black arrowhead). **E** *Sall4* expression in a control embryo. **F** *Sall4* expression in a *Tbx5$^{lox/lox}$; Prx1Cre(98)* mutant embryo. The left forelimb is reduced in size compared to the right (black arrowhead).

3.2 BILATERALLY SYMMETRIC HYPOMORPHIC LEVELS OF A *Prx1-Tbx* TRANSGENE IN THE RIGHT AND LEFT FORELIMB-FORMING REGIONS LEADS TO FORELIMB DEFECTS THAT ARE MORE SEVERE IN THE LEFT FORELIMB THAN THE RIGHT.

The deletion of the conditional *Tbx5* allele from the forelimb forming area in the *Tbx5$^{lox/lox}$; Prx1Cre* mutant leads to a loss of forelimb bud initiation from the LPM, resulting in a total failure of forelimb formation (Rallis et al., 2003). *Tbx4* is a paralogue of *Tbx5* and is expressed in the hindlimb-forming region of the LPM. Previously published work has shown that the expression of a *Tbx* transgene is able to rescue forelimb bud initiation in the *Tbx5$^{lox/lox}$; Prx1Cre* mutant embryo (Minguillon et al., 2009). This construct is composed of the N and T-Box DNA binding domains of Tbx5 and the C terminal of Tbx4 and is expressed in the limb-forming regions of the LPM through the control of the *Prx1* promoter element (*Prx1-5N5T4C*). Exogenous expression of the *Prx1-5N5T4C* transgene is able to rescue forelimb bud initiation when misexpressed in the forelimb-forming region of mutant embryos in which *Tbx5* expression is lost (Fig 3.5 A) (Minguillon et al., 2009).

During the course of the above-mentioned study, several transgenic mouse lines were independently generated through the random integration of the *Prx1-*

5N5T4C transgenic construct into the mouse genome. Expression of the *Prx1-5N5T4C* transgene in the published transgenic mouse line, *Prx1-M4C*, rescues forelimb bud initiation when combined with the conditional *Tbx5* null mutant (*Tbx5$^{lox/lox}$; Prx1Cre; Prx1-M4C* see Fig 3.5 B) (Minguillon et al., 2009). Interestingly, expression of the same *Prx1-5N5T4C* transgene in the unpublished transgenic mouse line, *Prx1-Tbx*, does not fully rescue forelimb bud initiation when combined with the conditional *Tbx5* null mutant (*Tbx5$^{lox/lox}$; Prx1Cre; Prx1-Tbx*). Instead, these mutants present with forelimb defects that are more severe in the left forelimb (Fig 3.6 B). As this is strongly reminiscent of the left-biased asymmetrical upper limb phenotype in HOS patients, I decided to analyze the left-sided bias to the forelimb defects in the *Tbx5$^{lox/lox}$; Prx1Cre; Prx1-Tbx* mutant. To validate further analysis and in the process demonstrate the robustness of the gene deletion-replacement strategy, I have shown that in *Tbx5$^{lox/lox}$; Prx1Cre; Prx1-Tbx* mutants the conditional allele for *Tbx5* is symmetrically deleted and the *Prx1-5N5T4C* construct is symmetrically expressed in the forelimb-forming regions.

***Cre recombinase* and the *Prx1-5N5T4C* transgene are expressed bilaterally symmetrically in the left and right forelimb-forming regions of the *Tbx5$^{lox/lox}$; Prx1Cre; Prx1-Tbx* mutant.**

The gene deletion/replacement approach utilizes tissue restricted cre recombinase-LoxP technology in combination with the expression of a transgenic construct. The conditional *Tbx5* allele is deleted from the forelimb-forming region using the limb-restricted cre deleter transgenic line, *Prx1Cre*. Simultaneous to the deletion of the conditional *Tbx5* allele, the limb-restricted *Prx1-5N5T4C* transgene is expressed in the forelimb-forming region (Fig 3.5 A). Thus, expression of *Tbx5* is effectively 'replaced' by expression of *Prx1-5N5T4C*. For this assay to be completely effective, the deletion of conditional *Tbx5* and the simultaneous expression of *Prx1-*

5N5T4C must be bilaterally symmetric between the left and right forelimb-forming regions of the LPM.

Asymmetric cre recombinase activity in the published *Prx1Cre* transgenic deleter line has not been reported. Additionally, I have not detected any asymmetry in the spatial or temporal activity of cre recombinase during my comparative analysis between the *Prx1Cre* and *Prx1Cre(98)* transgenic lines (see section 3.1). However, to determine whether the expression of *cre recombinase* in the *Prx1Cre* line is asymmetric, I have again used RT QT PCR to quantify the expression levels of *cre recombinase* in the left and right forelimb buds of E9.5 and E10.5 transgenic embryos. I designed forward and reverse primers against the ORF of *cre recombinase* such that an amplicon length of 129 bp is yielded. I extracted RNA from these tissue samples (n=10) and subsequently synthesized cDNA for the PCR reaction. The raw data obtained from the QT PCR was analysed as described in the Methods and Materials. In transgenic E9.5 embryos there is a less than 0.1 fold difference in the level of the transcript between the right and left forelimb bud. This difference is not significantly increased in transgenic embryos staged a day later at E10.5 (Fig 3.5 C). Statistical analysis using the two-tailed Student's *t*-test demonstrates that the difference in *cre recombinase* expression levels between the left and right forelimb buds is not significant ($p > 0.05$, $p = 0.46$). This data demonstrates that *cre recombinase* is expressed bilaterally symmetrically between the left and right forelimb-forming regions of *Prx1Cre* transgenic embryos.

I have shown that the conditional *Tbx5* allele is symmetrically deleted from the left and right forelimb-forming regions, which leads to a bilateral loss of *Tbx5* expression. As the *Prx1-5N5T4C* transgene 'replaces' *Tbx5* expression in *Tbx5*$^{lox/lox}$*; Prx1Cre; Prx1-Tbx* mutants, I decided to show that the expression of this transgene

is also symmetrical between the left and right forelimb-forming regions. I designed forward and reverse primers to yield an amplicon of 100bp against the *Tbx5/Tbx4* junction in the sequence of the *Prx1-5N5T4C* construct. This ensures that only the target transgene is amplified and not any endogenous *Tbx5* or *Tbx4* transcript. I extracted RNA from the forelimb buds of E9.5 and E10.5 transgenic *Prx1-Tbx* embryos expressing the *Prx1-5N5T4C* transgene (n=10). I then synthesized and subsequently processed cDNA for QT PCR analysis. My results show that there is a less than 0.1 fold difference in *Prx1-5N5T4C* expression levels between the left and right forelimb buds of transgenic embryos staged at E9.5. When examined a day later, at E10.5, there is no significant increase in the initial difference in expression levels between the left and right forelimb buds (Fig 3.5 D). At both stages these differences are not statistically significant according to the two-tailed Students *t*-test ($p > 0.05$, $p = 0.2$).

My quantitative analysis of cre recombinase and *Prx1-5N5T4C* transcript levels in the left and right forelimbs of *Tbx5*$^{lox/lox}$*; Prx1Cre; Prx1-Tbx* mutants confirms that the conditional *Tbx5* allele is deleted symmetrically and *Prx1-5N5T4C* is symmetrically expressed in the left and right forelimb regions. The gene deletion-gene replacement approach is therefore a robust system in which asymmetrical forelimb formation can be studied.

As I have described earlier, mutations in *TBX5* leading to functional haploinsufficiency are associated with HOS (Basson et al., 1999; Ghosh et al., 2001; Boogerd et al., 2010). The expression of *Prx1-5N5T4C* in the forelimb-forming regions of *Tbx5*$^{lox/lox}$*; Prx1Cre; Prx1-M4C* mutants is sufficient to rescue forelimb bud initiation, whereas the expression of the same construct in the *Tbx5*$^{lox/lox}$*; Prx1Cre; Prx1-Tbx* mutant is not. This suggests that the transgenic *Prx1-5N5T4C* construct is

fully capable of acting on the same transcriptional targets as *Tbx5*. Based on observations of HOS patients it is highly possible that the transgenic expression of *Prx1-5N5T4C* in the *Tbx5$^{lox/lox}$; Prx1Cre; Prx1-Tbx* mutant is hypomorphic compared to endogenous *Tbx5* expression levels.

To determine this I have analyzed transgenic Prx1-5N5T4C protein levels in the forelimb buds of *Tbx5$^{lox/lox}$; Prx1Cre; Prx1-Tbx* mutant embryos and compared them to endogenous Tbx5 protein levels in the forelimb buds of wildtype embryos. I extracted protein from E10.5 wildtype forelimb buds and E10.5 mutant forelimb buds, choosing to pool only the right forelimb buds in both samples as many *Tbx5$^{lox/lox}$; Prx1Cre; Prx1-Tbx* mutants at this stage have a small right forelimb bud and no prominent left forelimb bud (see Fig 3.7). I ran the samples on an acrylamide protein gel and then transferred this to a nitrocellulose membrane for western blot analysis. Endogenous Tbx5 protein and Prx1-5N5T4C transgenic proteins are detectable using an anti-Tbx5 polyclonal antibody. An anti-Actin antibody was used to detect levels of actin protein, which was analyzed as an internal control. At E10.5 there is less transgenic protein in the mutant forelimb bud compared to the level of endogenous Tbx5 protein in the wildtype forelimb bud (Fig 3.5 E). Actin bands are equivalent between the two protein samples, further demonstrating that *Tbx5$^{lox/lox}$; Prx1Cre; Prx1-Tbx* mutants have hypomorphic levels of the transgenic protein compared to endogenous levels of Tbx5 protein in the wildtype embryos.

Figure 3.5

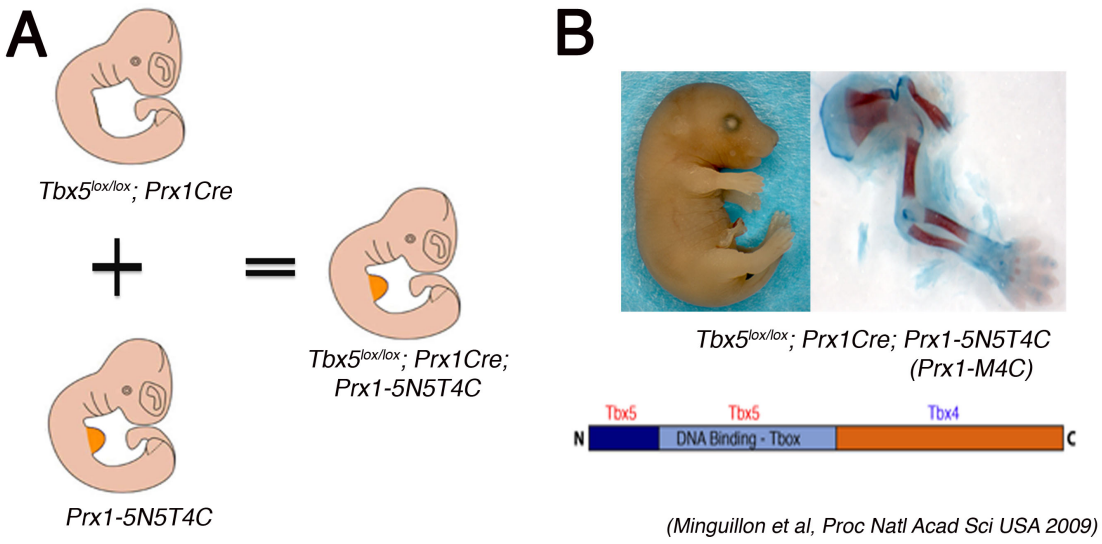
A
Tbx5lox/lox; Prx1Cre
+
=
Prx1-5N5T4C
Tbx5lox/lox; Prx1Cre;
Prx1-5N5T4C
B
Tbx5lox/lox; Prx1Cre; Prx1-5N5T4C
(Prx1-M4C)
Tbx5
Tbx5
Tbx4
N
DNA Binding - Tbox
C
(Minguillon et al, Proc Natl Acad Sci USA 2009)

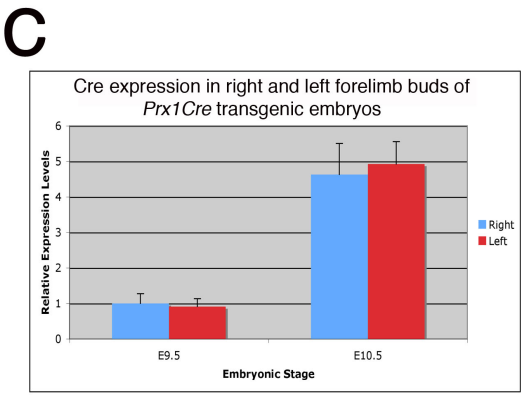
C
Cre expression in right and left forelimb buds of
Prx1Cre transgenic embryos
Relative Expression Levels
Embryonic Stage
E9.5
E10.5
Right
Left

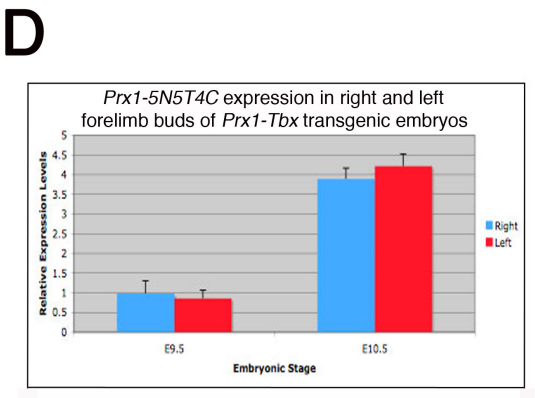
D
Prx1-5N5T4C expression in right and left
forelimb buds of Prx1-Tbx transgenic embryos
Relative Expression Levels
Embryonic Stage
E9.5
E10.5
Right
Left

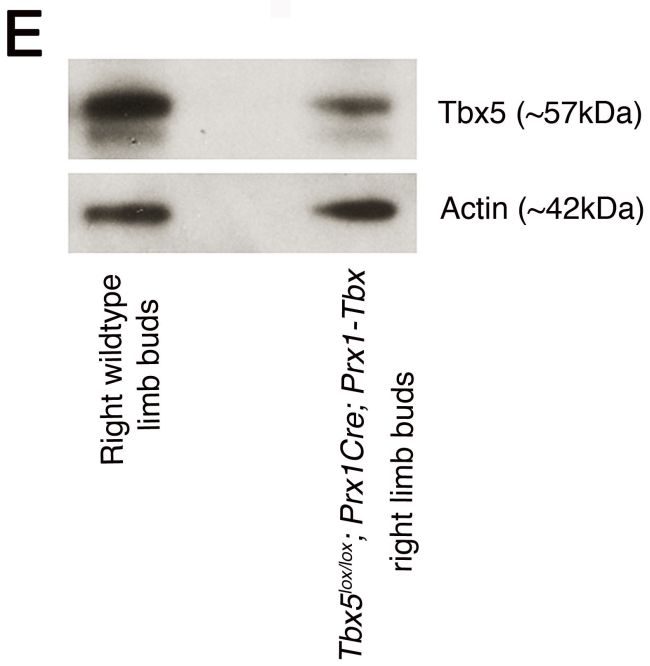
E
Tbx5 (~57kDa)
Actin (~42kDa)
Right wildtype
limb buds
Tbx5lox/lox; Prx1Cre; Prx1-Tbx
right limb buds

Figure 3.5 *Cre recombinase* and *Prx1-5N5T4C* transgene expression is bilaterally symmetric between the left and right forelimb buds of *Tbx5$^{lox/lox}$; Prx1Cre; Prx1-Tbx* mutant embryos.

A Schematic showing the gene deletion/gene replacement approach in which the conditional *Tbx5* allele is deleted and *Prx1-5N5T4C* is simultaneously expressed. **B** Lateral view of the right side of an E17.5 *Tbx5$^{lox/lox}$; Prx1Cre; Prx1-M4C* mutant embryo. The adjacent skeletal preparation is of the right forelimb of the same mutant embryo. The diagram shows the schematic of the *Prx1-5N5T4C* construct. (figures adapted from Minguillon et al., 2009). **C** Graph showing relative transcription levels of *cre recombinase* in the left and right forelimb buds of E9.5 and E10.5 transgenic *Prx1Cre* embryos. The expression levels in the left E9.5 forelimb bud, as well as the right and left E10.5 forelimb buds, are relative to the expression level of cre recombinase in the right E9.5 forelimb bud. ('y' axis – cre recombinase expression levels, 'x' – embryonic stage). **D** Graph showing relative levels of *Prx1-5N5T4C* transcript in the forelimb buds of E9.5 and E10.5 *Prx1-Tbx* transgenic embryos. The expression levels in the left E9.5 forelimb bud, as well as the right and left E10.5 forelimb buds, are relative to the expression level of *Prx1-5N5T4C* in the right E9.5 forelimb bud ('y' axis – Prx1-5N5T4C expression levels, 'x' – embryonic stage). **E** Western blot showing that compared to endogenous Tbx5 protein levels, Prx1-5N5T4C protein levels are reduced.

Tbx5$^{lox/lox}$; Prx1Cre; Prx1-Tbx mutant embryos present with forelimb defects that are more severe in the left forelimb than the right.

I have so far demonstrated that the conditional deletion of *Tbx5* from the left and right forelimb-forming regions, and then the subsequent hypomorphic expression of the *Prx1-5N5T4C* transgene in the forelimb-forming region results in the presentation of severe forelimb defects in *Tbx5$^{lox/lox}$; Prx1Cre; Prx1-Tbx* mutant embryos. Significantly, these forelimb defects are more severe in the left forelimb than the right. In an example of an individual mutant, the right forelimb has achieved relatively normal outgrowth but has only four digits. In contrast, the left forelimb is severely truncated and presents with a single digit (black arrow, Fig 3.6B). To identify whether the asymmetric presentation of the forelimb defects are consistent in every mutant, I analyzed the right and left forelimbs of

Tbx5$^{lox/lox}$*; Prx1Cre; Prx1-Tbx* mutant embryos. I have chosen to present skeletal preparations, using alcian blue to stain the cartilage and alizarin red to stain the bone, of 5 representative pairs of mutant forelimbs to demonstrate the varying extent and severity of forelimb defects. A total of 20 mutants were analysed.

In the first example of the most severely affected pair of forelimbs, the left forelimb is reduced to a rudimentary scapula whereas the right forelimb is severely truncated and mispatterned (red arrow, Fig 3.6 C1). In the second example, the right forelimb has achieved outgrowth however there are only three digits remaining from the autopod. Additionally this forelimb presents with a hypoplastic radius and malformed scapula. In contrast, the left forelimb is reduced to little more than a rudimentary scapula (Fig 3.6 C2). In the third example, the right forelimb presents with the radius and ulna, however the humerus is absent. Additionally, a digit is absent from the autopod. The left forelimb presents as a single digit attached to the scapula. The intermediate elements, the radius, ulna and humerus, are all absent (Fig 3.6 C3). The fourth and fifth examples demonstrate defects that are less severe than those previously described, however in both examples the left limb displays more defects than the right. In the fourth example the right forelimb has achieved relatively normal outgrowth, however the humerus and a digit from the autopod are absent from the left forelimb (Fig 3.6 C4). In the final example, the left forelimb has achieved outgrowth, although it is mispatterned due to the loss of the humerus and digit 1 in the autopod. The right forelimb presents with relatively normal limb elements, although the presence of a hole in the scapula indicates the presence of forelimb defects (red arrows, Fig 3.6 C5).

My analysis of the forelimb defects in E17.5 *Tbx5*$^{lox/lox}$*; Prx1Cre; Prx1-Tbx* mutant embryos clearly demonstrates a wide scale in the extent and severity of the

forelimb defects presented in mutant forelimbs. However, it is clear that despite the phenotypic variation, the left forelimb remains consistently more affected than the right forelimb.

Figure 3.6

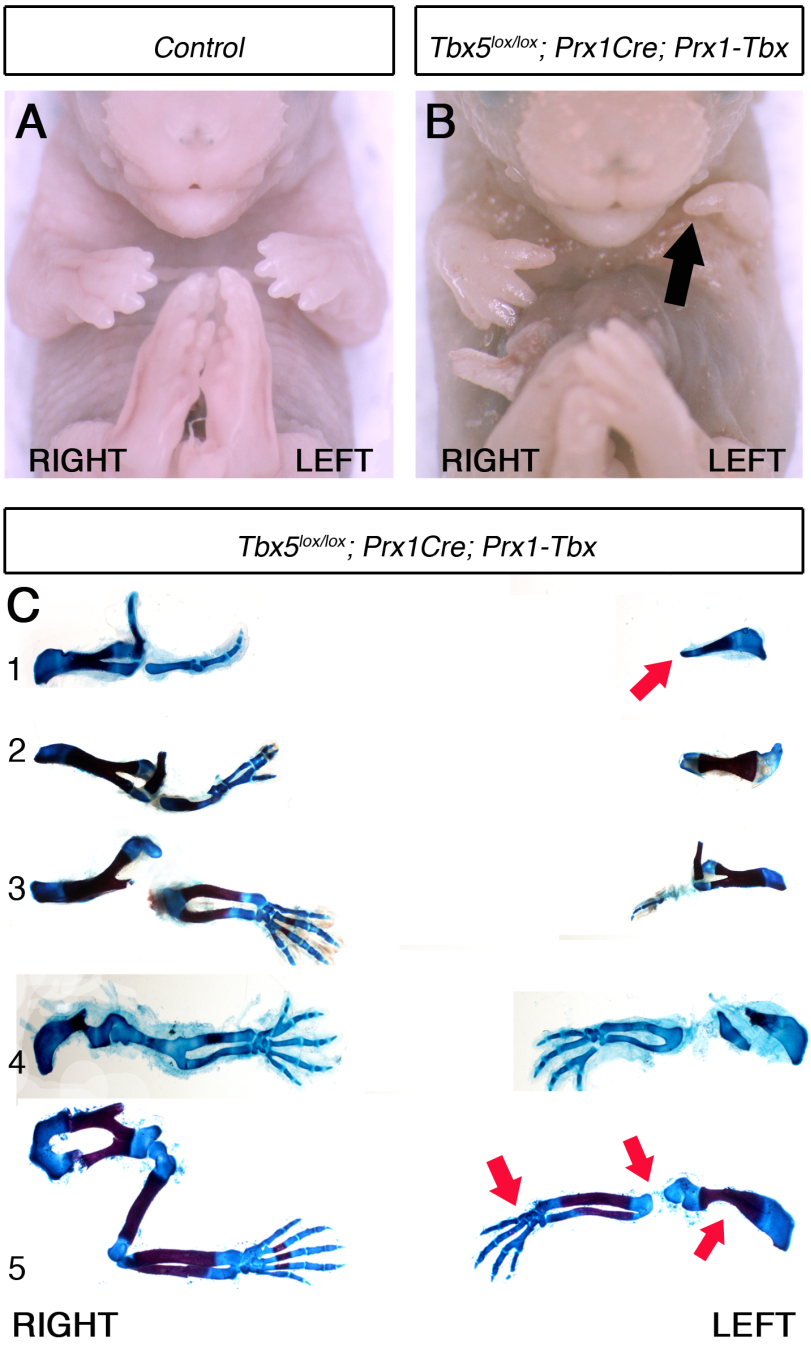

Figure 3.6 Hypomorphic expression levels of *Prx1-5N5T4C* lead to left-biased asymmetrical forelimb defects.

Panels **A-B** show ventral views of mutant embryos. Panel **C** shows dorsal views of 5 pairs of mutant forelimbs. The left and right forelimbs are labelled in all panels (**A-C**). **A** E17.5 control embryo. **B** E17.5 *Tbx5$^{lox/lox}$; Prx1Cre; Prx1-Tbx* mutant embryo. The left forelimb is severely truncated compared to the right forelimb (black arrow). **C** Series of skeletal preparations of 5 pairs of mutant forelimbs from 5 E17.5 mutant embryos. C1 – The left forelimb is reduced to a rudimentary scapula whereas the right forelimb is severely truncated (red arrow). C5 – The left forelimb presents with a malformed scapula and has lost the humerus and digit one (red arrows).

Left-biased asymmetrical forelimb defects are visible in E17.5 *Tbx5$^{lox/lox}$; Prx1Cre; Prx1-Tbx* mutant embryos. The gene deletion-gene replacement event used to generate these mutants takes place in the forelimb-forming region of the LPM prior to forelimb bud initiation. This raises the strong possibility that the left-biased asymmetrical forelimb differences are detectable from an early stage of forelimb formation. I have analyzed the right and left forelimb buds of E10.5 *Tbx5$^{lox/lox}$; Prx1Cre; Prx1-Tbx* mutant embryos using WMISH and probes for the genes *Fgf10*, *Fgf8* and *Sall4* as molecular markers. A minimum of 4 mutants for each phenotype were analysed with each probe (N=24)

At E10.5 the mutant embryos present with two clearly visible sets of phenotypes. In the first set, there is no obvious left limb bud and a small right limb bud (black arrowheads, Fig 3.7 B, E, H). In the second set there is a small left limb bud and a relatively larger right limb bud (black arrowheads, Fig 3.7 C, F, I). This is consistent with the variation in forelimb defects observed in E17.5 *Tbx5$^{lox/lox}$; Prx1Cre; Prx1-Tbx* mutants. An examination of *Fgf10* expression in the left and right limb buds of control embryos does not reveal any discernable difference in expression between the left and right forelimb bud (Fig 3.7 A). In mutant embryos from the first phenotypic set, *Fgf10* cannot be detected in the LPM but is present in the right forelimb bud (Fig 3.7 B) In mutant embryos from the second phenotypic set,

Fgf10 expression is detectable in both forelimb buds, although it appears to be downregulated in the left limb bud compared to the right (Fig 3.7 C). Similarly, *Fgf8* expression is apparently bilaterally symmetric in the ectoderm of right and left control forelimb buds (Fig 3.7 D). *Fgf8* expression is detectable in the ectoderm of the right forelimb bud of mutant embryos from the first phenotypic set, but cannot be detected in the left LPM (Fig 3.7 E). In mutant embryos from the second phenotypic set, *Fgf8* expression is disrupted in the ectoderm of the left forelimb bud and is detectable in the right (Fig 3.7 F). *Sall4* expression is bilaterally symmetric in the mesenchyme of the left and right forelimb buds of control embryos (Fig 3.7 G). Consistent with the previous WMISH data, *Sall4* expression is detectable in the right forelimb bud of mutants from the first phenotypic set (Fig 3.7 H). In mutant embryos from the second phenotypic set, *Sall4* expression is detectable in both the left and right forelimb buds with no discernable difference in expression (Fig 3.7 I).

My analysis of gene expression in the second phenotypic set of mutants indicates that *Fgf8* expression is disrupted in the AER of the left forelimb bud, suggesting a partial breakdown in signal transduction between the mesoderm and ectoderm. However, in all the mutant embryos analyzed the left forelimb bud is more affected than the right. This is consistent with the data generated using the *Tbx5$^{lox/lox}$; Prx1Cre(98)* mutant (see section 3.1). As I mentioned earlier, it is unclear from this WMISH analysis whether the difference in gene expression between the left and right limb bud is related to the smaller size of the left limb bud or is in fact the cause of the of smaller size.

Figure 3.7

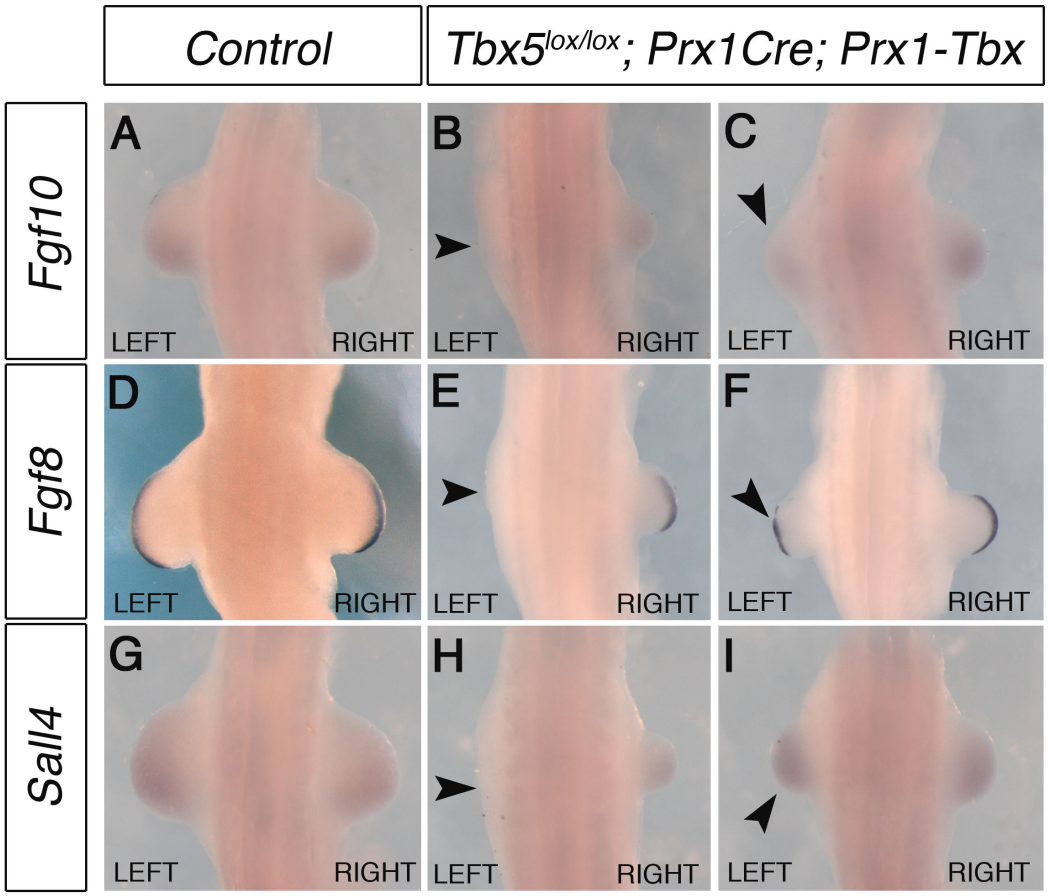

Figure 3.7 There is a discernable difference in limb bud size between the left and right forelimb buds of E10.5 *Tbx5$^{lox/lox}$; Prx1Cre; Prx1-Tbx* mutant embryos.

All panels **(A-I)** show dorsal views of E10.5 embryos that have been processed using whole mount in situ hybridisation. The left and right forelimb buds are labelled in each panel. **A** *Fgf10* expression in a control embryo. **B** *Fgf10* expression in a mutant embryo. The left forelimb bud has not formed (black arrowhead). **C** *Fgf10* expression in a mutant embryo, in which the left forelimb bud is reduced in size compared to the right (black arrowhead). **D** *Fgf8* expression in a control embryo. **E** *Fgf8* expression in a mutant embryo in which the left forelimb bud has not formed (black arrowhead). **F** *Fgf8* expression in a mutant embryo. *Fgf8* in the left forelimb ectoderm is disrupted compared to the right (black arrowhead). **G** *Sall4* expression in a control embryo. **H** *Sall4* expression in the right forelimb of a mutant embryo in which the left forelimb bud has not formed (black arrowhead). **I** *Sall4* expression in the forelimbs of a mutant embryo in which the left forelimb bud is reduced in size compared to the right (black arrowhead).

In this chapter I have shown, through the use of two separate genetic strategies, that the bilaterally symmetric disruption of Tbx5 activity in the left and right forelimb-forming regions of the LPM leads to the presentation of forelimb defects that are more severe in the left than the right. Both mouse models effectively recapitulate the upper limb phenotypes observed in HOS patients, and as I show in the next chapter, can be used to further elucidate the events leading to left-biased asymmetrical forelimb defects.

CHAPTER FOUR:

MECHANISTIC INSIGHT INTO THE GENETIC EVENTS LEADING TO THE FORMATION OF LEFT-BIASED ASYMMETRICAL FORELIMB DEFECTS

Introduction

In the previous chapter I have shown, using two separate approaches, that the bilaterally symmetric disruption of *Tbx5* in the left and right forelimb-forming regions of the LPM leads to the presentation of forelimb defects that occur with greater severity in the left forelimb than the right. In this chapter, I describe how I have used various mutant mouse strains to establish the events that lead to the formation of left-biased asymmetrical forelimb defects. Due to the consistent left-biased asymmetrical forelimb defects that are detectable in individual mutant embryos, I have chosen to use the *Tbx5$^{lox/lox}$; Prx1Cre; Prx1-Tbx* mouse mutant. I show that the left-biased asymmetrical forelimb defects that present in *Tbx5$^{lox/lox}$; Prx1Cre; Prx1-Tbx* mutants can be reversed to right-biased asymmetrical defects in *Tbx5$^{lox/lox}$; Prx1Cre; Prx1-Tbx; INV/INV* mutant embryos. I also show that expression of transgenic *Fgf10* is able to partially rescue the forelimb defects but does not affect the left-sided bias of their presentation.

4.1 *Tbx5$^{lox/lox}$; Prx1Cre; Prx1-Tbx; INV/INV* MUTANT EMBRYOS WITH SITUS INVERSUS PRESENT WITH FORELIMB DEFECTS THAT ARE MORE SEVERE IN THE RIGHT FORELIMB THAN THE LEFT.

A key feature of the mammalian body plan is the bilateral symmetry of exterior organs such as the eyes, face, and limbs. Interior organs, however, such as the heart, stomach, spleen, and liver are patterned in an asymmetric manner. The heart and stomach are situated in the left side of the body, whereas the liver is in the right. This is referred to as ‘situs solitus’. The asymmetric positioning of the visceral organs is stereotypic, and manifests due to the actions of the left-right pathway. The left-right pathway is established during early embryogenesis, when events at the node lead to the asymmetric expression of specific genes. Genes such as *Nodal*, *Lefty*, and *Pitx2* are expressed solely on the left side of the LPM. Apart from *Pitx2*,

the expression of these genes is transient and does not persist in the LPM of embryos older than E8.5. The disruption of left-right axis formation leads to the right-sided expression of *Nodal*, *Lefty*, and *Pitx2*. This can manifest as 'situs inversus' where the positioning of the inner organs is now reversed. In situs inversus organs that were formerly situated in the left side of the body, such as the heart and stomach, are now in the right side and organs that were in the right side, such as the liver, are now in the left side.

A study by Brown and Wolpert showed that administration of acetazolamide to dams causes right-sided asymmetrical forelimb defects in embryos with situs solitus and left-sided asymmetrical forelimb defects in embryos with situs inversus (Brown et al., 1989). Subsequent studies using genetic mouse models support this observation that asymmetric unilateral limb defects are subject to mirror reversal upon occurrence of situs inversus (Kocher-Becket et al., 1991; Schreiner et al., 1993). I was therefore interested in determining whether, in the event of the disruption of the left-right pathway, *Tbx5$^{lox/lox}$; Prx1Cre; Prx1-Tbx* mutant embryos would present with forelimb defects that are more severe in the right forelimb rather than the left.

Previous studies have involved the use of the *iv* mutant mouse strain, in which 50% of homozygous mutant embryos present with situs inversus and 50% present with situs solitus. The *INV* mouse mutant strain was generated due to the disruption of *inv* gene expression, due to the insertion of a tyrosine receptor transgene. *Inv* expression in the node is believed to be required during the establishment of the left-right pathway, the disruption of which leads to situs inversus. Homozygous *INV* mutant embryos are reported to present with situs

inversus, which is purported to be a fully penetrant phenotype (Yokoyama et al., 1993). Due to the complex breeding regimes involved in generating *Tbx5$^{lox/lox}$; Prx1Cre; Prx1-Tbx* mutant embryos, I chose to use the *INV* mutant mouse strain rather than the *iv* mutant mouse strain to disrupt the establishment of the left-right pathway during early embryogenesis.

Situs inversus is reported as the mirror reversal of the interior visceral organs. Therefore, in situs solitus the heart is positioned in the left side, whereas in embryos presenting with situs inversus the heart is positioned in the right side. Using this criteria to determine organ situs, I have identified *Tbx5$^{lox/lox}$; Prx1Cre; Prx1-Tbx; INV/INV* mutant embryos that display situs inversus. Situs solitus in E14.5 *Tbx5$^{lox/lox}$; Prx1Cre; Prx1-Tbx* mutants is shown by the left-sided laterality of the heart apex (black asterisk, Fig 4.3 A). In this example, the left forelimb is more severely affected as the right forelimb has 4 digits and the left has 3 digits (red arrow, Fig 4.1 B). In contrast, *Tbx5$^{lox/lox}$; Prx1Cre; Prx1-Tbx; INV/INV* mutants with situs inversus, indicated by right-sided heart laterality (black asterisk, Fig 4.1 C), have forelimb defects that are more severe in the right forelimb. Analysis of the skeleton using bone and cartilage stains show that the left forelimb has 4 digits, whereas the right forelimb has 3 digits (red arrow, Fig 4.1 D). These results show that upon reversal of the left-right axis, the asymmetrical forelimb defects undergo mirror reversal.

Figure 4.1

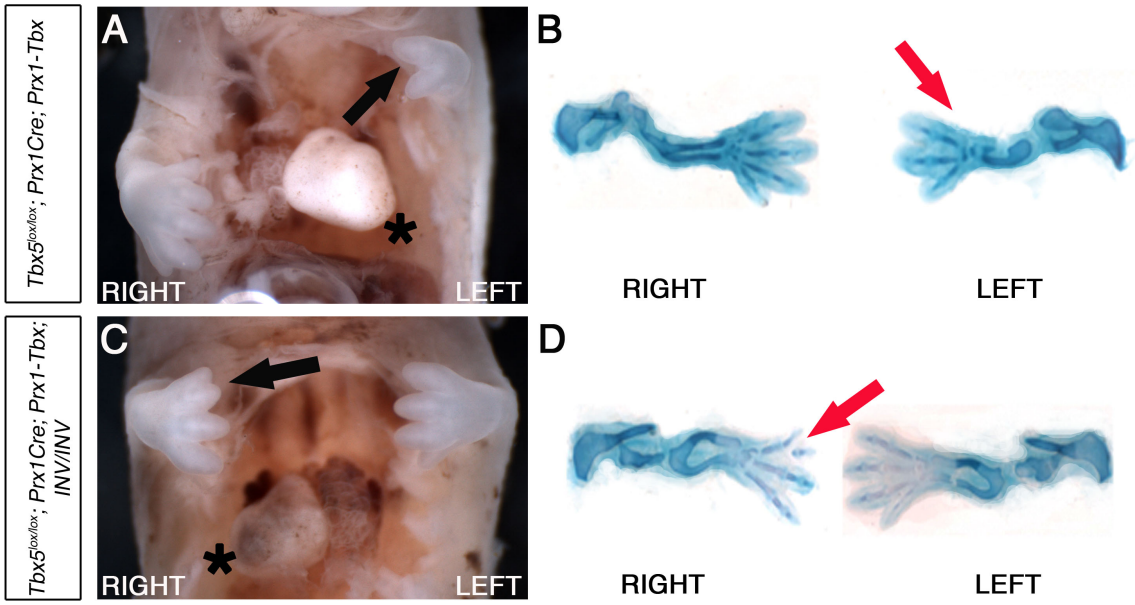

Figure 4.1 *Tbx5$^{lox/lox}$; Prx1Cre; Prx1-Tbx; INV/INV* mutants with situs inversus have right biased asymmetrical forelimb defects.

Panels **A**, **C** are ventral views of E14.5 embryos. Panels **B**, **D** are dorsal views of the forelimbs of E14.5 embryos. The right and left sides are labelled in all panels. **A** A *Tbx5$^{lox/lox}$; Prx1Cre; Prx1-Tbx* mutant embryo. The heart apex points to the left (black asterisk). The left forelimb is more severely affected than the right as it presents with 2 digits (black arrow). **B** Skeletal preparation of a *Tbx5$^{lox/lox}$; Prx1Cre; Prx1-Tbx* right forelimb with 4 digits and a left forelimb with 3 digits (red arrow). **C** A *Tbx5$^{lox/lox}$; Prx1Cre; Prx1-Tbx; INV/INV* mutant embryo. The heart apex points to the right (black asterisk). The right forelimb is more severely affected than the left as it presents with 3 digits, one of which is bifurcated (black arrow). **D** Skeletal preparation of the forelimbs of a *Tbx5$^{lox/lox}$; Prx1Cre; Prx1-Tbx; INV/INV* mutant embryo in which the right forelimb has 3 digits and the left forelimb has 4 digits (red arrow).

It was originally reported that homozygous *INV/INV* mutant embryos present with full penetration of the situs inversus phenotype (Yokoyama et al., 1993). I have found that during the course of my experiments only 30% of *INV/INV* mutants display situs inversus, which I have identified by the right-sided laterality of the heart. Due to these circumstances, I have only been able to identify a total of 2 *Tbx5$^{lox/lox}$; Prx1Cre; Prx1-Tbx; INV/INV* mutants from a total of 150 embryos.

My analysis has shown that in *Tbx5$^{lox/lox}$; Prx1Cre; Prx1-Tbx; INV/INV* mutants with situs inversus, the right forelimb displays more defects than the left. This result is consistent with previously reported studies that showed that the asymmetric bias of the limb defects is reversed following disruption of the left-right pathway during embryogenesis.

4.2 THE INCREASE OF *Fgf10* EXPRESSION IN THE LEFT AND RIGHT FORELIMB-FORMING REGIONS OF *Tbx5$^{lox/lox}$; Prx1Cre; Prx1-Tbx* MUTANT EMBRYOS DOES NOT LEAD TO SYMMETRICAL FORELIMB FORMATION.

During initiation of forelimb bud formation from the LPM, *Tbx5* acts to directly regulate *Fgf10* expression in the nascent forelimb bud mesenchyme. The Fgf10 ligand signals via Fgf receptors in the ectoderm to initiate the transcription of *Fgf8* in a strip of ectodermal cells that ultimately form the AER. In turn, *Fgf8* then signals via mesenchymal Fgf receptors to positively regulate the expression of *Fgf10* in the underlying mesenchyme. The establishment of this positive feedback loop drives nascent forelimb bud outgrowth.

Deletion of the conditional *Tbx5* allele from the forelimb-forming regions leads to the absence of *Fgf10* expression, the result of which is a complete failure of forelimb bud initiation and subsequent formation (Rallis et al., 2003). *Fgf10$^{-/-}$* null mutant embryos display a rudimentary scapula and pelvic girdle, demonstrating that the limbs have failed to form (Sekine et al., 1999). *Tbx5* is believed to positively regulate *Fgf10* transcription during forelimb bud initiation (Sekine et al., 1999; Agarwal et al., 2003; Rallis et al., 2003). Hypomorphic levels of *Tbx5*, or *Prx1-Tbx*, could be predicted to lead to hypomorphic levels of *Fgf10* in the *Tbx5$^{lox/lox}$; Prx1Cre; Prx1-Tbx* mutant. It is therefore possible that the forelimb defects observed in

Tbx5$^{lox/lox}$*; Prx1Cre; Prx1-Tbx* mutant embryos are due to hypomorphic *Fgf10* levels in the left and right forelimb buds during limb bud initiation.

If hypomorphic levels of *Fgf10* expression in the forelimb-forming regions of *Tbx5*$^{lox/lox}$*; Prx1Cre; Prx1-Tbx* mutant embryos lead to left-biased asymmetrical forelimb defects, then it would be predicted that restoring optimal *Fgf10* expression levels in this same mutant background would be sufficient to rescue the bilaterally symmetric formation of the left and right forelimbs. If this proves to be the case, then this would support a model in which optimal expression of *Tbx5* regulates symmetrical forelimb formation through its direct impact on *Fgf10* transcription. To test this hypothesis, I have used an *Fgf10*-expression inducible transgenic line in combination with the *Prx1-Tbx* hypomorphic mutant.

The *Z/EGFgf10* transgene enables Cre-inducible activation of *Fgf10* expression.

To increase *Fgf10* transcript levels in *Tbx5*$^{lox/lox}$*; Prx1Cre; Prx1-Tbx* mutants, I have used the *Z/EGFgf10* transgenic mouse line previously generated in the lab (Logan MPO, unpublished). The *Z/EGFgf10* transgenic mouse line was produced as a means of manipulating the exogenous delivery of transgenic *Fgf10* transcript in the developing mouse embryo. The *Z/EGFgf10* construct is derived from the *Z/EG* transgenic backbone originally produced by Novak et al in 2000 (Novak et al., 2000). The *Z/EGFgf10* construct contains a β-Geo cassette, flanked by two *LoxP* sites (Fig 4.2). This cassette is placed downstream of the chick β-actin promoter and the CMV enhancer, which acts to direct widespread expression of the construct. The β-Geo cassette contains *LacZ* and a neomycin resistance site, as well as a 3x polyadenalation site that serves as a transcriptional stop signal. Located 3' to the β-Geo cassette is another cassette containing the cDNA for *Fgf10* and the sequence

for an internal ribosome entry site (*IRES)* and *eGFP* followed by a β-globin polyadenalation site.

In the absence of cre recombinase the β-actin promoter and CMV elements, commonly referred to as CAGGS, drives β-galactosidase transcription in the β-Geo cassette. This is detectable through the identification of LacZ-positive cells and can act as a reporter of the transgenic construct in the absence of cre activity (Fig 4.2). In the presence of cre recombinase, the β-Geo cassette is recombined out of the construct and the *Fgf10*/*IRES*/*eGFP* cassette comes under the control of the CMV/β-actin promoter (Fig 4.2). This enables the transcription of *Fgf10*, and *eGFP* as a histological tag, in regions of the embryo where cre recombinase is active.

Figure 4.2

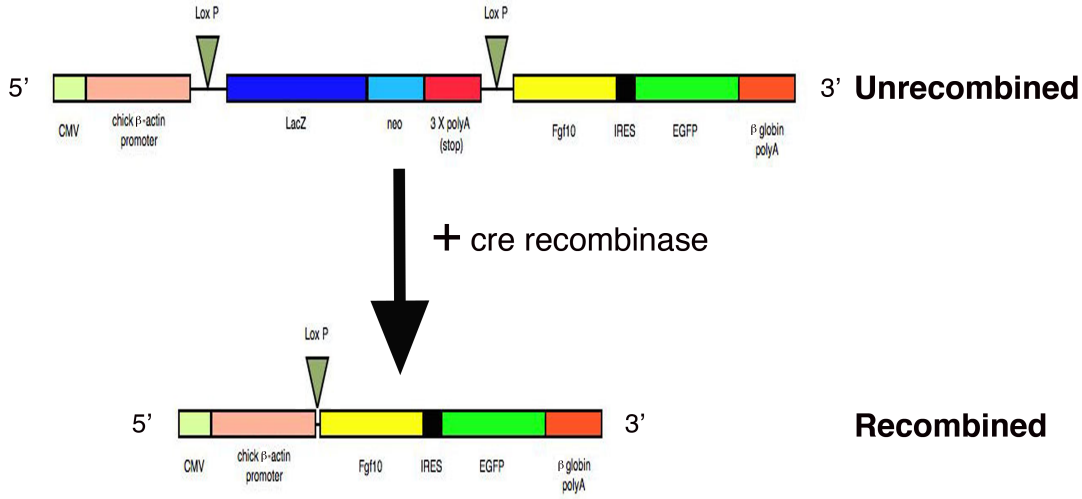

Figure 4.2 Cre recombinase recombines the *LoxP* flanked cassette to enable transgenic *Fgf10* transcription in the *Z/EGFgf10* construct.

My analysis of cre recombinase activity in the *Prx1Cre* line (see Chapter Three) shows that cre recombinase is expressed symmetrically in the left and right forelimb-forming regions of the LPM. I have therefore chosen to use the *Prx1Cre* transgenic line in combination with *Z/EGFgf10* transgenic line.

Expression of transgenic *Fgf10* in the *Fgf10$^{-/-}$; Prx1Cre; Z/EGFgf10* mutant rescues symmetrical forelimb outgrowth.

The loss of *Fgf10* expression in the *Fgf10$^{-/-}$* null mutant embryo leads to the reduction of the forelimb and hindlimb to a rudimentary scapula and pelvis, respectively. To test the efficiency of the *Z/EGFgf10* transgenic line, I used it in combination with the *Prx1Cre* to attempt to rescue limb outgrowth in the *Fgf10$^{-/-}$* null mutant. In E17.5 control embryos, the forelimb has formed (Fig 4.3 A, B) and the skeletons of the right and left limbs are bilaterally symmetric (Fig 4.3 C). At the same stage in *Fgf10$^{-/-}$* mutants, there is an absence of forelimb and hindlimb outgrowth (black arrow Fig 4.3 D, E). The right and left scapula rudiments are equally affected (Fig 4.3 F). In contrast, the stylopod, zeugopod and autopod elements are present in *Fgf10$^{-/-}$; Prx1Cre; Z/EGFgf10* forelimbs demonstrating that forelimb outgrowth has been rescued (black arrow, Fig 4.3 G, H). There is no detectable difference between the right and left rescued forelimbs of *Fgf10$^{-/-}$; Prx1Cre; Z/EGFgf10* mutants (Fig 4.3 I).

My results show that transgenic *Fgf10 (tgFgf10)*, as delivered by the *Z/EGFgf10* line, is capable of rescuing symmetrical forelimb outgrowth in the *Fgf10$^{-/-}$* null mutant. This shows that the levels of *tgFgf10* delivered by the *Z/EGFgf10* transgene are similar to those of endogenous *Fgf10*. Importantly *tgFgf10* is apparently delivered symmetrically between the left and right forelimb-forming regions.

Figure 4.3

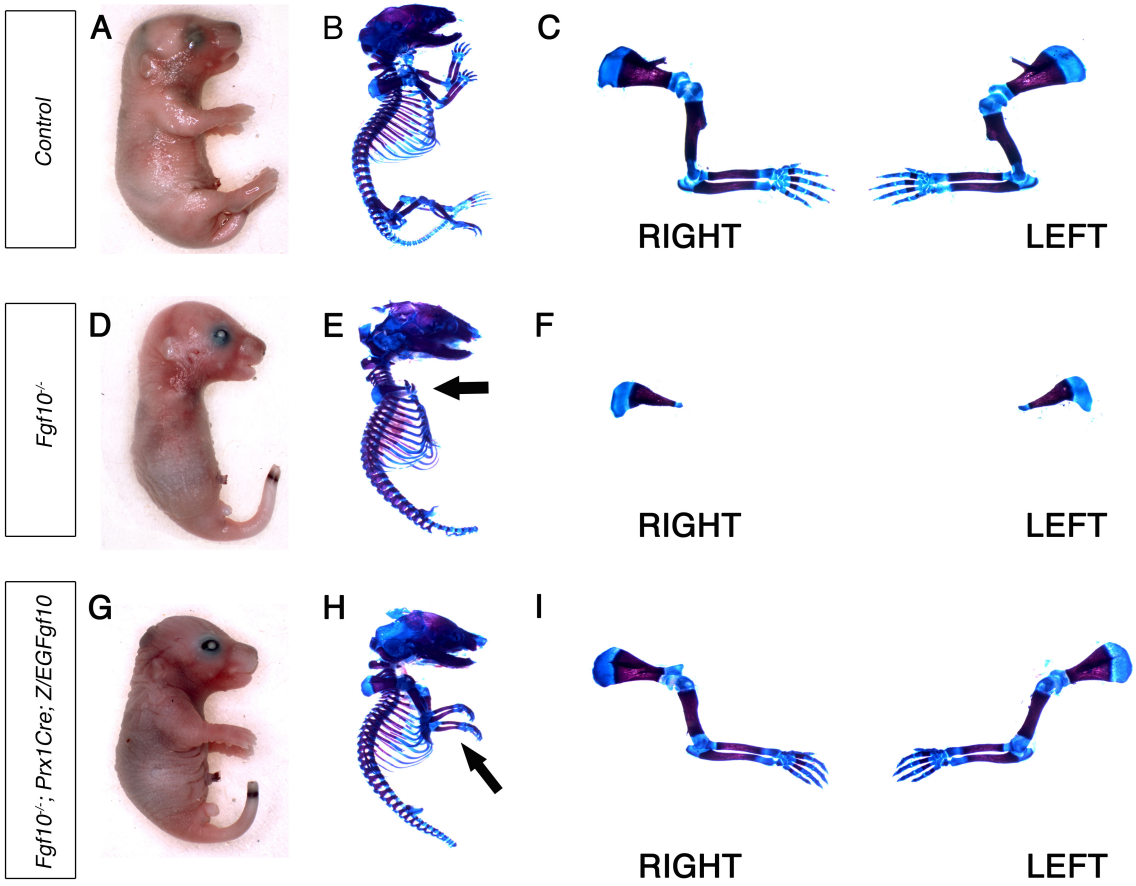

Figure 4.3 Exogenous delivery of transgenic *Fgf10* expression in the forelimb area is sufficient to rescue forelimb outgrowth in *Fgf10* null mutant embryos.

Panels **A**, **B**, **D, E**, **G, H** show right-side lateral views of E17.5 embryos. Panels **C**, **F**, **I** show dorsal views of skeletal preparations of forelimbs from E17.5 embryos. The right and left forelimbs are labelled in panels **C**, **F**, and **I**. **A** Control embryo. **B** A skeletal preparation of the control embryo. **C** A skeletal preparation of the right and left forelimbs of the control embryo. **D** An *Fgf10*$^{-/-}$ null mutant embryo. **E** A skeletal preparation of the *Fgf10*$^{-/-}$ mutant embryo. The elements of the forelimb have not formed (black arrow). **F** Skeletal preparation of the right and left rudimentary scapula elements of an *Fgf10*$^{-/-}$ mutant embryo. **G** An *Fgf10*$^{-/-}$*; Prx1Cre; Z/EGFgf10* mutant embryo. **H** A skeletal preparation of the *Fgf10*$^{-/-}$*; Prx1Cre; Z/EGFgf10* mutant embryo, in which the forelimbs have formed (black arrow). **I** A skeletal preparation of the left and right forelimbs of an *Fgf10*$^{-/-}$*; Prx1Cre; Z/EGFgf10* mutant embryo.

By E17.5, the formation of the pelvis is largely complete in the control embryo. In the *Fgf10*$^{-/-}$ mutant embryo the pelvic rudiment is greatly reduced and

hindlimb elements have not formed. There is no obvious difference in the morphology of the pelvic rudiment between the *Fgf10*$^{-/-}$ mutant and the *Fgf10*$^{-/-}$*; Prx1Cre; Z/EGFgf10* mutant embryo (black arrows Fig 4.4 B, C). In the *Prx1Cre* transgenic line the onset of cre activity in the hindlimb bud is delayed compared to that in the forelimb, taking place after hindlimb bud initiation has taken place (Logan et al., 2002). The relative delay in onset of transgene *Fgf10* expression in the hindlimb buds of *Fgf10*$^{-/-}$*; Prx1Cre; Z/EGFgf10* mutants likely accounts for the failure to rescue hindlimb outgrowth.

Figure 4.4

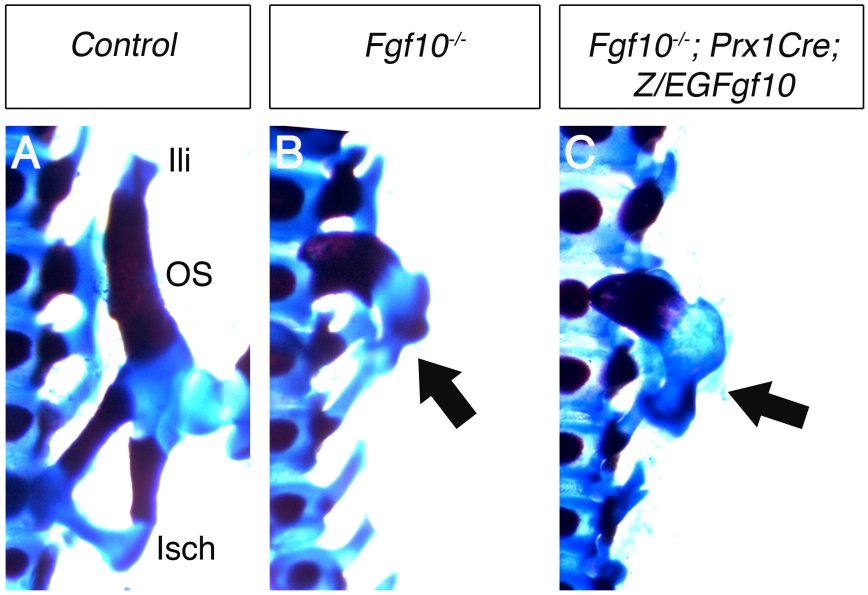

Figure 4.4 Expression of transgenic *Fgf10* under actions of the transgenic activator line, *Prx1Cre*, does not rescue hindlimb outgrowth in *Fgf10*$^{-/-}$ mutants.

All panels show the ventral left-sided view of the pelvic regions of E17.5 embryos

A Control embryo, in which the elements of the pelvis are labelled. **B** An *Fgf10*$^{-/-}$ mutant embryo in which the pelvis is reduced to a single rudimentary element (black arrow). **C** An *Fgf10*$^{-/-}$*; Prx1Cre; Z/EGFgf10* embryo in which the pelvis is a single rudimentary element (black arrow). Ili – ilium, OS – ossa coxae, Isch – ischium

Ectopic expression of *Fgf10* in the *Tbx5$^{lox/lox}$; Prx1Cre; Prx1-Tbx* mutant does not rescue the left-biased asymmetrical presentation of the forelimb defects.

When crossed into the *Tbx5$^{lox/lox}$; Prx1Cre; Prx1-Tbx* background, the *Z/EGFgf10* transgenic line delivers transgenic *Fgf10* mRNA at equal levels in the right and left forelimb areas, therefore raising *Fgf10* transcript levels. I used the *Z/EGFgf10* line in combination with the *Tbx5$^{lox/lox}$; Prx1Cre; Prx1-Tbx* mutant to determine whether increased *Fgf10* expression will rescue symmetrical forelimb formation.

Tbx5$^{lox/lox}$; Prx1Cre; Prx1-Tbx mutants have extensive forelimb defects, which are more severe in the left forelimb than the right. In an example, the left forelimb is truncated with a solitary digit and the right forelimb has four digits instead of five (black arrow, Fig 4.5 A). *Tbx5$^{lox/lox}$; Prx1Cre; Prx1-Tbx; Z/EGFgf10* mutants have increased right and left forelimb outgrowth, however the presence of a rudimentary digit 1 on the left forelimb indicates left-biased asymmetrical forelimb defects (black arrow, Fig 4.5 B). Skeletal staining of the left and right forelimbs of four mutant embryos reveals that the prevalence of forelimb defects is reduced. However, the left forelimb in each individual mutant embryo presents with significantly more severe defects than the right. In example one, the left forelimb presents with the loss of digit one, aplasia of the humerus, and a partially formed scapula (red arrows, Fig 4.5 C1), whereas the right forelimb displays a hole in the scapula. In example two, the left forelimb presents with a malformed scapula and a humerus that is reduced in length compared to the right, while the right forelimb displays a hole in the scapula (Fig 4.5 C2). Example three is of a pair of forelimbs in which both forelimbs display the same defects apart from the more severely scapula of the left forelimb (Fig 4.5 C3). Similarly, in example four the only difference in the defects observed in the left and right forelimbs is the presence of a bifurcated digit in

the left forelimb (Fig 4.5 C4). A total of four mutants were analysed and are presented here. While this is a relatively small sample size, the left forelimb in all four examples consistently presents with more severe forelimb defects than the right. An increase in the sample size may serve to further illustrate this difference, however that has yet to be determined.

My analysis shows that the left forelimb consistently presents with more severe forelimb defects than the right in the *Tbx5*$^{lox/lox}$*; Prx1Cre; Prx1-Tbx; Z/EGFgf10* mutant embryo. This demonstrates that optimal levels of *Fgf10* are unable to rescue symmetrical forelimb formation. This suggests that in the presence of hypomorphic levels of Prx1-Tbx (or Tbx5) activity, the left left forelimb-forming region is less responsive to Fgf10 ligand activity than the right.

Figure 4.5

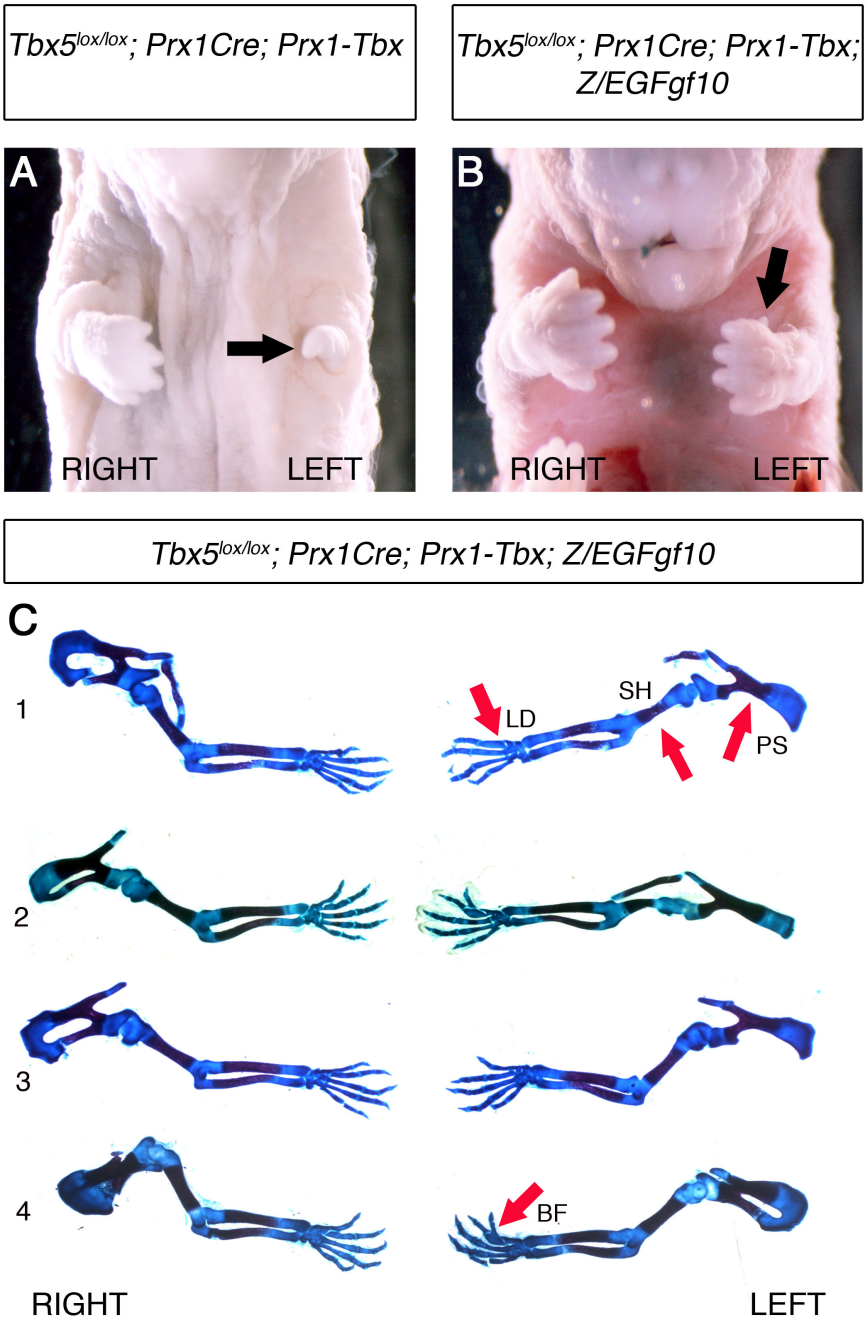

Figure 4.5 Exogenous delivery of transgenic *Fgf10* expression in the left and right forelimb areas of *Tbx5$^{lox/lox}$; Prx1Cre; Prx1-Tbx* mutants does not result in symmetric forelimb formation. Panels **A**-**B** are ventral views of E17.5 mutant embryos. Panel **C** presents a dorsal view of 4 pairs of forelimbs from E17.5 mutant embryos. The left and right sides are labelled in all panels. **A** A *Tbx5$^{lox/lox}$; Prx1Cre; Prx1-Tbx* mutant embryo. The left forelimb is severely truncated compared to the right (black arrow). **B** A *Tbx5$^{lox/lox}$; Prx1Cre; Prx1-Tbx; Z/EGFgf10* mutant embryo. The left forelimb has loss digit one (black arrow). **C** Series of skeletal preparations of the right and left forelimbs of 4 *Tbx5$^{lox/lox}$;*

Prx1Cre; Prx1-Tbx; Z/EGFgf10 mutant embryos. C1 – The left forelimb presents with a partial scapula (PS), shortened humerus (SH) and the loss of digit one (LD) (red arrows). C4 – The left forelimb presents with a bifurcated digit (BF) (red arrow).

PS- partial scapula, SH – shortened humerus, LD- loss of digit one, BF – bifurcated digit

In this chapter, I have demonstrated that the left-biased asymmetric forelimb defects observed in *Tbx5*$^{lox/lox}$*; Prx1Cre; Prx1-Tbx* mutants are linked to the formation of the left-right axis as the disruption of the latter leads to the mirror reversal of the former. I have also demonstrated that hypomorphic levels of *Tbx5* in the left and right forelimb-forming regions of the LPM result in the formation of left-biased asymmetrical forelimb defects in a mechanism that is independent of the direct role of *Tbx5* in *Fgf10* transcription during forelimb bud initiation from the LPM.

CHAPTER FIVE:

THE ROLE OF *Tbx4* DURING HINDLIMB BUD INITIATION

In chapters 3 and 4, I have demonstrated that the bilaterally symmetric disruption of *Tbx5* expression during left and right forelimb bud initiation results in forelimb defects that are consistently more severe in the left forelimb than the right. *Tbx4* is the paralogue of *Tbx5* and is thought to play an equivalent role in the hindlimb to that of *Tbx5* in the forelimb. In this chapter, I show that the deletion of the conditional *Tbx4* allele from the hindlimb-forming region of the LPM leads to the formation of mispatterned hindlimbs with defects that are more severe in the left hindlimb than the right. I also show that *Pitx1*, a paired-like homeodomain transcription factor, is able to partially compensate for the loss of *Tbx4* expression during hindlimb bud initiation thus leading to the formation of the mutant hindlimb.

Introduction

The conditional deletion of *Tbx5* from the forelimb-forming region of the LPM, using the limb-restricted *Prx1Cre* transgenic deleter line (*Tbx5*$^{lox/lox}$*; Prx1Cre*), leads to the total loss of forelimb bud initiation and subsequent limb formation (Rallis et al., 2003). *Tbx4*, the paralogue of *Tbx5*, is expressed in the hindlimb-forming region of the LPM. Using a *Prx1-Tbx4* line, transgenic expression of *Tbx4* in the forelimb-forming regions of the *Tbx5*$^{lox/lox}$*; Prx1Cre* mutant embryo (*Tbx5*$^{lox/lox}$*; Prx1Cre; Prx1-Tbx4*) rescues forelimb bud initiation and formation (Minguillon et al., 2005). Additionally, the similar expression of transgenic fusion constructs containing domains of both Tbx5 and Tbx4 are also able to rescue forelimb bud initiation and formation in the *Tbx5*$^{lox/lox}$*; Prx1Cre* mutant (Minguillon et al., 2009). These experiments show that although the endogenous expression of *Tbx5* and *Tbx4* is restricted to the forelimb and hindlimb respectively, the two transcription factors can act on the same downstream targets during the initiation of the forelimb bud from the LPM.

Tbx5 is thought to act directly upstream of *Fgf10* to positively regulate its expression in the limb bud mesenchyme during forelimb bud initiation (Agarwal et al., 2003; Rallis et al., 2003). Expression of *Fgf10* during nascent forelimb bud formation is vital for continued outgrowth. The loss of *Tbx5* expression from the forelimb-forming region of the LPM leads to the failure to initiate *Fgf10* expression. As a result, the elements of the forelimb completely fail to form. Based on these observations and the results described earlier, it could be predicted that the loss of *Tbx4* expression from the hindlimb-forming region of the LPM would lead to a similar loss of *Fgf10* expression and thus a failure of hindlimb bud initiation. It has since been shown, however, that the conditional deletion of *Tbx4* from the hindlimb-forming region of the LPM leads to the formation of a small hindlimb bud (Naiche and Papaioannou., 2003). This study was performed using mouse lines carrying a conditional *Tbx4* allele in combination with the transgenic cre deleter line, *β-actinCre* (*Tbx4*$^{lox/lox}$*; β-actinCre*). In *β-actinCre* transgenic embryos cre activity starts to take place throughout every cell in the embryo from the blastocyst stage (Lewandowski and Martin., 1997). The conditional *Tbx4* allele is therefore deleted from every cell in the developing embryo many stages prior to hindlimb bud initiation. However, in the absence of *Tbx4* expression from the hindlimb-forming region of the LPM a small hindlimb bud is detectable showing that hindlimb bud initiation has taken place.

As mentioned earlier, *Fgf10* expression in the nascent limb bud mesenchyme is essential for limb bud outgrowth (Sekine et al., 1999). In the absence of *Tbx4*, *Fgf10* is still expressed albeit at lower levels than normal in the hindlimb buds of *Tbx4*$^{lox/lox}$*; β-actinCre* mutants (Naiche and Papaioannou., 2003). These results suggest that in the absence of *Tbx4*, another factor is able to positively regulate expression of *Fgf10* thus leading to the formation of a nascent hindlimb bud in the absence of *Tbx4*.

In *Tbx4*$^{lox/lox}$*; β-actinCre* mutant embryos the loss of *Tbx4* expression throughout the embryo leads to a failure of the chorion and allantois to fuse. This failure of fusion results in the disruption of normal placenta formation. In addition to this, vasculogenesis and umbilical cord formation are also disrupted. The cumulative effects of these developmental problems lead to embryonic lethality at E10.5 and therefore examination of the *Tbx4*$^{lox/lox}$*; β-actinCre* mutant hindlimb bud is not possible at later stages. To examine whether the mutant hindlimb bud is capable of continuing outgrowth in the absence of *Tbx4*, the authors cultured hindlimb bud explants. Control hindlimb bud explants continue outgrowth 3 days post-explantation, while in comparison *Tbx4*$^{lox/lox}$*; β-actinCre* mutant hindlimb bud explants fail to continue outgrowth (Naiche and Papaioannou., 2003). From this experiment the authors concluded that the small hindlimb, which forms in the absence of *Tbx4*, does not continue further outgrowth.

To aid my analysis of the role of *Tbx4* during hindlimb bud initiation I have characterised a novel transgenic cre deleter line, *RetRV5Cre*, that I show has cre activity throughout the hindlimb-forming region of the LPM. I have used this line in combination with the conditional *Tbx4* allele to delete *Tbx4* from the hindlimb-forming region of the LPM (*Tbx4*$^{lox/lox}$*; RetRV5Cre*). As cre activity does not take place in the chorio-allantois in these mutant embryos, the formation of the placenta is not disrupted. Therefore the early embryonic lethality is bypassed and *Tbx4*$^{lox/lox}$*; RetRV5Cre* mutant pups are viable beyond birth. The use of this transgenic cre line has allowed me to examine and characterize hindlimb bud formation and outgrowth in the total absence of *Tbx4* activity during both early and late stages of embryonic development. In addition, using the *Tbx4*$^{lox/lox}$*; RetRV5Cre* mutant in combination with the *Pitx1*$^{-/-}$ null mutant shows that no hindlimb elements

form suggesting that *Pitx1* is able to partially compensate for the absence of *Tbx4* expression during the initiation of hindlimb bud formation.

5.1 A MISPATTERNED HINDLIMB FORMS IN THE ABSENCE OF *Tbx4* FROM THE HINDLIMB-FORMING REGION.

Several cre transgenic deleter lines were generated and tested to develop a transgenic line in which cre recombinase is expressed specifically in the hindlimb area. Of these I have characterised two, the *RetRV5Cre* and *HoxB6Cre* transgenic cre deleter lines. I will describe the use and characterization of the *HoxB6Cre* transgenic line in detail later.

A ~10 kbp fragment of the Ret promoter was found to drive LacZ expression in caudal regions of the LPM that include the hindlimb-forming region of the LPM (Pachnis et al., 1993). A transgenic construct in which this promoter fragment is upstream of cre recombinase was subsequently used to generate transgenic founder animals using pronuclear injection methods by the Procedural Services Staff at the NIMR.

The *RetRV5Cre* transgenic deleter line was crossed into the *Tbx4* conditional background and breeding regimes were established to generate P0.0 $Tbx4^{lox/lox}$*; RetRV5Cre* mutants. Three mutant pups were obtained in a litter of eight, which is consistent with the expected Mendelian ratio of 25%. These mutants survived post-birth, showing that the embryonic lethality incurred by the global conditional deletion of *Tbx4* has been bypassed. I subsequently characterised the spatio-temporal activity to confirm that cre recombinase is active in the hindlimb-forming region of *RetRV5Cre* transgenic embryos.

Analysis of the spatio-temporal activity of cre recombinase in the *RetRV5Cre* transgenic deleter line.

The temporal and spatial dynamics of cre activity in the *RetRV5Cre* transgenic line were characterised using the *Rosa26RlacZ* reporter mouse line. The presence of blue stain corresponds to LacZ activity thus indicating the cells in which cre recombinase has been active.

At E9.0, prior to hindlimb bud formation, LacZ activity corresponding to cre activity is detectable in the hindlimb-forming region of the LPM that spans the region lateral to five somites (marked by black asterisks, Fig 5.1A). At this stage, LacZ activity is not detectable in any other region of the embryo. Transverse cryosections through the hindlimb-forming region of E9.0 *Rosa26RlacZ/+; RetRV5Cre* embryos reveal that cre activity is present in the mesenchyme, but not the overlying ectoderm (red arrowhead, Fig 5.1C). Cre recombinase is also active in the splanchnic component of the LPM, which will eventually form the wall of the hindgut (black arrowhead, Fig 5.1B).

At E9.5, cre activity is detectable throughout the left and right hindlimb buds (black arrowhead, Fig 5.1 E). LacZ-positive cells are also now detectable in the posterior region of the forelimb bud and also in a small number of isolated cells in the inter-limb region (black arrowheads, Fig 5.1 D). Transverse cryosections through the hindlimb buds of E9.5 *Rosa26RlacZ/+; RetRV5Cre* embryos shows that while LacZ activity is detectable throughout the limb bud mesenchyme, it is not detectable in the overlying ectoderm (red arrowhead, Fig 5.1 F). Cre activity is also detectable in the tissue surrounding the hindgut diverticulum (black arrowhead, Fig 5.1F) and anterior to the vitelline artery (black asterisk, Fig 5.1F). By E10.5 the limb buds are prominent outgrowths from the LPM. LacZ positive cells are detectable throughout

the hindlimb bud (black arrowhead, Fig 5.1H). Isolated LacZ positive cells are now detectable in the anterior of the forelimb bud (black arrowhead, Fig 5.1 G). Transverse cryosections of E10.5 *Rosa26RlacZ/+; RetRV5Cre* embryos shows that LacZ positive cells are not detectable in the ectoderm of the hindlimb bud (red arrow, Fig 5.1 I). Cre activity is detectable throughout the tissue of the hindgut (black arrowhead, Fig 5.1I), including the dorsal mesentery (black asterisk, Fig 5.1I)

Figure 5.1

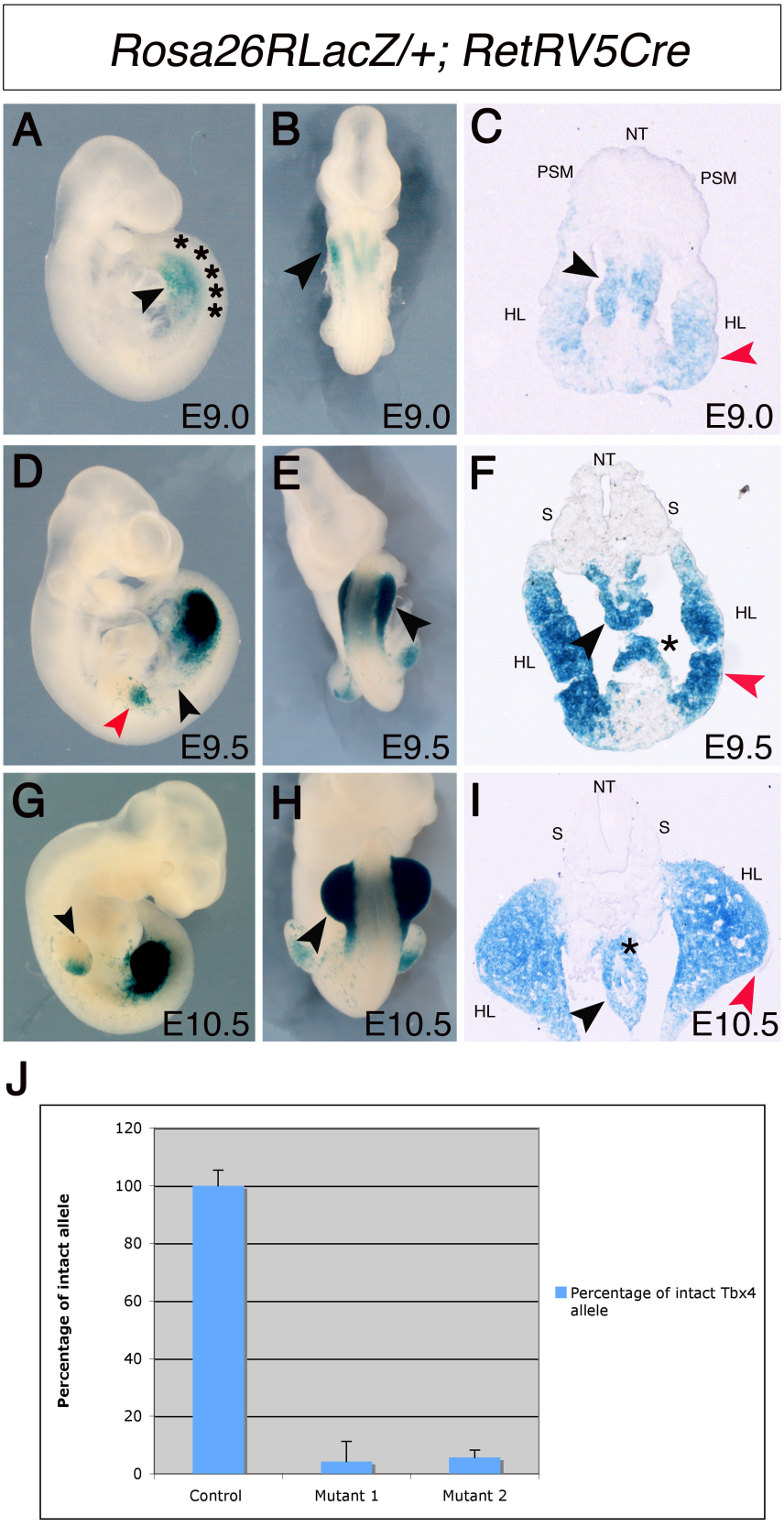
Rosa26RLacZ/+; RetRV5Cre
A
E9.0
B
E9.0
C
NT
PSM
PSM
HL
HL
E9.0
D
E9.5
E
E9.5
F
NT
S
S
HL
HL
E9.5
G
E10.5
H
E10.5
I
NT
S
S
HL
HL
E10.5
J
Percentage of intact allele
120
100
80
60
40
20
0
Control
Mutant 1
Mutant 2
Percentage of intact Tbx4 allele

Figure 5.1 Cre recombinase is active in the hindlimb-forming region of the LPM in the *RetRV5Cre* transgenic deleter line.

Panels **D+G** are right-side lateral views of embryos. Panels **B, E, H** are ventral views of embryos. Panels **C, F, I** are transverse cryosections through the hindlimb regions of embryos. **A** E9.0 *Rosa26RlacZ/+; RetRV5Cre* embryo. LacZ activity is detected in the hindlimb-forming region of the LPM (marked by black asterisks and indicated by the black arrowhead). **B** Dorsal view of the embryo in panel A. LacZ activity is detectable in the nascent hindlimb bud (black arrowhead). **C** Transverse cryosection through the hindlimb region of an E9.0 *Rosa26RlacZ/+; RetRV5Cre* embryo. LacZ activity is detectable in the mesenchyme of the hindlimb forming region (red arrowhead), and the hindgut (black arrowhead). **D** An E9.5 *Rosa26RlacZ/+; RetRV5Cre* embryo in which LacZ activity is detectable in the interlimb region (black arrowhead) and the posterior region of the forelimb bud (red arrowhead). **E** LacZ activity is detectable in the hindlimb buds of the embryo shown in panel D. **F** Transverse cryosection through the hindlimb region of an E9.5 *Rosa26RlacZ/+; RetRV5Cre* embryo. LacZ activity is not detectable in the ectoderm (red arrowhead). LacZ activity is additionally present in the hindgut diverticulum (black arrowhead) and anterior to the vitelline artery (black asterisk). **G** An E10.5 *Rosa26RlacZ/+; RetRV5Cre* embryo in which LacZ activity is detectable in the anterior forelimb bud (black arrowhead). **H** LacZ activity is detectable throughout the hindlimb buds of the embryo shown in panel G (black arrowhead). **I** Transverse cryosection through the hindlimbs of an E10.5 *Rosa26RlacZ/+; RetRV5Cre* embryo, in which LacZ activity is not detectable in the ectoderm (red arrowhead). LacZ activity is detectable in the mesoderm of the hindgut (black arrowhead) and the dorsal mesentery (black asterisk). **J** Graph showing that 96% of conditional DNA has been excised out in $Tbx4^{lox/lox}$*; RetRV5Cre* mutant hindlimbs. ('y' - percentage of intact conditional allele, 'x' – embryo) NT – Neural tube, S – somite, PSM – presomitic mesoderm, HL – hindlimb

My analysis of *Rosa26RlacZ/+; RetRV5Cre* embryos shows that cre recombinase is active in the hindlimb-forming region of the LPM prior to the initiation of the hindlimb bud. I therefore expect that when the *RetRV5Cre* is used in combination with the *Tbx4* conditional allele, the allele will be deleted throughout the hindlimb-forming region. To confirm this, I have analyzed how much of the target conditional allele remains intact in the hindlimb buds of $Tbx4^{lox/lox}$*; RetRV5Cre* mutants. The two *LoxP* sites in the $Tbx4^{lox/lox}$ mouse genome flank exon 5 of *Tbx4*.

Cre recombinase acts at the LoxP sites to recombine exon 5 out of the conditional *Tbx4* allele therefore in the absence of cre recombinase activity the conditional *Tbx4* allele will be intact. To detect levels of the intact conditional *Tbx4* allele, I designed primers flanking the LoxP site that is located 1.5kb 5' of exon 5. The length of the amplicon product yielded is 100bp. Cre characterization results show that cre activity is not present in the hindlimb ectoderm, therefore to prevent contamination of the genomic DNA samples I harvested *Tbx4*$^{lox/lox}$*; RetRV5Cre* and control E10.5 hindlimb buds and used dispase treatment to remove the overlying ectoderm. I then extracted genomic DNA from the remaining limb bud mesenchyme and subjected it to QT PCR analysis. I compared the amount of conditional *Tbx4* allele in control hindlimb buds (n=4) to the amount of conditional *Tbx4* allele in mutant hindlimb buds (n=4). Compared to control hindlimb buds, in which 100% of the target allele is intact, mutant hindlimb buds have only 4% of the intact conditional *Tbx4* allele. This shows that 96% of the conditional *Tbx4* alleles have been recombined in the mesenchyme of the mutant hindlimb buds (Fig 5.1 J). In summary, these results demonstrate that cre recombinase is efficiently recombining the conditional *Tbx4* alleles in mutant hindlimb buds therefore ablating normal *Tbx4* expression in the hindlimb.

Conditional deletion of *Tbx4* from the hindlimb-forming region of the LPM leads to the formation of a truncated and mispatterned hindlimb.

My analysis of the spatio-temporal activity of cre recombinase delivered by the *RetRV5Cre* indicates that the *Tbx4* conditional allele is deleted from the hindlimb-forming region of the LPM prior to hindlimb bud initiation in *Tbx4*$^{lox/lox}$*;RetRV5Cre* mutants. In contrast to previously reported results that suggested that in the absence of *Tbx4* the small hindlimb bud fails to undergo subsequent outgrowth, my results show that the mutant hindlimb bud continues

through outgrowth to form a severely mispatterned hindlimb (black arrow, Fig 5.2 E). Staining with alcian blue and alizarin red reveals that the pelvis and femur are completely missing (red arrows, Fig 5.2F). A single zeugopodal skeletal element is present, which although malformed, is most morphologically like a tibia suggesting that the fibula element has failed to form. A rudimentary nodule of cartilage is present, however it is unclear whether this is a rudiment of the femur or pelvis (red arrow, Fig 5.2 G). The sacrum, the element of the pelvic girdle that connects the ilium and ischium of the pelvis to the spine, is present despite the failure of the entire pelvis to form (Fig 5.2 G).

The distal elements of the hindlimb are relatively mildly affected by the loss of *Tbx4* compared to the proximal elements, which have completely failed to form. The autopod, the distal most element of the hindlimb, is composed of tarsals, metatarsals, and phalanges. A tarsal element, the calcaneus, is a morphologically characteristic hindlimb anklebone. Although small, the calcaneus is still present in *Tbx4$^{lox/lox}$; RetRV5Cre* mutant hindlimbs indicating that some characteristics of hindlimb morphology have not been lost (Fig 5.2 H). Other tarsal elements are fused (red arrow, Fig 5.2H). *Tbx4$^{lox/lox}$; RetRV5Cre* mutant hindlimbs display only four digits instead of the characteristic five. Digit one is identified by the presence of two phalanges (asterisk 1, Fig 5.2D), whereas other digits of the autopod have three phalanges. Although the speculative digit one in the mutant autopod displays two phalanges, these two phalanges are elongated to the extent that the mutant digit one appears much larger compared to the control digit one (asterisks 1, Fig 5.2 H).

Figure 5.2

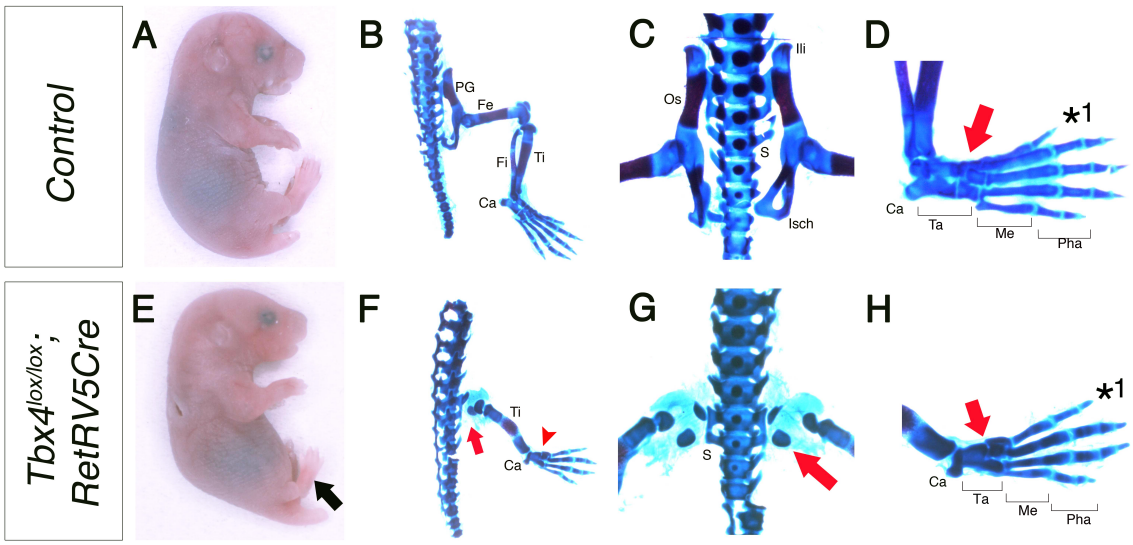

Figure 5.2 *Tbx4$^{lox/lox}$; RetRV5Cre* mutants have mispatterned hindlimbs and the proximal elements are absent.

Panels **A, B, E, F** are right-side lateral views of E17.5 embryos. Panels **C, G** are ventral views of the pelvic regions of E17.5 embryos. Panels **D** and **H** are dorsal views of the right autopods of E17.5 embryos. **A** Control embryo. **B** Hindlimb skeletal elements. **C** Magnified view of the hindlimb pelvic elements. **D** Magnified view of the skeletal elements of the ankle and hindlimb autopod (red arrow). Black asterisk marks digit one. **E** A *Tbx4$^{lox/lox}$; RetRV5Cre* mutant embryo. The hindlimbs are truncated (black arrow). **F** In the *Tbx4$^{lox/lox}$; RetRV5Cre* mutant the pelvic region and femur fail to form (red arrow). A single zeugopodal element, most likely the tibia, and only 4 digits form (red arrowhead). **G** A cartilage nodule is present in the pelvic regions of *Tbx4$^{lox/lox}$; RetRV5Cre* mutants (red arrow). **H** The tarsals are are fused in the mutant autopod (red arrow). Digit one has two elongated phalanges (black asterisk). PG – pelvic girdle, Fe – femur, Fi – Fibula, Ti – Tibia, Ca – calcaneus, S – sacrum, OS – ossae coxae, Ili – Ilium, Isch – ischium, Ta – Tarsals, Me – Metatarsals, Pha - Phalanges

Proximal elements cannot be detected prior to cartilage condensation in the hindlimbs of *Tbx4$^{lox/lox}$; RetRV5Cre* mutants.

One of the features of the hindlimb phenotype in the *Tbx4$^{lox/lox}$; RetRV5Cre* mutant is the complete loss of the proximal elements including the pelvic girdle and the femur. This feature is visible by E17.5, however skeletal preparations using alcian blue and alizarin red staining are unable to distinguish whether the formation

of these elements are disrupted earlier during embryogenesis or simply do not form at all. Type II Collagen (*Col2a*) forms part of the extracellular matrix of cartilage and is crucial for skeletal development. *Col2a* gene expression can be detected during embryogenesis (~E13.5) in the cells that are condensing to form the skeletal elements of the mouse. I have examined the expression pattern of *Col2a* in E13.5 control and mutant embryos to determine whether the proximal skeletal elements of the hindlimb are initially present in *Tbx4$^{lox/lox}$; RetRV5Cre* mutants. In E13.5 control embryos, *Col2a* can be clearly detected in the regions of the hindlimb that will give rise to the tibia, fibula and digits 1-5 of the autopod (Fig 5.3A). It is also expressed in cells in the proximal region, although whether this is the precursor to the pelvic girdle and femur is unclear (black arrowhead, Figure 5.3A). In E13.5 *Tbx4$^{lox/lox}$; RetRV5Cre* mutants, *Col2a* expression cannot be detected in the fibula-forming region of the hindlimb suggesting that fibula has completely failed to form (red arrowhead, Fig 5.3B). *Col2a* expression can be detected in the proximal region of the hindlimb, however this analysis is not sufficient to determine whether this is an indication of the pelvic girdle or femur (black arrowhead, Fig 5.3B). Expression of *Col2a* in the digits of the mutant hindlimb shows that a 5th digit does not form in the autopod, indicating that events prior to pre-cartilage cell condensation are leading to the loss of one of five digits.

Figure 5.3

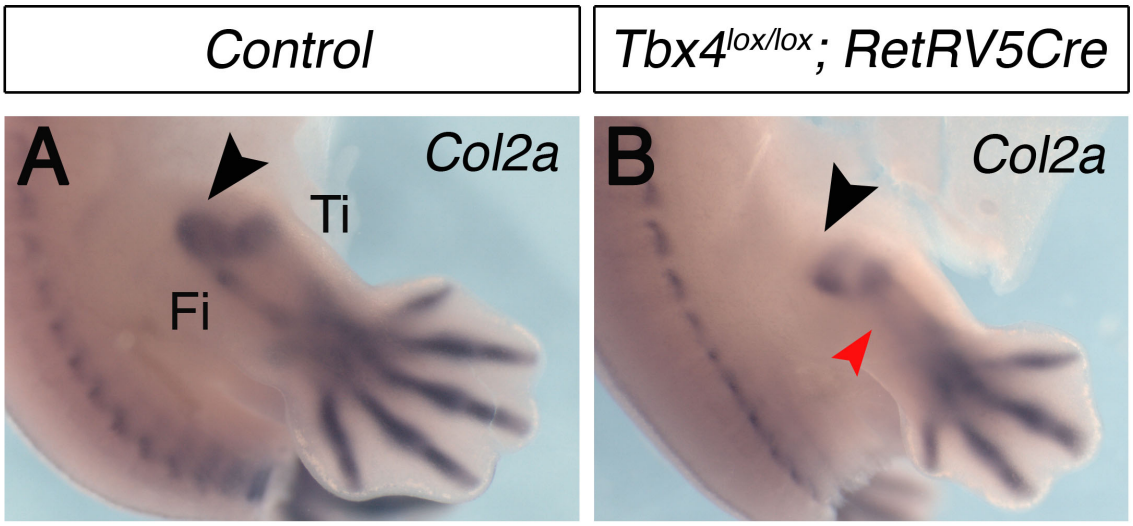

Figure 5.3 *Col2a* gene expression in the cartilage precursors is absent from the fibula-forming region of E13.5 mutant embryos.

Panels **A+B** show the right-side dorsal view of E13.5 hindlimbs. **A** *Col2a* gene expression is present in the proximal region of the hindlimb (black arrowhead), as well as the regions that will give rise to the tibia, fibula and all five digits of the autopod. **B** *Col2a* expression is absent from the fibula-forming region of *Tbx4$^{lox/lox}$; RetRV5Cre* mutants (red arrowhead), and can be detected in the proximal region (black arrowhead). Ti – tibia, Fi – fibula

My analysis of *Col2a* expression in E13.5 *Tbx4$^{lox/lox}$; RetRV5Cre* mutants suggests that the nascent fibula element does not condense. However, an extended analysis of 16 E17.5 mutant embryos shows that in some cases a fibula has formed and is fused to the tibia (Fig 5.5). Therefore to fully determine whether a fibula forms, I would need to extend my initial analysis to include a similar number of mutants at stages E13.5 and later. The formation of the fibula in *Tbx4$^{lox/lox}$; RetRV5Cre* mutants may be developmentally delayed, in which case *Col2a* expression may be detected in the fibula-forming region at later stages. It is also possible that the loss of the fibula is not a fully penetrant phenotype, which can be examined through the analysis of *Col2a* expression in a larger sample of mutant embryos.

In the absence of *Tbx4, Fgf10* expression is affected in the hindlimb bud.

Naiche and Papaioannou originally demonstrated that in the absence of *Tbx4*, a small hindlimb bud forms. They also showed that *Fgf10* expression can still be detected in these mutant hindlimbs, indicating that another factor may be compensating for the loss of *Tbx4* during hindlimb bud initiation (Naiche and Papaioannou., 2003). During limb bud outgrowth, mesenchymal Fgf10 signals via ectodermal FgfR receptors to initiate the expression of *Fgf8* in the overlying ectoderm. Fgf8 then signals via mesenchymal FgfR receptors to positively upregulate *Fgf10* expression in the underlying mesenchyme. This activity results in the establishment of the FGF signalling positive feedback-loop required to drive nascent limb bud outgrowth. *Tbx4$^{lox/lox}$; RetRV5Cre* mutants have mispatterned hindlimbs that have achieved a form of outgrowth despite the absence of *Tbx4* expression. Using whole mount in situ hybridisation (WMISH) I have examined the expression patterns of *Fgf10* and *Fgf8* in E10.0 – E11.5 control and *Tbx4$^{lox/lox}$; RetRV5Cre* embryos to determine how the FGF signalling pathway is established in the mutant hindlimbs.

At E10.0 the nascent hindlimb bud is starting to form and by E11.5 outgrowth of the hindlimb is well underway. At E10.0 *Fgf10* expression is detected throughout the early hindlimb bud mesenchyme and *Fgf8* expression is detected in the apical ectodermal ridge (AER) confirming the presence and activity of the Fgf10 ligand (Fig 5.4 A, D). By E10.5 the spatial expression pattern of *Fgf10* and *Fgf8* remains unchanged (Fig 5.4 B, E). In E11.5 hindlimbs, *Fgf10* expression is restricted to the most distal region of the hindlimb autopod whereas *Fgf8* expression is detected throughout the apical ectodermal ridge (Fig 5.4 C, F).

In E10.0 *Tbx4*$^{lox/lox}$*; RetRV5Cre* mutant embryos, *Fgf10* expression is detectable in the hindlimb bud (black arrowhead, Fig 5.4 G). However, *Fgf8* expression can only be detected in the posterior region of the apical ectodermal ridge (black arrowhead, Fig 5.4 J). The restricted expression of *Fgf8* in the posterior of the hindlimb bud indicates that the Fgf10 ligand is not present in the anterior hindlimb bud. Therefore *Fgf8* is only transcribed in the posterior hindlimb bud or is present at insufficient levels to induce ectodermal *Fgf8*. In E10.5 mutant embryos, *Fgf8* expression remains restricted to the posterior of the hindlimb bud (black arrowhead, Fig 5.4 K). *Fgf10* expression is detectable in the posterior of the hindlimb, suggesting that the Fgf8 ligand in the posterior region of the AER is acting to positively upregulate *Fgf10* in the posterior region of the mesenchyme (black arrowhead, Fig 5.4 H). Interestingly, the *Fgf10* expression detected in the posterior of the mutant hindlimb bud appears to be at higher levels than that in the control. However, this may simply be an artifact of the experiment. The use of a quantitative assay would be sufficient to determine this. By E11.5, *Fgf10* expression is detectable in the hindlimb bud throughout the distal mesenchyme that underlies the ectoderm (black arrowheads, Fig 5.4 I). Similarly, *Fgf8* expression is detectable throughout the AER (black arrowheads, Fig 5.4 L).

The restriction of *Fgf8* expression to the posterior AER in the absence of *Tbx4* suggests that the level of Fgf10 ligand in the anterior hindlimb bud may not be sufficient to initiate transcription of *Fgf8* in the anterior AER. To determine whether *Fgf10* is expressed in the anterior hindlimb bud I chose to use RT QT PCR to quantify the level of mRNA transcript. I collected 4 pairs of E10.0 mutant hindlimbs, which were separated into two halves, anterior and posterior and then pooled to generate 4 sample sets: anterior mutant buds, anterior control buds, posterior mutant buds, and posterior control buds. RNA was extracted from these samples,

and used to synthesis cDNA. I designed primers against *Fgf10*, to produce an amplicon product of 113 bp. I chose to analyze a sequence that spans the junction between exons 1 and 2 to ensure that only the cDNA is used as the template sequence rather than any contamination of genomic DNA. I compared the amount of *Fgf10* transcript in the anterior of the hindlimb bud to the amount in the posterior of the hindlimb bud. Again, as in previous chapters, the raw data was analysed as described in Methods and Materials. Compared to the anterior region of the mutant hindlimb bud, there is a statistically significant 0.6 fold increase in *Fgf10* transcript in the posterior of the hindlimb bud ($p < 0.05$, $p = 0.007$). Interestingly, there is no significant decrease in *Fgf10* transcript in the anterior region although there is a 0.2 fold decrease in mRNA levels (Fig 5.4 M) ($p > 0.05$, $p = 0.22$).

Figure 5.4

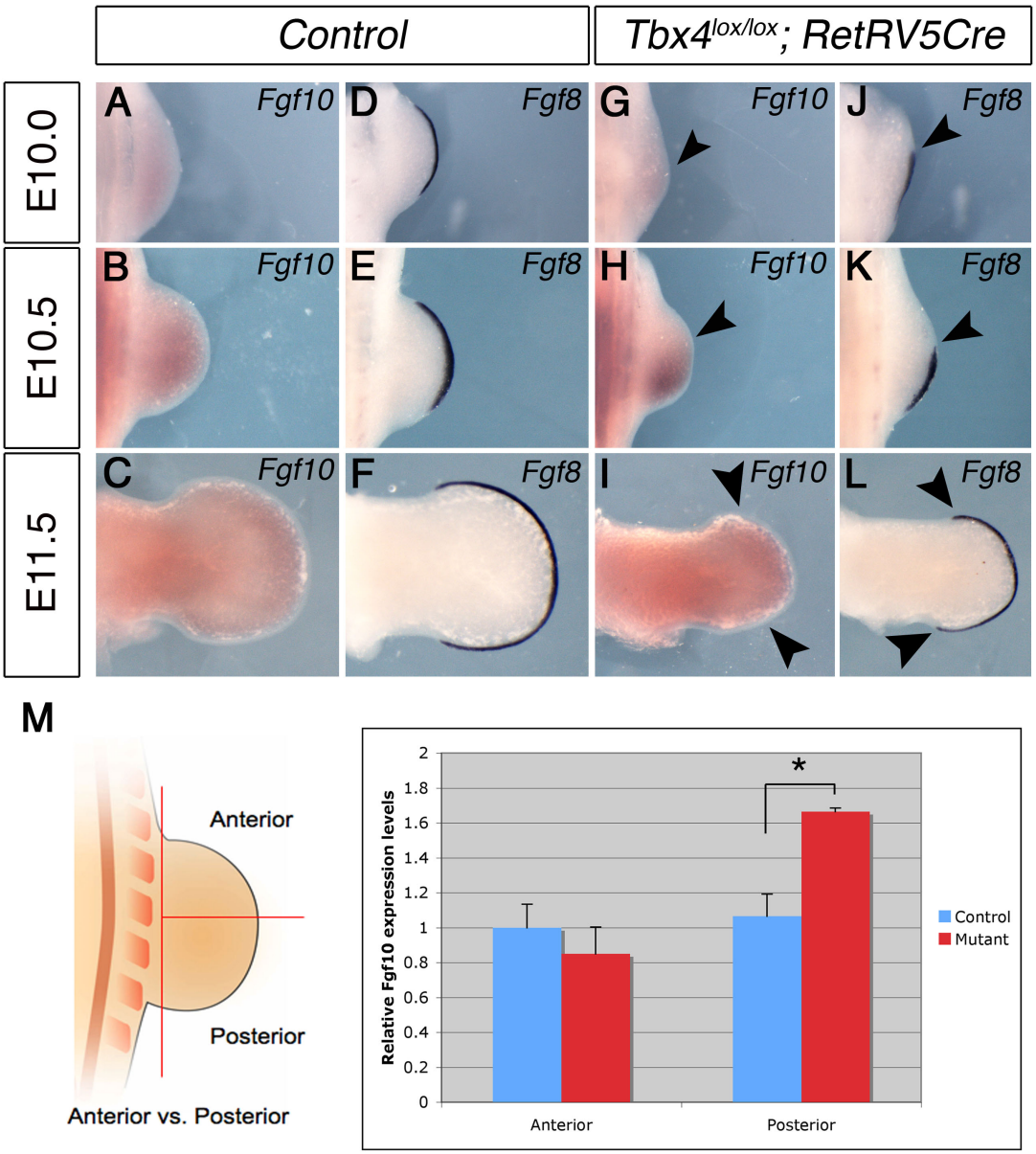

Figure 5.4 *Fgf10* is expressed in the posterior region of *Tbx4*$^{lox/lox}$*; RetRV5Cre* mutant hindlimb buds during hindlimb bud outgrowth.

Panels **A**-**L** show dorsal views of the right hindlimbs of embryos. Panels **A**-**F** are hindlimbs from control embryos. Panels **G**-**L** are hindlimbs from *Tbx4*$^{lox/lox}$*; RetRV5Cre* mutant embryos. **A-C** *Fgf10* expression in control hindlimb buds at stages E10.0 (**A**), E10.5 (**B**), and E11.5 (**C**) embryos. **D-F** *Fgf8* expression in the AER of control hindlimb buds at stages E10.0 (**D**), E10.5 (**E**), and E11.5 (**F**) embryos. **G** *Fgf10* expression in the hindlimb mesenchyme (black arrowhead). **H** *Fgf10* expression in the posterior mesenchyme (black arrowhead). **I** *Fgf10* expression in the distal mesenchyme. *Fgf8* expression is restricted to the posterior AER at stages E10.0 (**J**) and E10.5 (**K**). **L** *Fgf8* expression

throughout the AER. **M** The schematic shows the dissection of the anterior hindlimb bud vs. the posterior hindlimb buds. The graph shows the amount of *Fgf10* transcript in the anterior region of E10.0 control (blue) and mutant (red) hindlimb buds compared to the amount of transcript in the posterior regions. There is a difference of 0.6 fold in transcript levels between the anterior and posterior regions of the mutant hindlimb bud. ('y' – *Fgf10* expression levels 'x' – region of hindlimb bud)

In summary, my whole mount in situ (WMISH) results show that in the absence of *Tbx4*, *Fgf10* is expressed at lower levels in the nascent hindlimb bud than in the control. My RT QT PCR data indicates that *Fgf10* is expressed in both the anterior and posterior regions of the mutant hindlimb buds at levels that are not significantly lower than the *Fgf10* expression in the control hindlimb buds. This data, taken together with my WMISH results, suggests that signalling activity of the Fgf10 ligand does not take place in the anterior mutant hindlimb bud, which results in the posterior-restricted expression of *Fgf8* in the AER. The expression of *Fgf8* in the posterior AER of the mutant hindlimb buds allows for the establishment of FGF signalling positive feedback loop in the posterior hindlimb. This therefore drives outgrowth of the posterior region, leading to the formation of the truncated hindlimb.

Conditional deletion of *Tbx4* from the left and right hindlimb forming region leads to left-biased asymmetrical hindlimb defects.

In previous chapters, I have shown that the disruption of *Tbx5* leads to left-biased asymmetrical defects. As *Tbx5* and *Tbx4* are speculated to have the same role during limb bud initiation, I was interested in whether *Tbx4*$^{lox/lox}$*; RetRV5Cre* mutants present with any consistent asymmetric hindlimb defects. Mutations in *TBX4* have been associated with Small-Patella Syndrome (SPS) [OMIM #147891]. SPS patients present with small or absent patellas, an increased space between the first and second toes, and shortened fourth and fifth toes. These defects are significantly milder than the forelimb defects reported in HOS patients, who are

purported to have mutations in *TBX5*. A left-side bias to the severity of these defects is not a clinical feature of SPS and has not been reported.

To assess whether *Tbx4$^{lox/lox}$; RetRV5Cre* mutants present with asymmetrical hindlimb defects, I tabulated defects in 16 different mutant embryos. As in previous chapters, I have chosen to present the left and right hindlimbs of 5 mutant embryos as representational examples (Fig 5.5B). *Tbx4$^{lox/lox}$; RetRV5Cre* mutants present with hindlimb defects that are typically much more severe than those observed in SPS patients. I have tabulated certain defects such as hypoplastic tibias, bifurcated digits, the loss of more than one digit and fused metacarpals. In addition, I have observed the presence of fused tibia and fibulas in some of the 16 mutants.

Example 1 of Fig 5.5B shows a pair of mutant hindlimbs that are apparently bilaterally affected and there are no obvious differences between these two hindlimbs (Fig 5.5 B1). Example 2 shows a pair of mutant hindlimbs in which the left hindlimb presents with a partially fused fibula and tibia. In contrast, the right hindlimb displays a hypoplastic tibia (Fig 5.5 B2). In example 3, there is a bifurcated digit in the left hindlimb (Fig 5.5 B3). In example 4 the tibia of the left hindlimb is severely hypoplastic and is partially fused to the fibula. The right hindlimb does not present with a hypoplastic tibia (Fig 5.5 B4). There are obvious left-biased asymmetrical differences between the two hindlimbs in example 5. The left hindlimb presents with an elongated tibia and only three digits are present. In contrast, in the right hindlimb four digits and a partially fused fibula-tibia are present (Fig 5.5 B5).

Defects that are more prevalent on the right side include the loss of the fibula and the partial fusion of the fibula and tibia. There are considerably more defects present in the left hindlimb such as bifurcated digits, loss of more than one digit, fused fibula and tibia. Interestingly, fused metacarpals occur with equal frequency in

the left and right hindlimb (Table 6). Out of the total number of defects tabulated in both the left and right hindlimbs, 60% were observed in the left hindlimb compared to the right hindlimb in which 40% were observed. Although I have not yet determined whether this analysis is statistically significant, this would suggest that in the absence of *Tbx4*, the hindlimbs that form display defects that occur with greater frequency in the left hindlimb compared to the right.

Figure 5.5

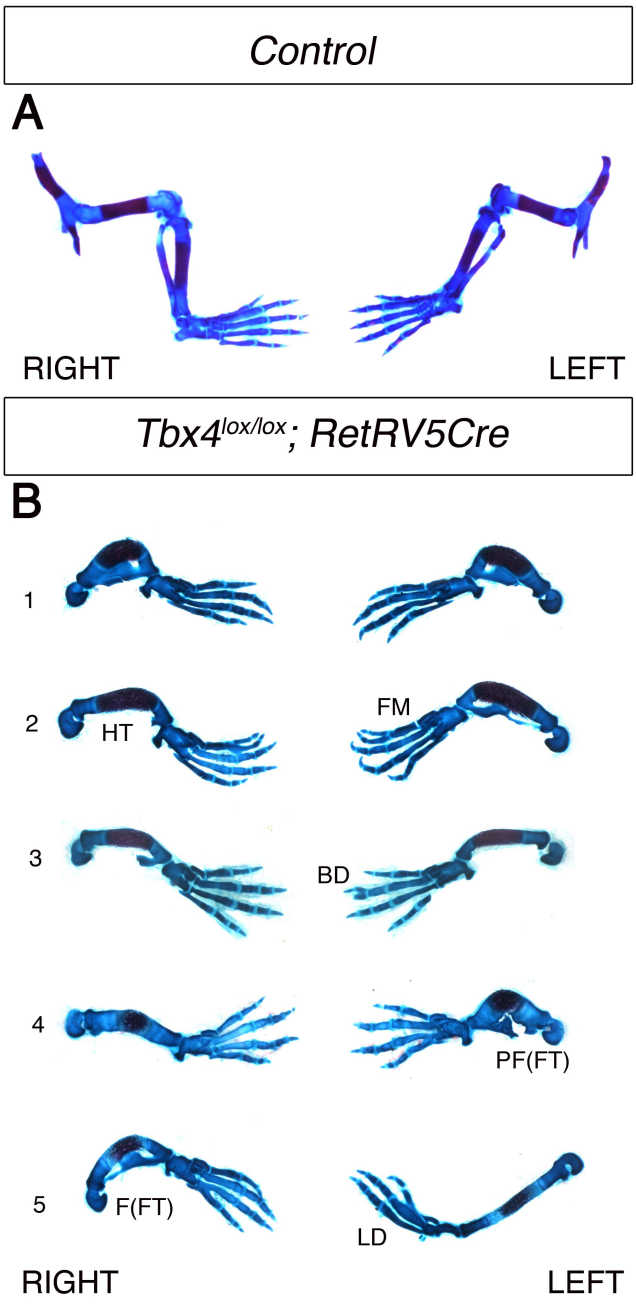

Figure 5.5 *Tbx4$^{lox/lox}$; RetRV5Cre* mutants present with left-biased asymmetrical hindlimb defects.

A Lateral views of the left and right hindlimbs of an E17.5 control embryo. **B** Lateral views of the left and right hindlimbs of 5 E17.5 *Tbx4$^{lox/lox}$; RetRV5Cre* mutant embryos. B2 - (HT) Hypoplastic tibia in the right hindlimb. (FM) An example of fused metacarpals in the left hindlimb. B3 - (BD) Bifurcated digit in the left hindlimb. B4 – (PF(FT)) Partially fused fibula and tibia in the left hindlimb. B5 – (F(FT))

Fused fibula and tibia in the right hindlimb, whereas LD is the loss of more than one digit from the left hindlimb.

FM – fused metacarpals, HT – hypoplastic tibia, BD – bifurcated digit, PF(FT) – partially fused fibula and tibia, LD – loss of more than one digit, F(FT) – fused fibula and tibia

Table 6.

RIGHT

	no fibula	fused fibtib	part. Fu	loss >1	bifu	fused meta	hypoplastic tibia
1	*						
2		*				*	
3	*				*		
4			*				
5	*						
6		*					*
7	*						
8		*					*
9	*						
10			*				
11		*					*
12		*					
13	*						
14	*						
15			*				
16			*				

LEFT

	no fibula	fused fibtib	part. Fu	loss >1	bifu	fused meta	hypoplastic tibia
1	*			*			
2	*						
3		*			*		
4	*				*		
5		*					*
6		*					*
7	*			*			*
8		*					*
9			*				
10		*			*		*
11		*				*	*
12				*			*
13				*			*
14	*				*		
15			*				
16			*				

Table 6. Graph tabulating the total number and type of defects in the right and left hindlimbs of 16 mutants.

5.2 A HINDLIMB BUD FORMS IN THE ABSENCE OF BOTH *Tbx5* AND *Tbx4*.

Tbx5 and *Tbx4* are paralogous genes encoding transcription factors that have been shown to have a similar role during the initiation of the limb bud from the LPM (Minguillon et al., 2005; Minguillon et al., 2009). Conditional deletion of *Tbx5* from the forelimb-forming region leads to a loss of forelimb bud initiation and formation, however in a similar experiment I have shown that deletion of conditional *Tbx4* from the hindlimb forming region of the LPM leads to the formation of a severely mispatterned hindlimb. My analysis of *Fgf10* expression during the initiation of hindlimb bud formation, using WMISH and RT QT PCR, shows that *Fgf10* is still expressed in the absence of *Tbx4.* This indicates that another factor can at least partially compensate for the loss of *Tbx4* expression to activate *Fgf10* transcription.

I have investigated the possible roles of two factors, *Tbx5* and *Pitx1*, during hindlimb bud initiation. *Tbx5* and *Tbx4* are described in the literature as being exclusively expressed in the forelimb and hindlimb (Agulnik et al., 1996; Gibson-Brown et al., 1996). However, there may be some transient expression of *Tbx5* in the hindlimb, which may be a reflection of the activity of the ancestral enhancer of the preduplicate *Tbx5*/*Tbx4* gene. Therefore one possible explanation is that in the absence of *Tbx4*, low levels of *Tbx5* transcript may be able to initiate low levels of *Fgf10* expression that result in the formation of a small hindlimb bud. This explanation is dependent on the presence of low levels of *Tbx5* transcript in the hindlimb-forming region of the LPM. WMISH may not be sensitive enough to detect any *Tbx5* expression in the hindlimb-forming region therefore I have had to pursue an alternative approach to examine the expression of *Tbx5* in the hindlimb.

I have chosen to use RT QT PCR to analyze *Tbx5* and *Tbx4* transcript levels in the hindlimb, as this is a more sensitive assay in which transcript levels can be quantified. Hindlimb bud initiation does not start to take place until E9.75 – E10.0, however it is possible that *Tbx5* may be expressed in the hindlimb-forming region prior to hindlimb bud formation. Therefore I have chosen to analyze expression over a series from E8.75, before a hindlimb is formed, through to E10.5, when a hindlimb bud is established. I harvested the hindlimb-forming regions of E8.75, E9.0, E9.5, and E10.5 wildtype embryos and subsequently extracted RNA. The RNA samples were then used to synthesise cDNA. To analyze the levels of *Tbx5*, I designed forward and reverse primers against an exon-exon junction to yield an amplicon of 100bp in length. The same was done for *Tbx4*. I then analyzed the levels of transcript.

To provide a comparison with the *Tbx5* transcript levels, I have also analyzed the transcript levels of *Tbx4*. Throughout all the stages analyzed, *Tbx5* transcript is detected. At E8.75, the level of *Tbx5* transcript is 25% that of the level of *Tbx4* transcript. At E9.0, the level of *Tbx5* transcript is reduced to 7% compared to the level of *Tbx4* transcript. At E9.5 this is reduced even further to 0.09% and by E10.5 this is 0.03% (Fig 5.6). This result shows that *Tbx5* transcript is detectable in the hindlimb-forming region. However, it does not determine whether *Tbx5* is partially compensating for the absence of *Tbx4* in *Tbx4*$^{lox/lox}$*; RetRV5Cre* mutants. The levels of *Tbx5* detected at E9.5 and E10.5 are extremely low compared to the levels of *Tbx4* transcript detected and it is unclear whether this would be sufficient to initiate the transcription of low levels of *Fgf10* in the absence of *Tbx4*.

Figure 5.6

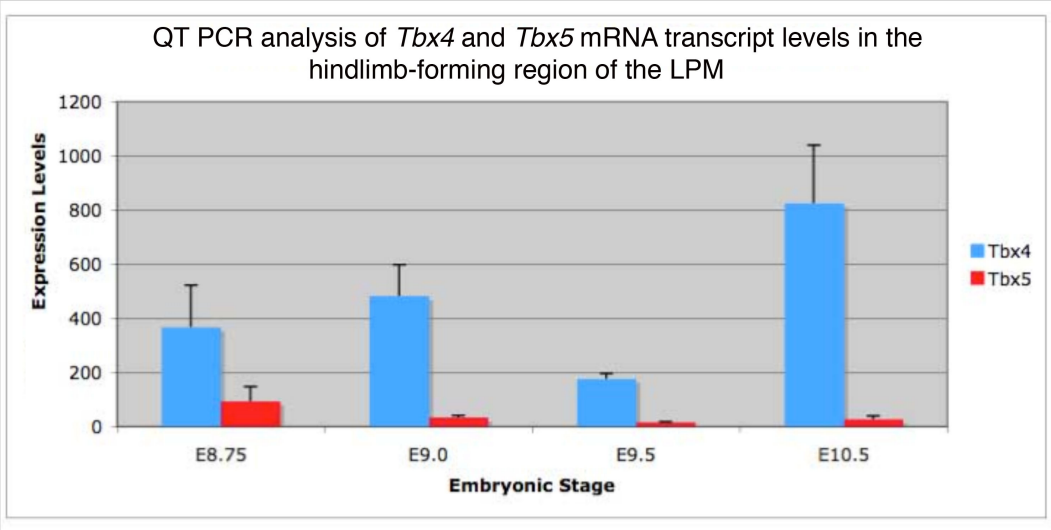

Figure 5.6 *Tbx5* transcript can be detected in the hindlimb-forming region.

('y' – expression levels compared to those in the midbrain of the embryo, 'x' – embryonic stage)

While my analysis indicates that *Tbx5* transcript is briefly produced in the hindlimb region, the levels of transcript are extremely low. It is unlikely that this would contribute, even partially, to *Fgf10* expression in the absence of *Tbx4*. However, as RT QT PCR analysis is not sufficient to determine this, I have chosen

to conditionally delete both *Tbx5* and *Tbx4* in the hindlimb-forming region. This approach will fully determine whether *Tbx5* is able to compensate in the event of the loss of *Tbx4* expression from the hindlimb.

Analysis of the spatio-temporal activity of cre recombinase in the *HoxB6Cre* transgenic cre deleter line.

In order to conditionally delete both *Tbx5* and *Tbx4* from the hindlimb-forming region of the LPM, I have chosen to use mice carrying homozygous conditional alleles for both *Tbx5* and *Tbx4* (*Tbx5*$^{lox/lox}$*; Tbx4*$^{lox/lox}$) in combination with the appropriate cre deleter line. For this experiment cre recombinase is required to act at 4 allele sites rather than 2. Therefore cre recombinase activity must be robust enough to fully recombine the target DNA at all 4 sites. The *HoxB6Cre* deleter line was produced using an enhancer fragment of the homeobox transcription factor, *HoxB6*. It was originally produced to generate *Tbx4*$^{lox/lox}$*; HoxB6Cre* mutant embryos, so that the mutant hindlimb that forms in the absence of *Tbx4* could be analyzed past E10.5. However, although cre recombinase activity is robust, it was found that it is active in the chorio-allantois of *HoxB6Cre* transgenic embryos. Thus when used in combination with conditional *Tbx4*, mutant embryos die at E11.0. As I have already demonstrated, the use of the *RetRV5Cre* to delete conditional *Tbx4* from the hindlimb-forming region leads to the development of embryos that are viable post-birth. Therefore *Tbx4*$^{lox/lox}$*; RetRV5Cre* mutants rather than *Tbx4*$^{lox/lox}$*; HoxB6Cre* mutants were analyzed.

While cre activity in the *RetRV5Cre* line is sufficient to recombine homozygous conditional *Tbx4*, it may not be robust enough to recombine two homozygous conditional targets. As I will show, cre activity in the *HoxB6Cre* transgenic line is robust and sufficient to recombine 4 target sites in

Tbx5$^{lox/lox}$*; Tbx4*$^{lox/lox}$*; HoxB6Cre* mutants. Although the mutant embryos die at E11.0 due to the loss of *Tbx4* expression from the forming chorio-allantois, this is sufficient to determine whether a hindlimb bud forms in the absence of *Tbx5* and *Tbx4*.

I have characterised the spatio-temporal activity of cre recombinase in the *HoxB6Cre* transgenic deleter line by using the *Rosa26RlacZ* reporter mouse line. At E9.0 the hindlimb bud has not yet formed. Cre activity is detectable throughout the hindlimb-forming region (marked by black asterisks, Fig 5.7A). LacZ positive cells are also detectable in the interlimb region as well as the posterior of the nascent forelimb bud (black arrowheads, Fig 5.7A). Cre activity is also detectable in the midbrain of the embryo. Transverse cryosections taken through the hindlimb-forming regions of E9.0 *Rosa26RlacZ/+; HoxB6Cre* embryos show that cre activity is detectable in the mesenchyme of the hindlimb bud (Fig 5.7C). Cre activity is also detectable in the splanchnic component of the mesenchyme. At E9.5 the hindlimb bud starts to bud form from the LPM. LacZ activity corresponding to cre activity is detectable throughout the nascent hindlimb bud (black arrowhead, Fig 5.7D).LacZ positive cells are also detectable in the somites in the caudal region of the embryo (black arrowhead, Fig 5.7 E). Transverse cryosections through the hindlimb buds of E9.5 *Rosa26RlacZ/+; HoxB6Cre* embryos show that while cre activity is present throughout the hindlimb mesoderm and in a mosaic manner in the somites and neural tube, it cannot be detected in the hindlimb bud ectoderm (black arrowhead, Fig 5.7 F). By E10.5 the hindlimb buds are prominent protrusions from the LPM. Again, cre activity is detectable throughout the hindlimb bud, interlimb region, posterior region of the forelimb bud and the caudal regions of the notochord (black arrowheads, Fig 5.7 G, H). Transverse cryosections taken through the hindlimb buds of E10.5 *Rosa26RlacZ/+; HoxB6Cre* embryos show that LacZ positive cells are not detectable in the hindlimb bud ectoderm (black arrowhead, Fig 5.7 I).

However, at this stage cre activity is detectable in the posterior region of the heart, which may lead to certain complications when used this cre line is used in combination with the conditional *Tbx5* (not shown).

Figure 5.7

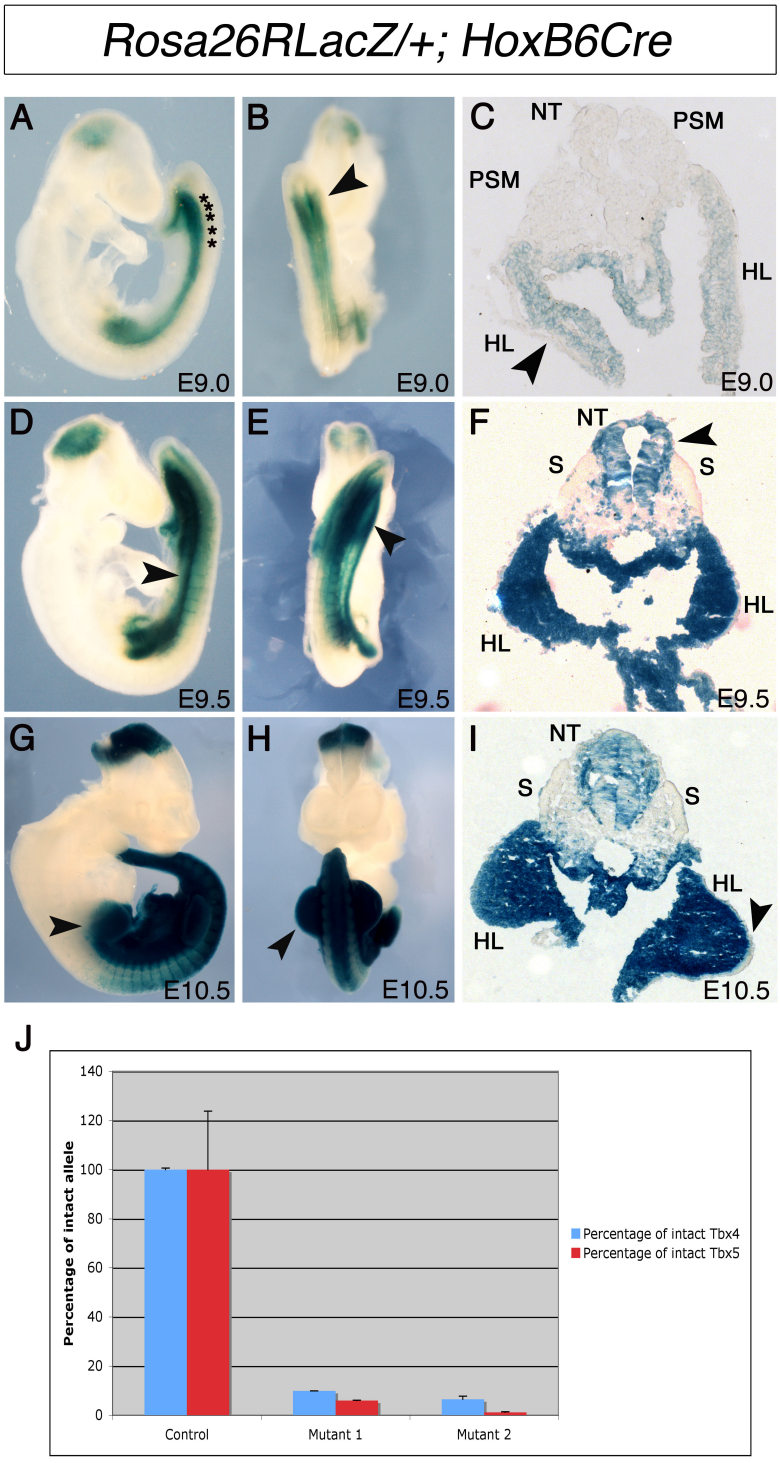

Figure 5.7 Cre recombinase activity takes place throughout the hindlimb bud, interlimb region, posterior forelimb bud, and midbrain in *HoxB6Cre* transgenic embryos.

Panels **A, D, G** are right-side lateral views of embryos. Panels **B, E, H** are ventral views of embryos. Panels **C, F, I** are transverse cryosections through the hindlimb regions of embryos. **A** E9.0 *Rosa26RlacZ/+; HoxB6Cre* embryo. LacZ activity corresponding to cre activity is throughout the hindlimb-forming region, interlimb region and posterior forelimb bud. **B** LacZ activity is detectable in the hindlimb-forming region of the embryo shown in panel A (black arrowhead). **C** Transverse cryosection through the hindlimb-forming region of an E9.0 *Rosa26RlacZ/+; HoxB6Cre* embryo. LacZ activity is in the hindlimb mesenchyme. **D** E9.5 *Rosa26RlacZ/+; HoxB6Cre* embryo. LacZ activity can be detected in the somites (black arrowhead). **E** LacZ activity is in the hindlimb buds of the embryo shown in panel D. **F** Transverse cryosection through the hindlimb buds of E9.5 *Rosa26RlacZ/+; HoxB6Cre* embryos, in which LacZ activity is in regions of the neural tube (black arrowhead). **G** E10.5 *Rosa26RlacZ/+; HoxB6Cre* embryo. LacZ activity is detectable in the posterior forelimb bud (black arrowhead). **H** LacZ activity is throughout the hindlimb buds of the same embryo shown in panel G. **I** Transverse cryosection through the hindlimb buds of an E10.5 *Rosa26RlacZ/+; HoxB6Cre* embryo. Cre activity is not detectable in the ectoderm (black arrowhead). **J** Graph showing that cre recombinase in $Tbx4^{lox/lox}$; $Tbx5^{lox/lox}$; *HoxB6Cre* recombines 96% of the target conditional DNA for both *Tbx5* and *Tbx4* ('y' - percentage of intact conditional allele, 'x' – embryo)

NT – neural tube, S – somite, PSM – presomitic mesoderm, HL - hindlimb

The deletion of *Tbx4* and *Tbx5* leads to the formation of a small mutant hindlimb bud.

I have shown that in *HoxB6Cre* embryos cre recombinase is active in the hindlimb-forming region prior to the initiation of the hindlimb bud from the LPM. I have subsequently used this line in combination with the mice carrying the conditional alleles for *Tbx5* and *Tbx4*. Cre recombinase in $Tbx5^{lox/lox}$; $Tbx4^{lox/lox}$; *HoxB6Cre* mutants is required to act upon 4 conditional alleles to fully delete both *Tbx5* and *Tbx4* in the hindlimb buds. Therefore to confirm that all 4 conditional alleles are recombined I have used QT PCR to analyze the levels of the intact alleles in mutant hindlimb buds. I have taken advantage of the primers

designed against the *LoxP* site of the conditional *Tbx4* allele as well as previously published primers designed against the *LoxP* sites of the conditional *Tbx5* allele (Hasson et al., 2005). I harvested hindlimb buds from E10.5 *Tbx5$^{lox/lox}$;Tbx4$^{lox/lox}$;HoxB6Cre* mutant embryos. As cre recombinase activity is not detected in the ectoderm, I removed it using dispase. Genomic DNA was extracted from the remaining mesenchyme and subjected to QT PCR analysis. I repeated this procedure for control hindlimb buds at the same stage.

I compared the levels of intact conditional *Tbx5* and *Tbx4* DNA from control hindlimb buds (n=4) to those in the mutant hindlimb buds (n=4). The level of intact conditional *Tbx5* and *Tbx4* in the control hindlimb bud is 100%, as these embryos are negative for cre recombinase. Compared to this, the mutant hindlimb buds carry 8% of intact *Tbx4* and 3% of intact *Tbx5*. These results therefore show that the vast majority of the conditional alleles for both *Tbx5* and *Tbx4* are recombined under the actions of cre recombinase (Fig 5.7J).

My analysis of cre recombinase activity in the *HoxB6Cre* transgenic line indicates that *Tbx5* and *Tbx4* expression is lost from the hindlimb-forming regions of *Tbx5$^{lox/lox}$; Tbx4$^{lox/lox}$; HoxB6Cre* mutant embryos. It should be noted that in *HoxB6Cre* transgenic embryos, cre activity is detectable in the forming chorio-allantois as well as the embryonic sac (not shown). Due to this, *Tbx4* expression is lost from the chorio-allantois leading to a failure of the placenta to form.

Tbx4$^{lox/lox}$; HoxB6Cre mutants do not survive past E11.0 and thus examination of the hindlimb phenotype is not possible past this stage. However, hindlimb bud formation takes place before E11.0, therefore hindlimb bud initiation can be examined in *Tbx5$^{lox/lox}$; Tbx4$^{lox/lox}$; HoxB6Cre* embryos.

During limb bud initiation, Fgf10 signals via ectodermal FgfR receptors to initiate the expression of *Fgf8* in the overlying ectoderm. This leads to the establishment of the positive feedback FGF signalling pathway, which drives limb bud outgrowth. *Fgf10* and *Fgf8* therefore serve as excellent molecular markers of hindlimb bud initiation and formation. I have used whole mount in situ hybridisation (WMISH) to examine the expression of *Fgf10* in the mesenchyme and *Fgf8* in the apical ectodermal ridge (AER). At E10.0, limb bud initiation has taken place and *Fgf10* expression is detectable in the hindlimb bud (Fig 5.8 A). At this same stage *Fgf8* expression is detectable in the AER (Fig 5.8 B). In E10.0 *Tbx4*$^{lox/lox}$*; HoxB6Cre* mutants, the size of the hindlimb bud is reduced and *Fgf10* expression is downregulated (Fig 5.8 C). Although reduced, *Fgf8* expression is detectable in the AER of the *Tbx4*$^{lox/lox}$*; HoxB6Cre* mutant hindlimb bud (Fig 5.8 D). *Tbx5*$^{lox/lox}$*; Tbx4*$^{lox/lox}$*; HoxB6Cre* mutant embryos have small hindlimb buds in which *Fgf10* expression is detectable, although at lower levels than both the control and *Tbx4*$^{lox/lox}$*; HoxB6Cre* mutant (Fig 5.8 E). *Fgf8* expression is also detectable at reduced levels in the AER of the hindlimb bud of the *Tbx5*$^{lox/lox}$*; Tbx4*$^{lox/lox}$*; HoxB6Cre* mutant embryo.

Figure 5.8

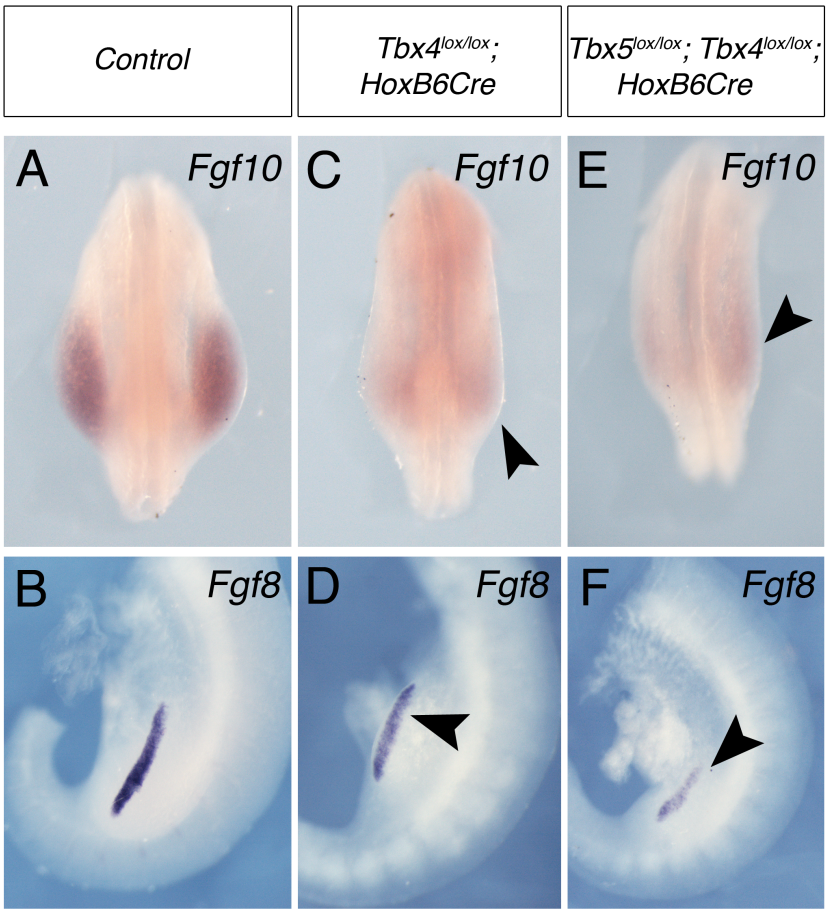

Figure 5.8 The double deletion of *Tbx5* and *Tbx4* from the hindlimb-forming region of the LPM results in the formation of a small mutant hindlimb bud.

Panels **A, C, E** are dorsal views of E10.0 hindlimb buds. Panels **B, D, F** are left-side lateral views of E10.5 hindlimb buds. **A** *Fgf10* is detectable throughout the hindlimb buds of control embryos. **B** *Fgf8* is detectable in the AER of control embryos. **C** *Fgf10* is downregulated in the hindlimb buds of *Tbx4$^{lox/lox}$; HoxB6Cre* mutant embryos (black arrowhead). **D** *Fgf8* is downregulated in the hindlimb bud AER of *Tbx4$^{lox/lox}$; HoxB6Cre* mutant embryos (black arrowhead). **E** *Fgf10* is downregulated in the hindlimb buds of *Tbx4$^{lox/lox}$; Tbx5$^{lox/lox}$; HoxB6Cre* mutant embryos (black arrowhead). **F** *Fgf8* is downregulated in the AER of *Tbx4$^{lox/lox}$; Tbx5$^{lox/lox}$; HoxB6Cre* mutant hindlimb buds (black arrowhead).

My analysis shows that a hindlimb bud still forms in the absence of both *Tbx5* and *Tbx4* from the hindlimb-forming region. *Tbx5$^{lox/lox}$; Tbx4$^{lox/lox}$; HoxB6Cre* mutant embryos appear to be smaller than *Tbx4$^{lox/lox}$; HoxB6Cre* mutants, which may be due to the activity of cre recombinase in the cardiac region of the embryo.

The deletion of *Tbx5* from parts of the forming heart may lead to a developmental delay, resulting in a small mutant embryo. This developmental delay may also account for the reduced size of the *Tbx5$^{lox/lox}$; Tbx4$^{lox/lox}$; HoxB6Cre* mutant hindlimb bud, as well as the reduced expression of *Fgf10* and *Fgf8*, compared to the size of the *Tbx4$^{lox/lox}$;HoxB6Cre* mutant hindlimb bud.

5.3 A HINDLIMB BUD FAILS TO FORM IN THE ABSENCE OF BOTH *Tbx4* AND *Pitx1*.

Pitx1 is a paired-like homeodomain transcription factor expressed in the hindlimb bud. It has previously been implicated in the specification of hindlimb identity (Lanctot et al., 1999; DeLaurier et al., 2006). It is possible that *Pitx1* expression is able to partially compensate for the loss of *Tbx4*, leading to the partial expression of *Fgf10* during hindlimb bud initiation.

The calcaneus, an identifiable feature of hindlimb identity, is present in *Tbx4$^{lox/lox}$; RetRV5Cre* hindlimbs showing that these mutant hindlimbs retain hindlimb specific features. This would suggest that *Pitx1* is still expressed in the absence of *Tbx4*, therefore conferring hindlimb identity on the mutant hindlimbs that form. To confirm this, I used WMISH to analyze *Pitx1* expression in the absence of *Tbx4*. In E10.5 control hindlimb buds at this stage, *Pitx1* is expressed throughout mesenchyme of the hindlimb bud(black arrowheads, Fig 5.9A). In E10.5 *Tbx4$^{lox/lox}$; RetRV5Cre* hindlimb buds, *Pitx1* expression can be detected throughout the hindlimb bud mesoderm (black arrowhead, Fig 5.9B). *Pitx1* expression does not appear to be downregulated in the mutant hindlimb bud.

Figure 5.9

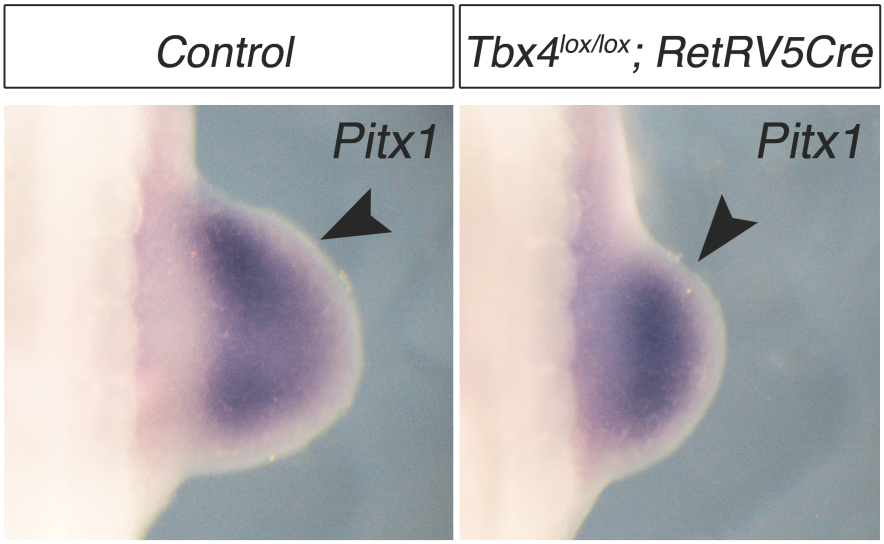

Figure 5.9 *Pitx1* expression is unchanged in the absence of *Tbx4* from the hindlimb.

Both panels (**A** + **B**) show dorsal views of the right hindlimb buds from E10.5 embryos. **A** *Pitx1* is expressed throughout the hindlimb bud of control embryos (black arrowhead). **B** *Pitx1* is expressed throughout the hindlimb bud of *Tbx4$^{lox/lox}$; RetRV5Cre* mutant embryos (black arrowhead).

These results are consistent with previously published data showing that *Pitx1* is upstream of *Tbx4* expression (Logan MP and Tabin CJ., 1999). It is therefore a possibility that *Pitx1* expression contributes towards hindlimb bud initiation. As I have already demonstrated, *Tbx4$^{lox/lox}$; RetRV5Cre* mutants live post birth, which allows for detailed analysis at late stages. For this reason I have chosen to use the *Tbx4$^{lox/lox}$; RetRV5Cre* mutant for this experiment in combination with the *Pitx1$^{-/-}$* null mutant (Szeto et al., 1999) to delete conditional *Tbx4* and *Pitx1* from the hindlimb-forming region.

By E17.5 control hindlimbs have achieved full limb outgrowth (Fig 5.10 A, A'). At this stage in *Pitx1$^{-/-}$* mutants, the femur and autopod are reduced in length (black arrow, Fig 5.10 B'). Additionally mutants also present with severe micrognathia lower jaw (recessed lower jaw) (black arrow, Fig 5.10 B). Hindlimb

defects are phenotypically more severe in *Tbx4*$^{lox/lox}$*; RetRV5Cre* mutant embryos, which present with severely shortened hindlimbs (black arrow Fig 5.10 C'). In striking contrast, *Pitx1*$^{-/-}$*; Tbx4*$^{lox/lox}$*; RetRV5Cre* mutants have lost hindlimb outgrowth as no residual elements of the hindlimb can be detected in embryos (Fig 5.10 D'). These mutants also present with micrognathia, which is consistent with the phenotype observed in *Pitx1*$^{-/-}$ null mutants (black arrow, Fig 5.10 D).

Figure 5.10

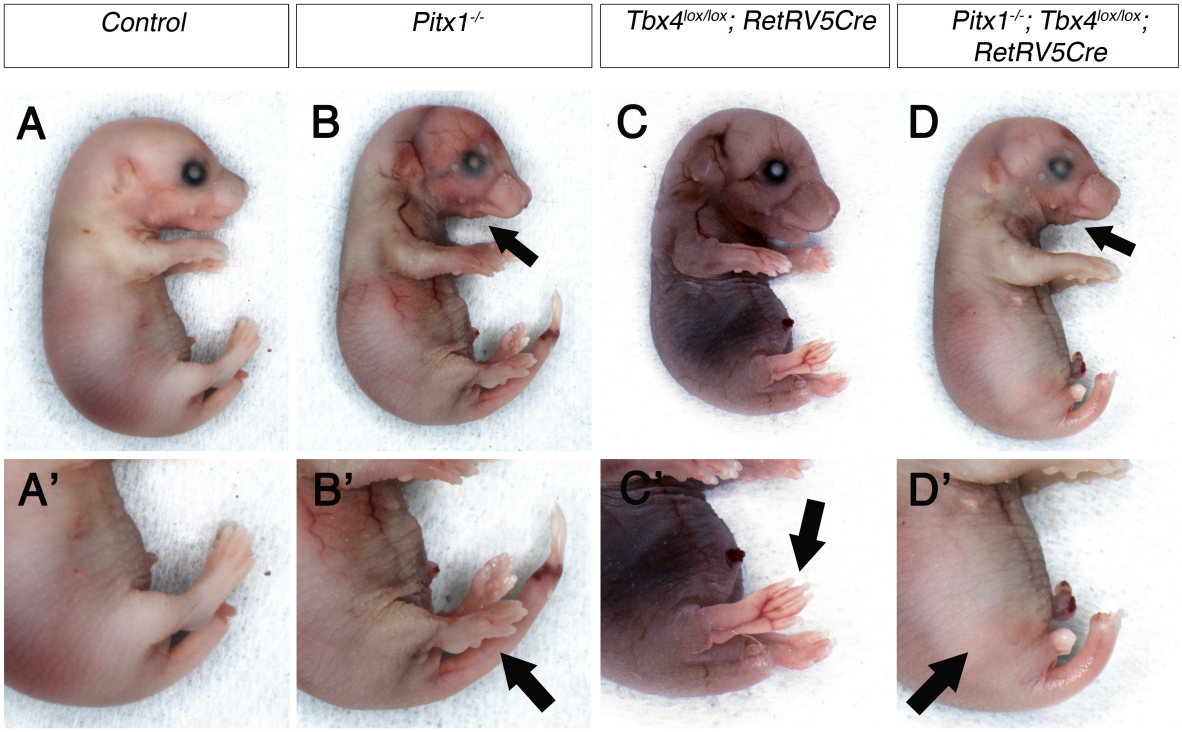

Figure 5.10 Deletion of both *Pitx1* and *Tbx4* from the hindlimb region of the LPM results in a loss of hindlimb outgrowth.

All panels show the right-side lateral views of E17.5 embryos. Panels marked **(')** are higher magnifications of the hindlimbs of E17.5 embryos shown in panels **A-D**.

A Control embryo. **A'** Closeup of the control hindlimb. **B** *Pitx1*$^{-/-}$ null mutant embryo. The lower jaw is recessed (black arrow) and the hindlimb is truncated (black arrow, **B'**). **C** *Tbx4*$^{lox/lox}$*; RetRV5Cre* mutant embryo. The hindlimb is severely truncated (black arrow, **C'**). **D** *Pitx1*$^{-/-}$*; Tbx4*$^{lox/lox}$*; RetRV5Cre* mutant embryo. The lower jaw is recessed (black arrow) and the hindlimb has not formed (black arrow, **D'**).

Skeletal preparations of control E17.5 embryos using alcian blue and alizarin red staining shows the presence of all the hindlimb elements including the pelvic girdle, femur, tibia, fibula and autopod (Fig 5.11A). Similar analysis of an E17.5 *Pitx1*$^{-/-}$*; Tbx4*$^{lox/lox}$*; RetRV5Cre* mutant reveals that all of these hindlimb elements are lost (red arrow, Fig 5.11B). Unlike previously published mouse mutants in which hindlimb outgrowth has been disrupted, there are no pelvic rudiments of the hindlimb present in *Pitx1*$^{-/-}$*; Tbx4*$^{lox/lox}$*; RetRV5Cre* mutants (Sekine et al., 1999; De Moerlooze et al., 2000).

Figure 5.11

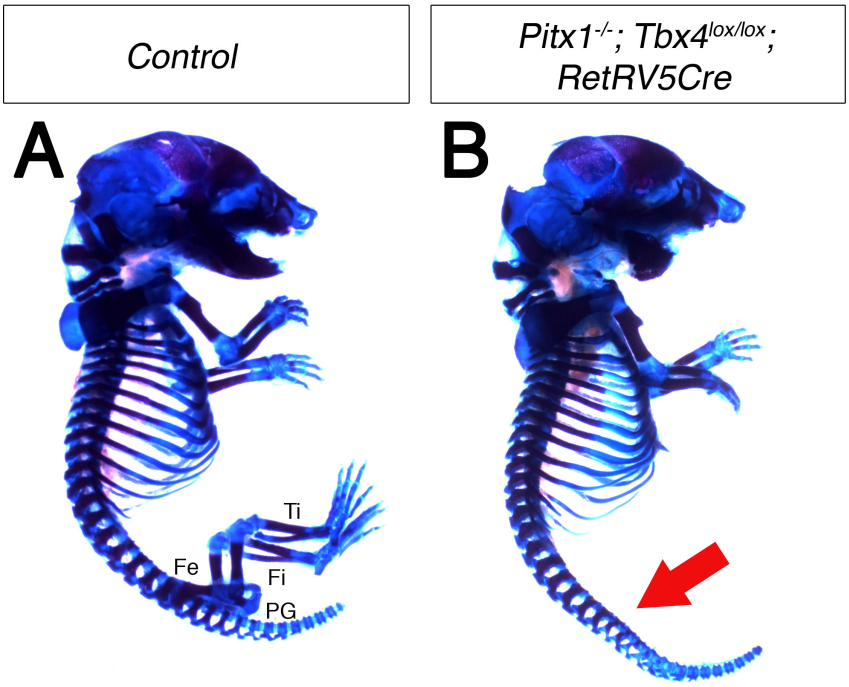

Figure 5.11 Deletion of *Pitx1* and *Tbx4* from the hindlimb region of the LPM leads to the total loss of all hindlimb skeletal elements.

Both panels show the right-side lateral views of skeletal staining of E17.5 embryos.

A Control embryo **B** *Pitx1*$^{-/-}$*; Tbx4*$^{lox/lox}$*; RetRV5Cre* mutant embryo. All elements of the hindlimb are lost, including the pelvic girdle (red arrow).

Fe – femur, Ti – tibia, Fi – fibula, PG – pelvic girdle

As I have written in previous chapters, limb outgrowth and formation is complete by E17.5 days. To examine whether the initiation of the hindlimb bud is affected in *Pitx1*$^{-/-}$*; Tbx4*$^{lox/lox}$*; RetRV5Cre* mutants I have analyzed *Fgf10* expression in E10.5 embryos. Hindlimb bud initiation takes place at E10.0 and by E10.5 a hindlimb bud has formed. In E10.5 control embryos, the hindlimb bud is a prominent outgrowth of the LPM and *Fgf10* expression can be detected in the limb bud mesenchyme (black arrowhead, Fig 5.12A). In contrast, it is clear that in *Pitx1*$^{-/-}$*; Tbx4*$^{lox/lox}$*; RetRV5Cre* embryos a hindlimb bud has not formed by E10.5. Significantly, *Fgf10* expression cannot be detected by WMISH. These results show that in the absence of *Tbx4* and *Pitx1*, *Fgf10* is not transcribed and as a consequence hindlimb bud initiation and subsequent outgrowth is completely lost. This implicates a partial contribution towards *Fgf10* transcription from *Pitx1* to complement the primary role of *Tbx4* during hindlimb bud initiation.

Figure 5.12

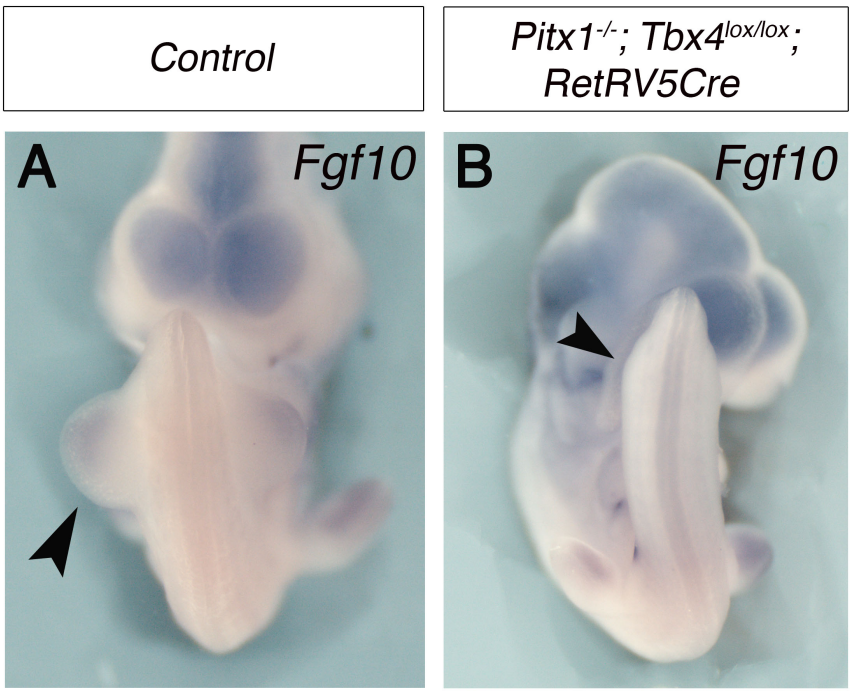

Figure 5.12 Hindlimb bud initiation fails to occur in the absence of both *Pitx1* and *Tbx4*.

Both panels are ventral views of E10.5 embryos. **A** *Fgf10* expression is detectable in the hindlimb bud of a control embryo (black arrowhead). **B** A hindlimb bud has not formed in a *Pitx1*$^{-/-}$*; Tbx4*$^{lox/lox}$*; RetRV5Cre* mutant embryo, nor can *Fgf10* expression be detected (black arrowhead)

CHAPTER SIX:

DISCUSSION

6.1 DISRUPTION OF *Tbx5* DURING FORELIMB BUD INITIATION LEADS TO LEFT-BIASED ASYMMETRICAL FORELIMB DEFECTS.

In this section I discuss the significance of the results that I presented in chapters three and four. Through my analysis of various mouse mutants, I have shown a novel role for threshold levels of *Tbx5* in ensuring the bilaterally symmetric formation of the left and right forelimb, the disruption of which was originally observed in HOS patients.

Hypomorphic levels of the *Prx1-Tbx* transgene in the *Tbx5$^{lox/lox}$;Prx1Cre;Prx1-Tbx* mutant demonstrate the importance of threshold levels of *Tbx5* during forelimb bud initiation.

Previously published work has demonstrated that in the total absence of *Tbx5*, the left and right forelimbs completely fail to form (Agarwal et al., 2003; Rallis et al., 2003). However, I have shown in chapter three that hypomorphic levels of the *Prx1-Tbx* transgene in the *Tbx5$^{lox/lox}$; Prx1Cre; Prx1-Tbx* mutant leads to the formation of substantial defects in both the left and right forelimb. Significantly, the left forelimb is always more affected than the right. When these data are taken together, the importance of threshold levels of *Tbx5* expression starts to become clear.

When levels of *Tbx5* reach a threshold in the left and right forelimb buds, normal symmetrical forelimb bud formation takes place. Forelimb defects start to develop in both the left and right forelimbs when levels of *Tbx5* fall below the threshold. The severity of the forelimb defects increases as the amount of *Tbx5* decreases in the left and right forelimb buds (Fig 6.1). When there is no *Tbx5* expression at all, forelimb bud initiation does not take place and the forelimbs fail to form (Agarwal et al., 2003; Rallis et al., 2003). The limb defects are consistently

more severe in the left limb than the right. This suggests that the threshold levels of Tbx5 activity required for symmetrical forelimb initiation may be different in the left and right forelimb-forming regions.

Figure 6.1

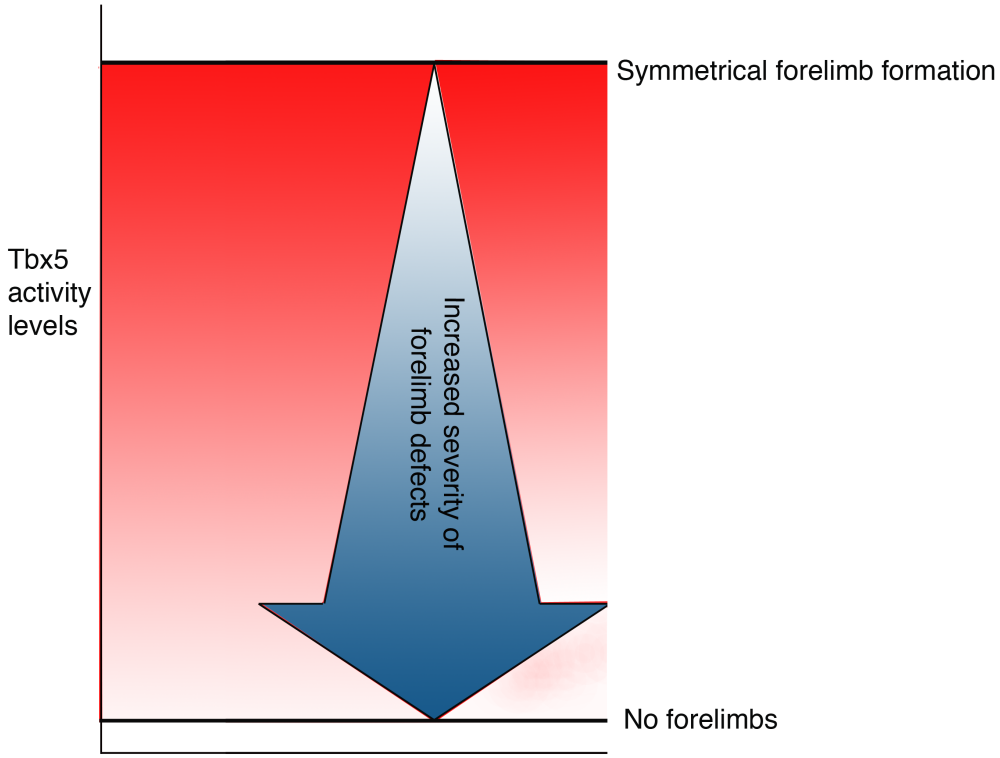

Figure 6.1 The severity of forelimb defects increases with the decrease in *Tbx5* expression in the left and right forelimb buds. When *Tbx5* activity levels reach a threshold across the left and right forelimb buds, symmetrical forelimb formation occurs. However, when *Tbx5* activity levels fall anywhere below this threshold, forelimb defects occur. The severity of the forelimb defects increase as the level of *Tbx5* decreases until forelimbs completely fail to form.

Previous work produced in this laboratory has demonstrated that when *Tbx5* is deleted post forelimb bud formation at E10.5, forelimb bud outgrowth is not impeded (Hasson et al., 2007). A small number of mutants, from which *Tbx5* is deleted during nascent forelimb bud formation, display forelimb defects predominantly in the left forelimb (Hasson et al., 2007). The results of this study indicate that there is a brief time window in which *Tbx5* expression is necessary for

forelimb bud initiation, and after this time window has passed *Tbx5* does not have a role in further forelimb outgrowth. My results in which asymmetrical limb bud differences can be detected at an early stage suggest that the threshold requirement for Tbx5 activity is during forelimb bud initiation and not the later stages of limb development.

Mutant embryos generated using two different approaches display the same phenotypic variation in forelimb defects.

Using two different strategies, I have generated and characterised mutants that both display left-biased asymmetrical forelimb defects. *Fgf10* is the only known direct target of Tbx5 activity during forelimb bud initiation. Therefore, as *Tbx5* is mosaically deleted in the *Tbx5$^{lox/lox}$; Prx1Cre(98)* mutant, it can be expected that the Fgf10 ligand will be mosaically expressed. In *Tbx5$^{lox/lox}$; Prx1Cre; Prx1-Tbx* mutants, the prediction would be that hypomorphic levels of *Prx1-Tbx* transgene activity would lead to hypomorphic levels of *Fgf10* in every cell in the nascent forelimb bud. Therefore, in both mouse mutants, the net amount of Fgf10 ligand secreted during left and right forelimb bud initiation will be sub-optimal.

Phenotypic variation in the extent of the forelimb defects can be observed across individual examples of both the *Tbx5$^{lox/lox}$; Prx1Cre(98)* and *Tbx5$^{lox/lox}$; Prx1Cre; Prx1-Tbx* mutants. The two strategies used to generate these mutant embryos rely on the activity of cre recombinase to delete a conditional allele of *Tbx5*. The onset of cre activity may also vary from embryo to embryo within a single litter. Any variation in the temporal activity of cre may affect the effective spatial activity, as cells within the forelimb-forming region will be exposed to different levels of Tbx5 activity at a fixed time point. It should be noted, however, that within families of HOS sufferers individuals carrying the same mutation in *TBX5* can often

present with an extreme range in the severity of the upper limb phenotypes (Basson et al., 1999; Boogerd et al., 2010).

The left forelimb is consistently more affected than the right in both *Tbx5$^{lox/lox}$; Prx1Cre(98)* and *Tbx5$^{lox/lox}$; Prx1Cre; Prx1-Tbx* mutants.

Significantly, a phenotypic variation I detected within individual embryos was that the left forelimb is consistently more affected than the right. In chapter three I have described various control experiments that I carried out to demonstrate, as accurately as possible, that the deletion of *Tbx5* is bilaterally symmetric. Therefore the left bias to the severity of the forelimb defects in both the *Tbx5$^{lox/lox}$; Prx1Cre(98)* and *Tbx5$^{lox/lox}$; Prx1Cre; Prx1-Tbx* mutants is not due to an increase in the temporal or spatial activity of cre recombinase in the left forelimb-forming region. Additionally, *Prx1-Tbx* expression is bilaterally symmetric in the left and right forelimb-forming regions of *Tbx5$^{lox/lox}$; Prx1Cre; Prx1-Tbx* mutant embryos, therefore the left-sided bias cannot be ascribed to lower rescue transgene levels in the left forelimb-forming region than the right. Additionally, optimal levels of Prx1-Tbx activity have been demonstrated to rescue forelimb bud initiation and subsequent formation (Minguillon et al., 2009), therefore the forelimb defects seen in the *Tbx5$^{lox/lox}$; Prx1Cre; Prx1-Tbx* mutant cannot be attributed to a difference between the activity of *Tbx5* and *Prx1-Tbx*. I have shown that the left-sided forelimb defects are not due to an experimental artefact thus demonstrating that the left forelimb-forming region of the LPM is more sensitive to sub-optimal levels of Tbx5 activity than the right.

The effects of the left-right pathway persist in the right and left forelimb forming regions of the LPM.

The occurrence of situs inversus in *Tbx5$^{lox/lox}$; Prx1Cre; Prx1-Tbx; INV/INV* mutants indicates that the left-right pathway has been reversed such that genes

previously expressed on the left side, i.e. *Nodal*, *Pitx2* and *lefty1/2* are now expressed on the right side. In these mutants, the right forelimb is more affected than the left. My results are consistent with previous studies such as those published by Kocher-Becker et al who found that the *polydactyly* (*py*) mutant displays forelimb defects that are more severe in the left forelimb than the right. However, when this mutant is bred onto an *iv* background, *py* mutants with situs inversus display forelimb defects that are more severe in the right forelimb than left (Kocher-Becker et al., 1991).

My results, as well as those mentioned above, suggest that the effects of the left-right pathway persist in the regions of the LPM that will give rise to the left and right forelimb buds. Expression of genes such as *Nodal* and *lefty1/2* is reported to be lost from the LPM by E8.0 (Meyers and Martin., 1999), however the downstream actions of these genes may persist to later stages. Additionally, *Pitx2* expression is reported to still persist in the left LPM at E9.5 (Shih et al., 2007). It is possible that the lingering effects of the left-right pathway in the LPM may negatively interfere with the ability of the forelimb-forming regions to initiate FGF signalling. If that were so, then the left forelimb-forming region would have less FGF signalling taking place than the right. In order to buffer against such an event, Tbx5 activity would need to reach threshold levels in both the left and right forelimb-forming regions to counteract the asymmetric effects of the left-right pathway in the LPM.

***Tbx5* has a role in ensuring the symmetrical initiation of the left and right forelimb buds in a manner that is independent of its direct role in *Fgf10* transcription.**

I demonstrated in chapter four that transgenic *Fgf10*, when delivered from the *Z/EGFgf10* line, bilaterally symmetrically rescues forelimb outgrowth in *Fgf10*$^{-/-}$ null mutants that otherwise lack forelimbs. However, when the same line is used to deliver transgenic *Fgf10* to the *Tbx5*$^{lox/lox}$*; Prx1Cre; Prx1-Tbx* mutant, left-biased asymmetrical forelimb defects are still present. This indicates that optimal levels of *Fgf10*, which are sufficient to rescue forelimb formation in the *Fgf10*$^{-/-}$ mutant, are unable to rescue asymmetrical forelimb formation in the presence of hypomorphic levels of *Tbx5.* This suggests that *Tbx5* has a role in ensuring symmetrical forelimb bud initiation that is independent of its role in positive regulation of *Fgf10* transcription.

In the limb-forming regions, the Fgf10 ligand signals via FgfR2b to positively regulate *Fgf8* transcription in the overlying ectoderm. The Fgf8 ligand signals through FgfR2c in the mesenchyme to positively regulate *Fgf10* expression as one of its activities. For FGF signalling to take place the expression of both the ligands and receptors are required. *Tbx5*$^{lox/lox}$*; Prx1Cre; Prx1-Tbx; Z/EGFgf10* embryos have optimal levels of the Fgf10 ligand, but may not have optimal levels of other components of the FGF signalling pathway. It is possible that *Tbx5* may have a role in the transcription of other signalling components, for example *FgfR2c*. *Tbx5* is purported to be upstream of *Sall4* (Harvey et al., 2006; Koshiba-Takeuchi et al., 2006). *Sall4*, a transcription factor belonging to the *Sall* gene family, is required for the formation of the pectoral fin in zebrafish, a structure that is analogous to the forelimb in mice (Harvey et al., 2006). *Sall4* acts downstream of *Tbx5* during forelimb bud initiation and may have a direct role in the transcription of the *FgfR2c*

isoform of the FgfR2 receptor, thus providing an indirect role for *Tbx5* in *FgfR* transcription (Harvey et al., 2006; Koshiba-Takeuchi et al., 2006).

The presence of left-biased asymmetrical forelimb defects in *Tbx5$^{lox/lox}$;Prx1Cre;Prx1-Tbx;Z/EGFgf10* mutants suggest that despite the increased levels of Fgf10 ligand, FGF signalling is taking place asymmetrically between the left and right forelimb buds. I have not observed an asymmetrical difference between the levels of di-phosphorylated ERK (dp-ERK), a downstream component of FGF signalling, in the left and right forelimb buds of E10.5 *Tbx5$^{lox/lox}$; Prx1Cre; Prx1-Tbx; Z/EGFgf10* mutants. However, this may be due to the fact that this assay is not sensitive enough to quantitatively detect any subtle differences.

Threshold levels of *Tbx5* buffer against an asymmetrical difference between the left and right forelimb-forming regions to ensure symmetrical forelimb bud initiation.

I have shown that mutants with optimal levels of Fgf10 ligand and hypomorphic Prx1-Tbx activity display forelimb defects that are more severe in the left forelimb than the right. My data suggests that there may be an asymmetrical difference in Fgf ligand signal transduction in the left and right forelimb-forming regions. Reduced FgfR2c receptor activity, or an increase in antagonistic activity at the level of the receptor, in the mesenchyme of the left forelimb region compared to the right would lead to lower FGF signalling in the left forelimb bud. Therefore, the left forelimb-forming region may have a higher threshold requirement for optimal FgfR2c receptor activity than the right. Bilaterally symmetric threshold levels of Tbx5 activity would then be required to ensure that both the left and right forelimb-forming regions experience optimal FGF signalling. When levels of Tbx5 activity fall below

this threshold in both the left and right forelimb regions, then FGF signalling in the left forelimb-forming region will be reduced to a greater extent than in the right. Therefore the left forelimb will form with more severe defects than the right (Fig 6.2).

Figure 6.2

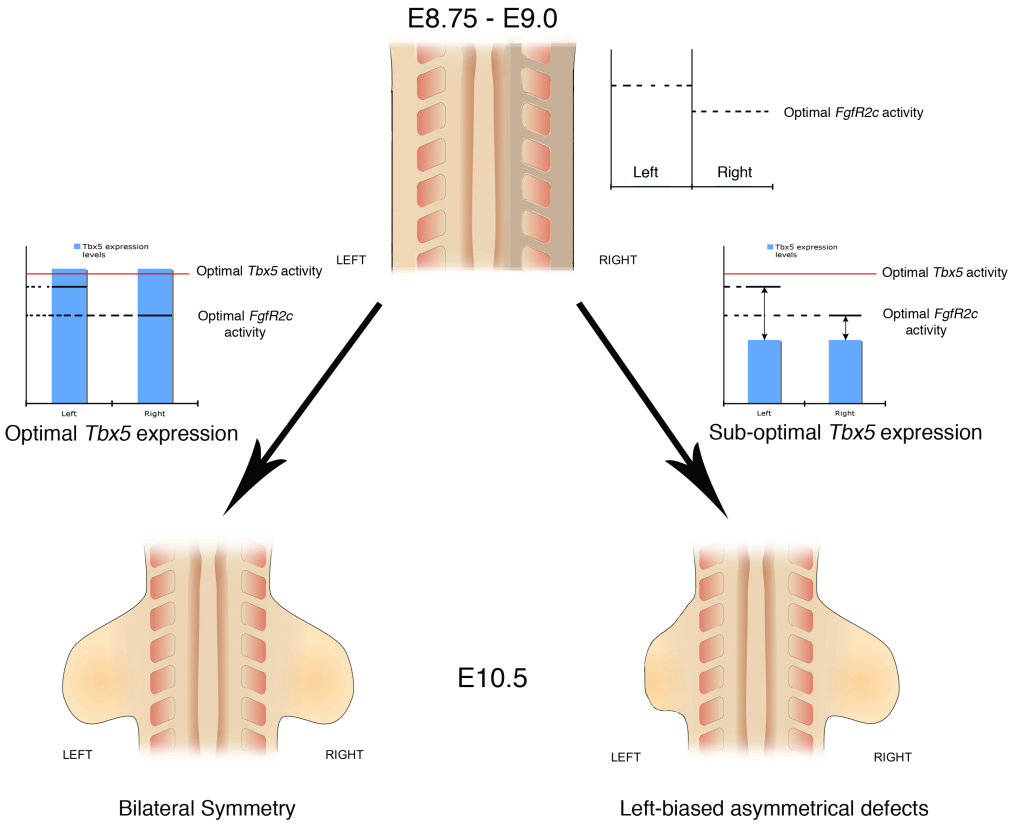

Figure 6.3 Threshold levels of Tbx5 activity are required to ensure the bilaterally symmetric initiation of the left and right forelimb buds from the lateral plate mesoderm (LPM).

An inherent asymmetrical difference in the left and right LPM prior to forelimb bud initiation at E8.75 (shown through a difference in colour) leads to a difference in threshold requirements for FgfR2c activity. Optimal Tbx5 activity in the left and right forelimb regions ensures that FgfR2c activity is at optimal levels in both the left and right forelimb regions. Sub-optimal Tbx5 activity levels in the left and right forelimbs leads to a reduction in FgfR2c activity in the left forelimb. This reduction is greater in the left than that in the right, so the left forelimb develops with more defects than the right.

FgfR2c is a trans-membrane tyrosine kinase receptor expressed in mesenchymal cells of the limb bud. It is possible that prior to forelimb bud initiation,

it is expressed at lower levels in the left forelimb-forming region of the LPM than the right. Threshold levels of Tbx5 activity would be required to ensure that *FgfR2c* is expressed at the threshold levels for both the left and right forelimb regions. In the presence of hypomorphic levels of Tbx5 activity, hypomorphic *FgfR2c* expression would be unable to compensate for the initial asymmetrical difference in expression. Therefore FGF signalling would take place at a reduced level in the left forelimb bud compared to the right.

Sproutys 2 and 3 are downstream components of the FGF signalling pathway, and also act as antagonists to the pathway. Sprouty 2 is believed to inhibit the phosphorylation of the downstream component Erk1/2 by binding to the intracellular component of FgfR2 (Hanafusa et al., 2002; Mason et al., 2004). High levels of Sprouty activity in the left forelimb region would lead to a reduction in FgfR2 activity. Tbx5 activity may act to inhibit or repress Sprouty so that optimal FGF signalling can take place during left and right forelimb bud initiation. Alternatively, Tbx5 activity may increase the levels of FGF signalling in the left and right forelimb-forming regions so that the asymmetrical differences due to Sprouty expression are overcome.

It has recently been reported, through analysis of a transgenic LacZ reporter line, that the isoform of *Pitx2*, *Pitx2c*, is expressed throughout the left LPM of E9.0 embryos (Furtado et al., 2011). It is therefore possible that Pitx2c activity may interfere with FGF signalling in the left LPM, thus restricting left forelimb bud initiation.

The possible mechanism that I have described postulates that were it not for the threshold levels of Tbx5 activity, limb initiation would take place asymmetrically. In 2005, Vermot and Pourquie proposed that somite formation requires retinoid

signalling to ensure that the somites form in bilateral symmetry. The authors found that the incubation of chick embryos in the presence of disulfiram, an inhibitor of retinoic acid synthesis, leads to a reduced number of left-sided somites compared to those on the right side (Vermot and Pourquie., 2005). This has since been repeated in the mouse using the *rere* mouse mutant to disrupt retinoid signalling, indicating a mechanistic conservation between species. Interestingly, in the mouse the number of right-side somites is reduced compared to the left. The authors also demonstrated that when crossed into the *iv* mutant background, *rere; iv/iv* mutants display a reduced number of left-sided somites (Vilhais-Neto et al., 2010).

The retinoid signalling pathway has been co-opted in the developmental program of organs such as the nervous system and the eye, and has been shown to play a substantial role during limb bud development (Grandel et al., 2002; Solomin et al., 1998; Mercader et al., 2000). Mutants that are hypomorphic for retinoid signalling in the left and right forelimb also present with left-biased asymmetrical forelimb defects (Niederreither et al., 2002; Sandell et al., 2007). However, it is possible that *Tbx5* is a downstream target of retinoid signalling, making it unclear whether these asymmetrical defects are a direct result of hypomorphic retinoic acid signalling in the left and right or are in fact due to hypomorphic levels of *Tbx5* caused by disrupted retinoid signalling. If the distinction could be determined and it was shown that hypomorphic levels of retinoid signalling directly leads to left-biased asymmetrical forelimb defects, then these mouse mutants could be used to further dissect the interplay between retinoid signalling and Tbx5 activity during the initiation of the left and right forelimb buds.

An alternative explanation to the model I have described above involves the vascular supply to the forelimbs during development. It has been observed that

during normal embryonic development the right forelimb receives a larger blood supply from the umbilical cord (Brown et al., 1989). Therefore formation of the left forelimb may be restricted due to the lesser supply of blood during development. However, there has not been a similar observation reported for the hindlimbs, which can present with asymmetrical defects.

The mosaic deletion of *Tbx5* in *Tbx5$^{lox/lox}$; Prx1Cre(98)* mutants may model the possible effects of allele silencing in HOS patients.

In *Tbx5$^{lox/lox}$; Prx1Cre(98)* mutants *Tbx5* is conditionally deleted in a mosaic manner from the left and right forelimb-forming regions. As a consequence, both forelimbs develop with substantial defects that are more severe in the left than the right. These forelimb defects model those observed in the majority of patients suffering from HOS, which is associated with heterozygous mutations in *TBX5* (Boogerd et al., 2010). It is, however, unclear how the mosaic loss of Tbx5 activity in *Tbx5$^{lox/lox}$; Prx1Cre(98)* mutants correlates with the reported heterozygous mutations in *TBX5* in HOS patients. A possible explanation involves the phenomenon of allele silencing.

The majority of autosomal genes require both the maternal and paternal alleles for normal gene expression. However, a small number of genes have been identified in which mono-allelic expression occurs (reviewed in Kacem and Feil 2009). For these genes a random decision is made during development in which either the maternal or paternal copy of the gene is repressed. This process is controlled by regions of DNA known as imprinting control regions (ICR), which are marked by DNA methylation. It appears that the mechanisms through which ICRs control the expression of certain alleles varies, depending on the gene and ICR. ICRs that are located nearby to the target allele may recruit chromatin-remodelling

proteins to the locus that modify the histones. This can cause the chromatin to become compact, interfering with the transcription of the target allele (reviewed in Kacem and Feil 2009). Another suggested mechanism involves the transcription of long non-coding RNAs from ICRs that may interfere with the transcription of the allele (reviewed in Brosnan and Voinnet 2009).

Insulin-like growth factor 2 (*Igf2)* is an example of an imprinted gene. *Igf2* acts as a growth factor during embryo development and is expressed only from the paternal allele, due to repression of the maternal allele (Wu et al., 1997). If the imprinting process is disrupted, then the subsequent overexpression of *Igf2* will lead to the formation of tumours and 'visceromegaly', an overgrowth of the visceral organs such as the kidneys and liver (Brown et al., 1996).

Although unreported to date, it is possible that *TBX5* may be subject to allele silencing. It is thought that both copies of *TBX5* are required for normal gene expression in humans. In the case of HOS, individuals who carry one mutated copy of the gene present with the characteristic upper limb and heart defects through haploinsufficiency for *TBX5*. Expression of one functional allele in the event of heterozygous loss-of-function mutations in *TBX5* is believed to be insufficient for the gene to carry out its normal functions. However, if *TBX5* were subject to allele silencing, then expression from one functional copy is sufficient for correct heart and upper limb formation. In HOS patients, the combination of a heterozygous loss-of-function mutation in one allele and silencing in the other allele would result in some cells that are effectively 'null' for *TBX5* expression. In other cells the allele carrying the mutation may be silenced, leaving one functional *TBX5* allele. In this scenario, the mono-allelic expression is sufficient and the cell would experience normal TBX5 activity (Fig 6.3). If this were the case, then HOS patients would be effectively

mosaic for cells in which *TBX5* is functioning normally and cells in which *TBX5* is non-functional. This will in turn lead to the development of various defects in the left and right upper limbs, with the left more affected than the right.

Figure 6.3

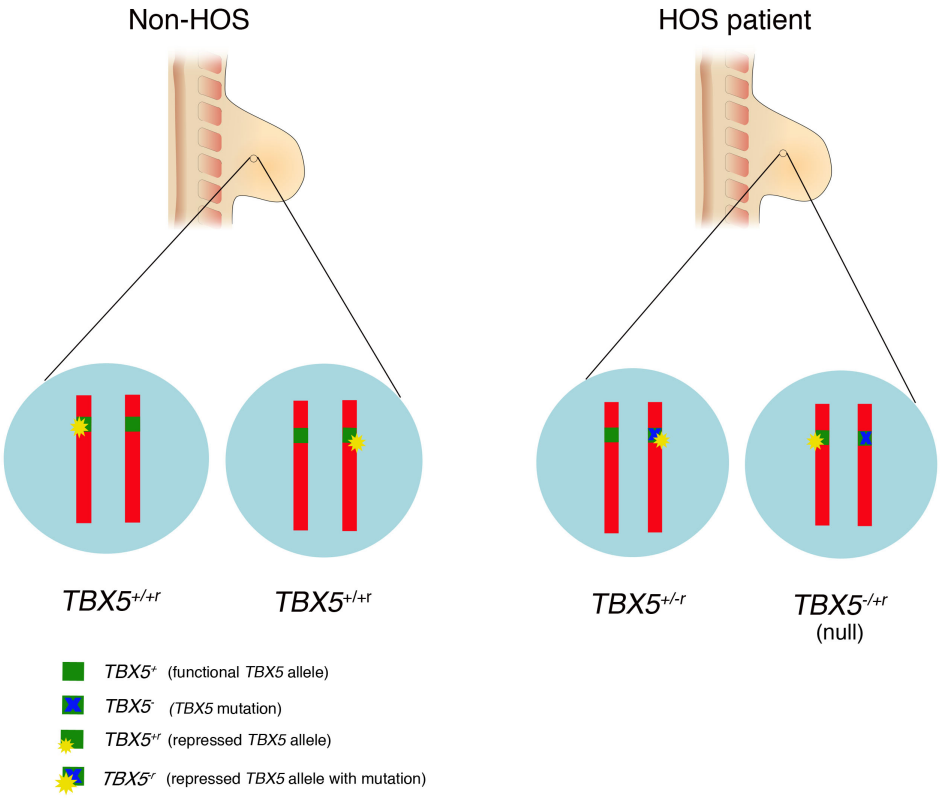

Figure 6.3 A model of how allele silencing in HOS patients may lead to a mosaic of cells in the forming limb that are effectively *TBX5* 'null' while other cells have functional *TBX5* expression levels. Allele silencing leading to the mono-allelic expression of *TBX5* is sufficient for normal upper limb formation. In HOS patients, however, allele silencing would produce a mosaic of cells that are *TBX5* null and cells expressing normal *TBX5* levels.

As I have mentioned in chapter three, *Tbx5*$^{lox/+}$*; Prx1Cre* and *Tbx5*$^{+/-}$ embryos do not display any obvious forelimb phenotypes (Bruneau et al., 2001; Rallis et al., 2003). If *Tbx5* is mono-allelicly expressed in the mouse, then these mutants should display a limb phenotype similar to that of HOS patients. The lack of any obvious

phenotype does not provide support for this model. However, it is entirely possible that *Tbx5* is bi-allelicly expressed in the mouse and mono-allelicly expressed in humans.

6.2 *Tbx4* AND *Pitx1* ARE BOTH REQUIRED FOR NORMAL HINDLIMB BUD INITIATION.

In this section I discuss the results presented in chapter five. *Tbx4* is the paralogue of *Tbx5*, expressed in the hindlimb-forming region of the LPM. I have demonstrated that in the absence of *Tbx4* the formation of a mispatterned hindlimb takes place and that both *Tbx4* and *Pitx1* are required for hindlimb bud initiation.

FGF signalling in the posterior hindlimb bud drives hindlimb outgrowth in the *Tbx4$^{lox/lox}$; RetRV5Cre* mutant.

The observation made in this study that a hindlimb is capable of being formed in the absence of *Tbx4* is in contradiction of those made by Naiche and Papaioannou in 2003 (Naiche and Papaioannou., 2003). In this study, the authors cultured wildtype and *Tbx4$^{lox/lox}$; β-actinCre* mutant hindlimb explants for 4-7 days. They observed the formation of hindlimb-like features in the wildtype cultures after three days, but at the same timepoint could not identify any hindlimb-like features in the cultured mutant explants (Naiche and Papaioannou., 2003). The authors concluded from this that in the absence of *Tbx4* hindlimb bud formation does not continue after the initiation stage. It is possible that the failure of the mutant hindlimb buds to develop further was due to problems with the technically challenging limb culture assay. By using the *RetRV5Cre* line to more precisely delete *Tbx4* from the hindlimb-forming region, I was able to bypass the early embryonic lethality observed in the *Tbx4$^{lox/lox}$; β-actinCre* mutants and generate embryos with hypoplastic hindlimbs.

In the absence of *Tbx4*, *Fgf10* is still expressed, albeit at lower levels, in the mesenchyme of the mutant hindlimb bud. However, *Fgf8* expression can only be detected in the posterior AER. A possible reason for the lack of *Fgf8* expression in the anterior AER may be due to a reduction in anterior mesenchymal *FgfR2c* expression compared to posterior. This would mean that Fgf8 signalling activity would not take place in the anterior mesenchyme. During hindlimb bud initiation in mutant embryos, Fgf10 signals through FgfR2b to initiate *Fgf8* transcription in the anterior AER. Fgf8 may not be able to signal in the underlying mesenchyme due to the lack of *Fgfr2c* expression, one of the results of which would be a failure in the upregulation of *Fgf10* in the anterior mesenchyme. As the initially hypomorphic expression of *Fgf10* is not upregulated in the anterior mesenchyme, the positive feedback loop breaks down and *Fgf8* expression in the anterior AER would decrease until it could no longer be detected (Fig 6.4). As a result a FGF signalling positive feedback loop will only be established in the posterior region of the hindlimb bud. Antibody staining against dp-ERK, a downstream component of FGF signalling, should be able to confirm whether this is correct.

Figure 6.4

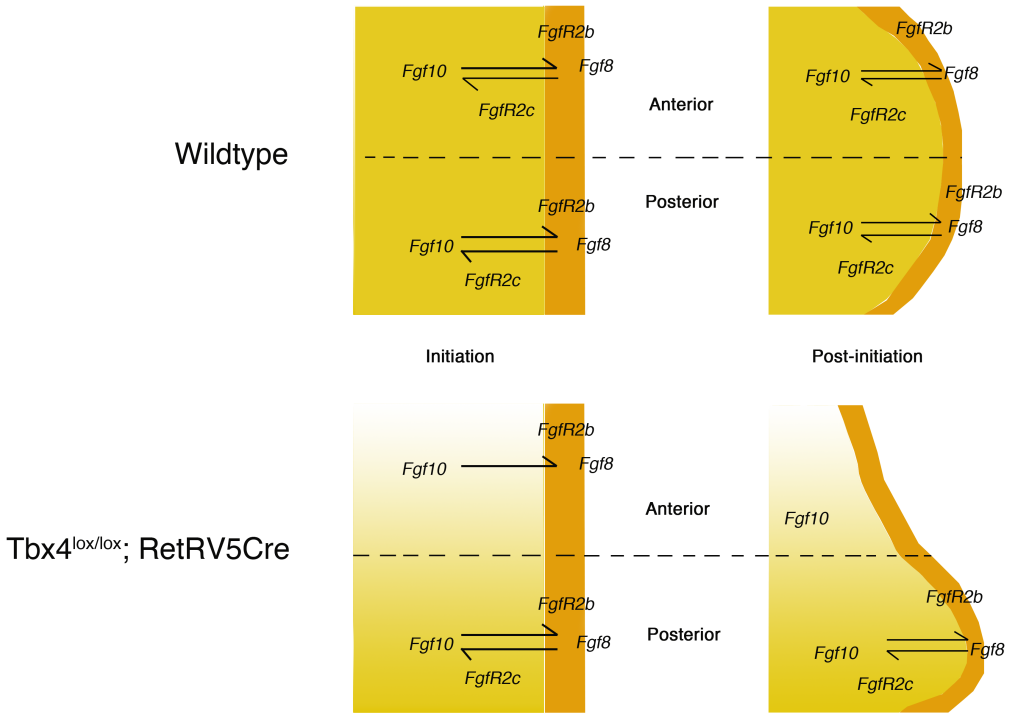

Figure 6.4 A lack of anterior *FgfR2c* expression may lead to the loss of *Fgf8* expression in the anterior AER of *Tbx4$^{lox/lox}$; RetRV5Cre* mutant hindlimbs. *FgfR2c* is expressed throughout the hindlimb bud, which enables Fgf8 to signal in the mesenchyme underlying the AER. During hindlimb initiation in the mutants, a lack of *FgfR2c* expression in the anterior mesenchyme (represented by the colour gradient) will lead to a failure of the Fgf8 ligand to signal in the mesenchyme. Due to the lack of *Fgf10* upregulation in later stage hindlimb buds, *Fgf8* expression is lost from the anterior AER and can no longer be detected.

It will be interesting to analyze *Fgf8* expression in the AER and *FgfR2c* expression in the mesenchyme of mutant and control hindlimb buds during the limb bud initiation stage. It may also be useful to investigate the possible roles of other components of the FGF signalling pathway, such as *Sproutys 2, 3,* and *4*. As well as being downstream components, these factors act as FGF signalling antagonists. In the absence of *Tbx4*, *Sprouty 2, 3,* or *4* may be overexpressed in the anterior

mesenchyme of the hindlimb bud thus inhibiting the anterior establishment of the FGF signalling pathway.

Loss of the anterior hindlimb bud may lead to the loss of the proximal structures of the hindlimb.

A key and striking feature of *Tbx4$^{lox/lox}$; RetRV5Cre* mutant hindlimbs is the lack of proximal elements, i.e. the pelvic girdle and the femur. Little is known about the development of the pelvic girdle. Work done in the chick has demonstrated that the pelvic girdle precursors are derived from the LPM through signals emanating from the somites and the region of the mesoderm that is distal to the somites (Malashichev et al., 2005; Malashichev et al., 2007). According to Pomikal and Streicher, the pelvis originates within the hindlimb as a small condensation of cartilage precursors that go on to form the ilium. During later development (E14.5 and onwards) the ilium elongates and thickens to narrow the gap between the hindlimb and spine and eventually forms the pelvic girdle (Pomikal and Streicher., 2010).

I have demonstrated that the anterior region of the *Tbx4$^{lox/lox}$; RetRV5Cre* mutant hindlimb bud does not continue outgrowth, although the posterior region does. It is possible that the proximal structures of the hindlimb may be derived from the anterior region of the nascent hindlimb. In *Tbx4$^{lox/lox}$; RetRV5Cre* hindlimbs the ilium may initially form, however due to the loss of the anterior hindlimb bud, it will not elongate. Therefore the gap between the axial skeleton and the hindlimb will not be bridged and the distal elements of the hindlimb will not be connected to the main body. This explanation would identify the cartilage fragment observed in the proximal region of the mutant hindlimb as the initial ilium rudiment.

To extend the initial whole mount in situ hybridisation analysis, a transgenic mouse line in which the *Col2a* promoter drives GFP fluorescence in the cartilage elements post E13.5 can be used (*Col2a-GFP*). By using optical projection tomography (OPT) to visualize the cartilage elements in *Col2a-GFP* embryos, a 3D model of pelvic girdle development can be produced. By using this transgenic line in combination with the *Tbx4*$^{lox/lox}$*; RetRV5Cre* mutant to visualize mutant hindlimb development, the formation of the hypoplastic hindlimb can be further analyzed.

Asymmetrical hindlimb defects develop in the absence of *Tbx4* expression from the left and right hindlimb-forming regions of the LPM.

In the *Tbx4*$^{lox/lox}$*; RetRV5Cre* mutants, the left hindlimb is often more affected than the right hindlimb. Asymmetrical hindlimb defects have been described in other mouse mutants such as the *R-spondin2* null. *R-spondin2* null mutants display syndactyly of the hindlimb defects, with greater severity in the left hindlimb observed in 100% of mouse embryos (Nam et al., 2007). R-spondin2 is believed to be an activator of canonical Wnt/β-catenin signalling, which in the ectoderm is thought to have a role in maintenance of the AER (Barrow JR et al., 2003; Kazanskaya et al., 2004; Nam et al., 2007).

My results indicate that Fgf10 levels are at hypomorphic levels in both the left and right hindlimb buds. If, like the forelimb-forming regions, the left hindlimb-forming region is less responsive to Fgf ligand signalling activity than the right then it will require higher threshold levels of FgfR2c receptor activity than the right. In the presence of hypomorphic Fgf10 signalling activity, which presumably leads to reduced Fgf8 signalling activity in the AER, FgfR2c activity in the left hindlimb region may not reach the required threshold level. As the threshold levels for optimal FgfR

activity in the left and right hindlimb-forming regions may differ, the left hindlimb will therefore form with more defects than the right.

***Pitx1* partially contributes to hindlimb bud initiation in the absence of *Tbx4*.**

The data presented in chapter five demonstrates that in the absence of both *Tbx4* and *Pitx1* hindlimb bud initiation fails to take place and all the elements of the hindlimb fail to form. When *Pitx1* is deleted from the hindlimb-forming region, *Tbx4* expression falls to hypomorphic levels and a shortened hindlimb forms (Szeto et al., 1999; Lanctot et al., 1999). In chapter five, I demonstrated that when *Tbx4* is deleted from the hindlimb-forming region, there is no apparent change in *Pitx1* expression but a hypoplastic hindlimb with severe defects forms. Therefore, it is probable that *Pitx1* has a partial contribution towards hindlimb bud initiation that complements the main contribution of *Tbx4*. *Fgf10* is detectable at lower levels in hindlimb buds from which *Tbx4* has been deleted, but is not detectable in the hindlimb regions of mutants in which *Pitx1* and *Tbx4* has been deleted. *Pitx1* may therefore be able to partially positively regulate *Fgf10* transcription during hindlimb bud initiation.

Based on the above, the following model for hindlimb bud initiation is proposed. During hindlimb bud initiation, *Tbx4* acts directly to positively regulate *Fgf10* expression. *Pitx1* partially contributes to the positive transcription of *Fgf10* as well as partially towards *Tbx4* expression, which is downstream of a transcriptional cue from within the LPM, during limb bud initiation (Fig 6.5). In the absence of both *Tbx4* and *Pitx1*, *Fgf10* transcription does not occur and hindlimb bud formation fails to take place.

Figure 6.5

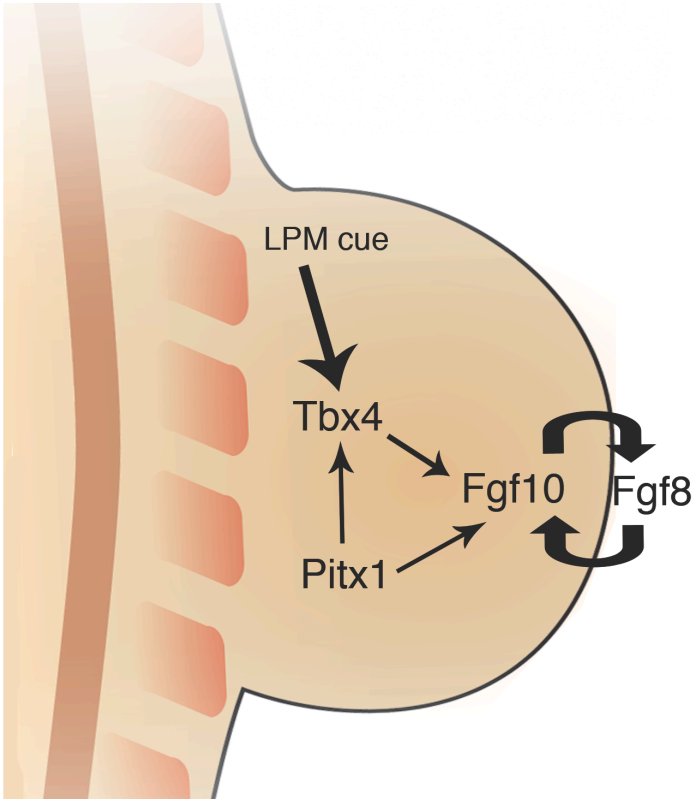

Figure 6.5 *Tbx4* and *Pitx1* both contribute towards FGF signalling during hindlimb bud initiation.

Tbx4 expression is induced in the presumptive hindlimb-forming region of the LPM. *Tbx4* is upstream of *Fgf10* expression in the hindlimb bud mesenchyme, which in turn leads to the establishment of the FGF signalling positive feedback loop. *Pitx1* expression in the nascent limb bud partially contributes towards the regulation of both *Tbx4* and *Fgf10* in the mesoderm, enabling limb bud outgrowth.

There is a forelimb and hindlimb specific difference in the initiation of limb bud formation.

My results reveal an unexpected difference in the mechanism regulating Fgf10 expression in the forelimb and hindlimb. When *Tbx5* is deleted from the forelimb-forming regions, no *Fgf10* expression is detected and forelimb bud formation completely fails to take place (Rallis et al., 2003; Agarwal et al., 2003). This indicates that *Tbx5* is exclusively required for *Fgf10* expression in the forelimb. When the paralogue of *Tbx5*, *Tbx4*, is expressed in the forelimb-forming regions of

these mutant embryos forelimb bud initiation and formation is rescued (Minguillon et al., 2005; Minguillon et al., 2009), indicating that *Tbx4* can replace the function of *Tbx5* in the forelimb-forming region. However, when *Tbx4* is deleted from the hindlimb-forming region, hindlimb bud initiation takes place due to the compensatory effects of *Pitx1* in regulating *Fgf10* expression. This indicates that although *Tbx5* and *Tbx4* may share the same transcriptional targets, the mechanisms by which *Fgf10* expression is regulated differ between the forelimb and hindlimb. In the context of hindlimb bud initiation, *Pitx1* influences *Fgf10* expression through two pathways. One of which is through its positive regulation of *Tbx4*, which in turn activates *Fgf10* expression, and the other through a *Tbx4* indirect pathway, which may or not be direct. The role of *Tbx4* in regulating *Fgf10* expression appears to be more significant than that of *Pitx1* since the outgrowth defects in *Tbx4*$^{lox/lox}$*; RetRV5Cre* hindlimbs are more severe than those observed in the *Pitx1*$^{-/-}$ mutant embryos. In contrast, *Tbx5* appears to be able to sufficient and completely necessary to induce *Fgf10* transcription during forelimb bud initiation (Fig 6.6).

Figure 6.6

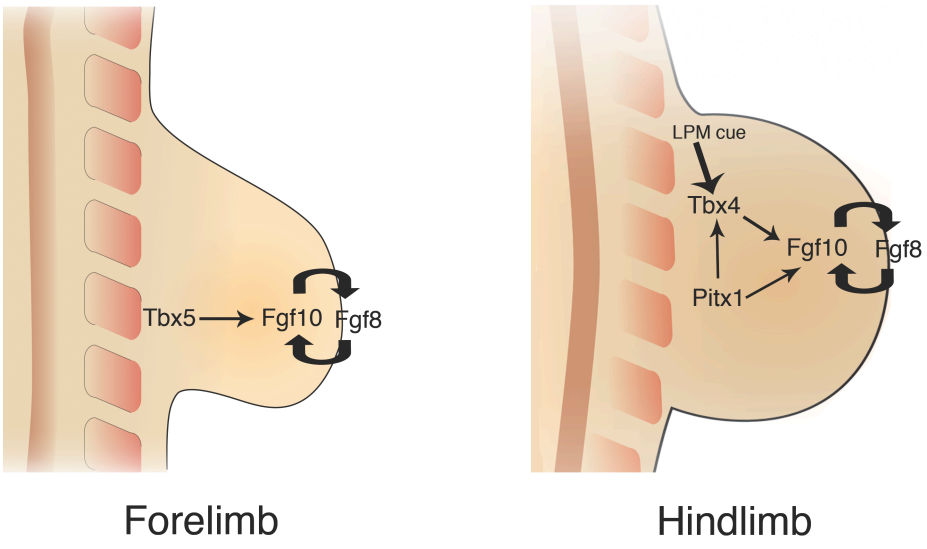

Figure 6.6 There is a forelimb and hindlimb specific difference in the positive regulation of *Fgf10* transcription during limb bud initiation. During forelimb bud initiation, *Tbx5* expression in the

LPM is sufficient for transcription of *Fgf10*. In contrast, during hindlimb bud initiation, *Fgf10* is positively regulated directly by *Tbx4* and either indirectly or directly by *Pitx1*. *Pitx1* has another input into *Fgf10* transcription through its positive regulation of *Tbx4*, which is secondary to the positive regulation of *Tbx4* by a cue from within the LPM.

6.3 PERSPECTIVES

Through the use of several transgenic mouse lines, I have demonstrated a novel role for Tbx5 in symmetrical forelimb bud initiation. Through the results presented in this study, a model has been developed in which threshold levels of Tbx5 activity are required to ensure that bilaterally symmetric forelimb buds are initiated and formed from the inherently asymmetric LPM. I have also demonstrated, through the use of conditional deletion and gene knockout strategies, that *Tbx4* has a significant role in *Fgf10* regulation, which is supplemented by *Pitx1*. This work has demonstrated a heretofore unrecognised role for *Pitx1* in the positive regulation of *Fgf10* transcription during hindlimb bud initiation.

REFERENCES

Aalfs, C.M., van Schooneveld, M.J., van Keulen, E.M., and Hennekam, R.C. (1996). Further delineation of the acro-renal-ocular syndrome. Am J Med Genet *62*, 276-281.

Agarwal, P., Wylie, J.N., Galceran, J., Arkhitko, O., Li, C., Deng, C., Grosschedl, R., and Bruneau, B.G. (2003). Tbx5 is essential for forelimb bud initiation following patterning of the limb field in the mouse embryo. Development *130*, 623-633.

Agulnik, S.I., Garvey, N., Hancock, S., Ruvinsky, I., Chapman, D.L., Agulnik, I., Bollag, R., Papaioannou, V., and Silver, L.M. (1996). Evolution of mouse T-box genes by tandem duplication and cluster dispersion. Genetics *144*, 249-254.

Akrami, S.M., Winter, R.M., Brook, J.D., and Armour, J.A. (2001). Detection of a large TBX5 deletion in a family with Holt-Oram syndrome. J Med Genet *38*, E44.

Al-Baradie, R., Yamada, K., St Hilaire, C., Chan, W.M., Andrews, C., McIntosh, N., Nakano, M., Martonyi, E.J., Raymond, W.R., Okumura, S., et al. (2002). Duane radial ray syndrome (Okihiro syndrome) maps to 20q13 and results from mutations in SALL4, a new member of the SAL family. Am J Hum Genet *71*, 1195-1199.

Alvarado, D.M., Aferol, H., McCall, K., Huang, J.B., Techy, M., Buchan, J., Cady, J., Gonzales, P.R., Dobbs, M.B., and Gurnett, C.A. (2010). Familial isolated clubfoot is associated with recurrent chromosome 17q23.1q23.2 microduplications containing TBX4. Am J Hum Genet *87*, 154-160.

Arman, E., Haffner-Krausz, R., Gorivodsky, M., and Lonai, P. (1999). Fgfr2 is required for limb outgrowth and lung-branching morphogenesis. Proc Natl Acad Sci U S A *96*, 11895-11899.

Basson, C.T., Bachinsky, D.R., Lin, R.C., Levi, T., Elkins, J.A., Soults, J., Grayzel, D., Kroumpouzou, E., Traill, T.A., Leblanc-Straceski, J., et al. (1997). Mutations in human TBX5 [corrected] cause limb and cardiac malformation in Holt-Oram syndrome. Nat Genet *15*, 30-35.

Basson, C.T., Huang, T., Lin, R.C., Bachinsky, D.R., Weremowicz, S., Vaglio, A., Bruzzone, R., Quadrelli, R., Lerone, M., Romeo, G., et al. (1999). Different TBX5 interactions in heart and limb defined by Holt-Oram syndrome mutations. Proc Natl Acad Sci U S A *96*, 2919-2924.

Bell, M.A., Ellis, K.E., and Sirotkin, H.I. (2007). Pelvic skeleton reduction and Pitx1 expression in threespine stickleback populations. Novartis Found Symp *284*, 225-239; discussion 239-244.

Bell, M.A., Khalef, V., and Travis, M.P. (2007). Directional asymmetry of pelvic vestiges in threespine stickleback. J Exp Zool B Mol Dev Evol *308*, 189-199.

Bell, S.M., Schreiner, C.M., Hess, K.A., Anderson, K.P., and Scott, W.J. (2003). Asymmetric limb malformations in a new transgene insertional mutant, footless. Mech Dev *120*, 597-605.

Boettger, T., Wittler, L., and Kessel, M. (1999). FGF8 functions in the specification of the right body side of the chick. Curr Biol *9*, 277-280.

Bongers, E.M., Duijf, P.H., van Beersum, S.E., Schoots, J., Van Kampen, A., Burckhardt, A., Hamel, B.C., Losan, F., Hoefsloot, L.H., Yntema, H.G., et al. (2004). Mutations in the human TBX4 gene cause small patella syndrome. Am J Hum Genet *74*, 1239-1248.

Bongers, E.M., Van Bokhoven, H., Van Thienen, M.N., Kooyman, M.A., Van Beersum, S.E., Boetes, C., Knoers, N.V., and Hamel, B.C. (2001). The small patella syndrome: description of five cases from three families and examination of possible allelism with familial patella aplasia-hypoplasia and nail-patella syndrome. J Med Genet *38*, 209-214.

Boogerd, C.J., Dooijes, D., Ilgun, A., Mathijssen, I.B., Hordijk, R., van de Laar, I.M., Rump, P., Veenstra-Knol, H.E., Moorman, A.F., Barnett, P., et al. (2010). Functional analysis of novel TBX5 T-box mutations associated with Holt-Oram syndrome. Cardiovasc Res *88*, 130-139.

Brosnan, C.A., and Voinnet, O. (2009). The long and the short of noncoding RNAs. Curr Opin Cell Biol *21*, 416-425.

Brown, K.W., Villar, A.J., Bickmore, W., Clayton-Smith, J., Catchpoole, D., Maher, E.R., and Reik, W. (1996). Imprinting mutation in the Beckwith-Wiedemann syndrome leads to biallelic IGF2 expression through an H19-independent pathway. Hum Mol Genet *5*, 2027-2032.

Brown, N.A., Hoyle, C.I., McCarthy, A., and Wolpert, L. (1989). The development of asymmetry: the sidedness of drug-induced limb abnormalities is reversed in situs inversus mice. Development *107*, 637-642.

Bruneau, B.G., Nemer, G., Schmitt, J.P., Charron, F., Robitaille, L., Caron, S., Conner, D.A., Gessler, M., Nemer, M., Seidman, C.E., et al. (2001). A murine model of Holt-Oram syndrome defines roles of the T-box transcription factor Tbx5 in cardiogenesis and disease. Cell *106*, 709-721.

Bueno, D., Skinner, J., Abud, H., and Heath, J.K. (1996). Spatial and temporal relationships between Shh, Fgf4, and Fgf8 gene expression at diverse signalling centers during mouse development. Dev Dyn *207*, 291-299.

Burckhardt, A. (1988). [The small patella syndrome. A combination of knee and pelvic dysplasia]. Z Orthop Ihre Grenzgeb *126*, 22-29.

Chan, Y.F., Marks, M.E., Jones, F.C., Villarreal, G., Jr., Shapiro, M.D., Brady, S.D., Southwick, A.M., Absher, D.M., Grimwood, J., Schmutz, J., et al. (2010). Adaptive evolution of pelvic reduction in sticklebacks by recurrent deletion of a Pitx1 enhancer. Science *327*, 302-305.

Chiang, C., Litingtung, Y., Lee, E., Young, K.E., Corden, J.L., Westphal, H., and Beachy, P.A. (1996). Cyclopia and defective axial patterning in mice lacking Sonic hedgehog gene function. Nature *383*, 407-413.

Cho, J.Y., Grant, T.D., Lunstrum, G.P., and Horton, W.A. (2001). Col2-GFP reporter mouse--a new tool to study skeletal development. Am J Med Genet *106*, 251-253.

Cole, N.J., Tanaka, M., Prescott, A., and Tickle, C. (2003). Expression of limb initiation genes and clues to the morphological diversification of threespine stickleback. Curr Biol *13*, R951-952.

Collignon, J., Varlet, I., and Robertson, E.J. (1996). Relationship between asymmetric nodal expression and the direction of embryonic turning. Nature *381*, 155-158.

De Moerlooze, L., Spencer-Dene, B., Revest, J.M., Hajihosseini, M., Rosewell, I., and Dickson, C. (2000). An important role for the IIIb isoform of fibroblast growth factor receptor 2 (FGFR2) in mesenchymal-epithelial signalling during mouse organogenesis. Development *127*, 483-492.

DeLaurier, A., Schweitzer, R., and Logan, M. (2006). Pitx1 determines the morphology of muscle, tendon, and bones of the hindlimb. Dev Biol *299*, 22-34.

Domning, D.P. (2001). The earliest known fully quadrupedal sirenian. Nature *413*, 625-627.

Dunn, N.R., Winnier, G.E., Hargett, L.K., Schrick, J.J., Fogo, A.B., and Hogan, B.L. (1997). Haploinsufficient phenotypes in Bmp4 heterozygous null mice and modification by mutations in Gli3 and Alx4. Dev Biol *188*, 235-247.

Echelard, Y., Epstein, D.J., St-Jacques, B., Shen, L., Mohler, J., McMahon, J.A., and McMahon, A.P. (1993). Sonic hedgehog, a member of a family of putative signaling molecules, is implicated in the regulation of CNS polarity. Cell *75*, 1417-1430.

Francannet, C., Vanlieferinghen, P., Dechelotte, P., Urbain, M.F., Campagne, D., and Malpuech, G. (1994). LADD syndrome in five members of a three-generation family and prenatal diagnosis. Genet Couns *5*, 85-91.

Furtado, M.B., Biben, C., Shiratori, H., Hamada, H., and Harvey, R.P. (2011). Characterization of Pitx2c expression in the mouse heart using a reporter transgene. Dev Dyn 240, 195-203.

Ghosh, T.K., Packham, E.A., Bonser, A.J., Robinson, T.E., Cross, S.J., and Brook, J.D. (2001). Characterization of the TBX5 binding site and analysis of mutations that cause Holt-Oram syndrome. Hum Mol Genet *10*, 1983-1994.

Gibert, Y., Gajewski, A., Meyer, A., and Begemann, G. (2006). Induction and prepatterning of the zebrafish pectoral fin bud requires axial retinoic acid signaling. Development *133*, 2649-2659.

Gibson-Brown, J.J., Agulnik, S.I., Chapman, D.L., Alexiou, M., Garvey, N., Silver, L.M., and Papaioannou, V.E. (1996). Evidence of a role for T-box genes in the evolution of limb morphogenesis and the specification of forelimb/hindlimb identity. Mech Dev *56*, 93-101.

Glauser, T.A., Zackai, E., Weinberg, P., and Clancy, R. (1989). Holt-Oram syndrome associated with the hypoplastic left heart syndrome. Clin Genet *36*, 69-72.

Grandel, H., Lun, K., Rauch, G.J., Rhinn, M., Piotrowski, T., Houart, C., Sordino, P., Kuchler, A.M., Schulte-Merker, S., Geisler, R., et al. (2002). Retinoic acid signalling in the zebrafish embryo is necessary during pre-segmentation stages to pattern the anterior-

posterior axis of the CNS and to induce a pectoral fin bud. Development *129*, 2851-2865.

Gurnett, C.A., Alaee, F., Kruse, L.M., Desruisseau, D.M., Hecht, J.T., Wise, C.A., Bowcock, A.M., and Dobbs, M.B. (2008). Asymmetric lower-limb malformations in individuals with homeobox PITX1 gene mutation. Am J Hum Genet *83*, 616-622.

Halal, F., Homsy, M., and Perreault, G. (1984). Acro-renal-ocular syndrome: autosomal dominant thumb hypoplasia, renal ectopia, and eye defect. Am J Med Genet *17*, 753-762.

Harfe, B.D., Scherz, P.J., Nissim, S., Tian, H., McMahon, A.P., and Tabin, C.J. (2004). Evidence for an expansion-based temporal Shh gradient in specifying vertebrate digit identities. Cell *118*, 517-528.

Harvey, S.A., and Logan, M.P. (2006). sall4 acts downstream of tbx5 and is required for pectoral fin outgrowth. Development *133*, 1165-1173.

Hasson, P., Del Buono, J., and Logan, M.P. (2007). Tbx5 is dispensable for forelimb outgrowth. Development *134*, 85-92.

Hasson, P., DeLaurier, A., Bennett, M., Grigorieva, E., Naiche, L.A., Papaioannou, V.E., Mohun, T.J., and Logan, M.P. (2010). Tbx4 and tbx5 acting in connective tissue are required for limb muscle and tendon patterning. Dev Cell *18*, 148-156.

Heinz, G.W., Bateman, J.B., Barrett, D.J., Thangavel, M., and Crandall, B.F. (1993). Ocular manifestations of the lacrimo-auriculo-dento-digital syndrome. Am J Ophthalmol *115*, 243-248.

Hummel, K.P.a.C., D.B (1959). Visceral inversion and associated anomalies in the mouse. J Hered *50*, 10-13.

Jenkins, D. (2009). Hedgehog signalling: emerging evidence for non-canonical pathways. Cell Signal *21*, 1023-1034.

Kacem, S., and Feil, R. (2009). Chromatin mechanisms in genomic imprinting. Mamm Genome *20*, 544-556.

Katagiri, T., Boorla, S., Frendo, J.L., Hogan, B.L., and Karsenty, G. (1998). Skeletal abnormalities in doubly heterozygous Bmp4 and Bmp7 mice. Dev Genet *22*, 340-348.

Kispert, A., and Hermann, B.G. (1993). The Brachyury gene encodes a novel DNA binding protein. EMBO J *12*, 4898-4899.

Kitamura, K., Miura, H., Miyagawa-Tomita, S., Yanazawa, M., Katoh-Fukui, Y., Suzuki, R., Ohuchi, H., Suehiro, A., Motegi, Y., Nakahara, Y., et al. (1999). Mouse Pitx2 deficiency leads to anomalies of the ventral body wall, heart, extra- and periocular mesoderm and right pulmonary isomerism. Development *126*, 5749-5758.

Kocher-Becker U, V.E., Kocher W. (1991). Correlation of asymmetries of mutant polydactyly and mutant situs. Teratology *44*.

Kohlhase, J., Heinrich, M., Schubert, L., Liebers, M., Kispert, A., Laccone, F.,

Turnpenny, P., Winter, R.M., and Reardon, W. (2002). Okihiro syndrome is caused by SALL4 mutations. Hum Mol Genet *11*, 2979-2987.

Koshiba-Takeuchi, K., Takeuchi, J.K., Arruda, E.P., Kathiriya, I.S., Mo, R., Hui, C.C., Srivastava, D., and Bruneau, B.G. (2006). Cooperative and antagonistic interactions between Sall4 and Tbx5 pattern the mouse limb and heart. Nat Genet *38*, 175-183.

Lajeunie, E., Cameron, R., El Ghouzzi, V., de Parseval, N., Journeau, P., Gonzales, M., Delezoide, A.L., Bonaventure, J., Le Merrer, M., and Renier, D. (1999). Clinical variability in patients with Apert's syndrome. J Neurosurg *90*, 443-447.

Lanctot, C., Moreau, A., Chamberland, M., Tremblay, M.L., and Drouin, J. (1999). Hindlimb patterning and mandible development require the Ptx1 gene. Development *126*, 1805-1810.

Lehotay, M., Kunkel, M., and Wehrbein, H. (2004). Lacrimo-auriculo-dento-digital syndrome. Case report, review of the literature, and clinical spectrum. J Orofac Orthop *65*, 425-432.

Levy, W.J. (1967). Mesoectodermal dysplasia. A new combination of anomalies. Am J Ophthalmol *63*, 978-982.

Lewandoski, M., and Martin, G.R. (1997). Cre-mediated chromosome loss in mice. Nat Genet *17*, 223-225.

Li, Q.Y., Newbury-Ecob, R.A., Terrett, J.A., Wilson, D.I., Curtis, A.R., Yi, C.H., Gebuhr, T., Bullen, P.J., Robson, S.C., Strachan, T., et al. (1997). Holt-Oram syndrome is caused by mutations in TBX5, a member of the Brachyury (T) gene family. Nat Genet *15*, 21-29.

Logan, M., Martin, J.F., Nagy, A., Lobe, C., Olson, E.N., and Tabin, C.J. (2002). Expression of Cre Recombinase in the developing mouse limb bud driven by a Prxl enhancer. Genesis *33*, 77-80.

Logan, M., Pagan-Westphal, S.M., Smith, D.M., Paganessi, L., and Tabin, C.J. (1998). The transcription factor Pitx2 mediates situs-specific morphogenesis in response to left-right asymmetric signals. Cell *94*, 307-317.

Logan, M., and Tabin, C.J. (1999). Role of Pitx1 upstream of Tbx4 in specification of hindlimb identity. Science *283*, 1736-1739.

MacDermot, K.D., and Winter, R.M. (1987). Radial ray defect and Duane anomaly: report of a family with autosomal dominant transmission. Am J Med Genet *27*, 313-319.

Mahmood, R., Bresnick, J., Hornbruch, A., Mahony, C., Morton, N., Colquhoun, K., Martin, P., Lumsden, A., Dickson, C., and Mason, I. (1995). A role for FGF-8 in the initiation and maintenance of vertebrate limb bud outgrowth. Curr Biol *5*, 797-806.

Malashichev, Y., Borkhvardt, V., Christ, B., and Scaal, M. (2005). Differential regulation of avian pelvic girdle development by the limb field ectoderm. Anat Embryol (Berl) *210*, 187-197.

Malashichev, Y., Christ, B., and Prols, F. (2008). Avian pelvis originates from lateral plate mesoderm and its development requires signals from both ectoderm and paraxial mesoderm. Cell Tissue Res *331*, 595-604.

Marcil, A., Dumontier, E., Chamberland, M., Camper, S.A., and Drouin, J. (2003). Pitx1 and Pitx2 are required for development of hindlimb buds. Development *130*, 45-55.

McGlinn, E., and Tabin, C.J. (2006). Mechanistic insight into how Shh patterns the vertebrate limb. Curr Opin Genet Dev *16*, 426-432.

McNeish, J.D., Scott, W.J., Jr., and Potter, S.S. (1988). Legless, a novel mutation found in PHT1-1 transgenic mice. Science *241*, 837-839.

Meno, C., Gritsman, K., Ohishi, S., Ohfuji, Y., Heckscher, E., Mochida, K., Shimono, A., Kondoh, H., Talbot, W.S., Robertson, E.J., et al. (1999). Mouse Lefty2 and zebrafish antivin are feedback inhibitors of nodal signaling during vertebrate gastrulation. Mol Cell *4*, 287-298.

Meno, C., Saijoh, Y., Fujii, H., Ikeda, M., Yokoyama, T., Yokoyama, M., Toyoda, Y., and Hamada, H. (1996). Left-right asymmetric expression of the TGF beta-family member lefty in mouse embryos. Nature *381*, 151-155.

Mercader, N., Leonardo, E., Piedra, M.E., Martinez, A.C., Ros, M.A., and Torres, M. (2000). Opposing RA and FGF signals control proximodistal vertebrate limb development through regulation of Meis genes. Development *127*, 3961-3970.

Metsaranta, M., Toman, D., De Crombrugghe, B., and Vuorio, E. (1991). Specific hybridization probes for mouse type I, II, III and IX collagen mRNAs. Biochim Biophys Acta *1089*, 241-243.

Meyers, E.N., and Martin, G.R. (1999). Differences in left-right axis pathways in mouse and chick: functions of FGF8 and SHH. Science *285*, 403-406.

Milunsky, J.M., Zhao, G., Maher, T.A., Colby, R., and Everman, D.B. (2006). LADD syndrome is caused by FGF10 mutations. Clin Genet *69*, 349-354.

Min, H., Danilenko, D.M., Scully, S.A., Bolon, B., Ring, B.D., Tarpley, J.E., DeRose, M., and Simonet, W.S. (1998). Fgf-10 is required for both limb and lung development and exhibits striking functional similarity to Drosophila branchless. Genes Dev *12*, 3156-3161.

Minguillon, C., Del Buono, J., and Logan, M.P. (2005). Tbx5 and Tbx4 are not sufficient to determine limb-specific morphologies but have common roles in initiating limb outgrowth. Dev Cell *8*, 75-84.

Minguillon, C., Gibson-Brown, J.J., and Logan, M.P. (2009). Tbx4/5 gene duplication and the origin of vertebrate paired appendages. Proc Natl Acad Sci U S A *106*, 21726-21730.

Naiche, L.A., and Papaioannou, V.E. (2003). Loss of Tbx4 blocks hindlimb development and affects vascularization and fusion of the allantois. Development *130*, 2681-2693.

Naiche, L.A., and Papaioannou, V.E. (2007). Tbx4 is not required for hindlimb identity or post-bud hindlimb outgrowth. Development *134*, 93-103.

Nam, J.S., Park, E., Turcotte, T.J., Palencia, S., Zhan, X., Lee, J., Yun, K., Funk, W.D., and Yoon, J.K. (2007). Mouse R-spondin2 is required for apical ectodermal ridge maintenance in the hindlimb. Dev Biol *311*, 124-135.

Newbury-Ecob, R.A., Leanage, R., Raeburn, J.A., and Young, I.D. (1996). Holt-Oram syndrome: a clinical genetic study. J Med Genet *33*, 300-307.

Niederreither, K., Subbarayan, V., Dolle, P., and Chambon, P. (1999). Embryonic retinoic acid synthesis is essential for early mouse post-implantation development. Nat Genet *21*, 444-448.

Niederreither, K., Vermot, J., Schuhbaur, B., Chambon, P., and Dolle, P. (2002). Embryonic retinoic acid synthesis is required for forelimb growth and anteroposterior patterning in the mouse. Development *129*, 3563-3574.

Nissim, S., Allard, P., Bandyopadhyay, A., Harfe, B.D., and Tabin, C.J. (2007). Characterization of a novel ectodermal signaling center regulating Tbx2 and Shh in the vertebrate limb. Dev Biol *304*, 9-21.

Niswander, L., Jeffrey, S., Martin, G.R., and Tickle, C. (1994). A positive feedback loop coordinates growth and patterning in the vertebrate limb. Nature *371*, 609-612.

Niswander, L., Tickle, C., Vogel, A., Booth, I., and Martin, G.R. (1993). FGF-4 replaces the apical ectodermal ridge and directs outgrowth and patterning of the limb. Cell *75*, 579-587.

Nonaka, S., Tanaka, Y., Okada, Y., Takeda, S., Harada, A., Kanai, Y., Kido, M., and Hirokawa, N. (1998). Randomization of left-right asymmetry due to loss of nodal cilia generating leftward flow of extraembryonic fluid in mice lacking KIF3B motor protein. Cell *95*, 829-837.

Novak, A., Guo, C., Yang, W., Nagy, A., and Lobe, C.G. (2000). Z/EG, a double reporter mouse line that expresses enhanced green fluorescent protein upon Cre-mediated excision. Genesis *28*, 147-155.

Ohuchi, H., Kimura, S., Watamoto, M., and Itoh, N. (2000). Involvement of fibroblast growth factor (FGF)18-FGF8 signaling in specification of left-right asymmetry and brain and limb development of the chick embryo. Mech Dev *95*, 55-66.

Ohuchi, H., Nakagawa, T., Yamamoto, A., Araga, A., Ohata, T., Ishimaru, Y., Yoshioka, H., Kuwana, T., Nohno, T., Yamasaki, M., et al. (1997). The mesenchymal factor, FGF10, initiates and maintains the outgrowth of the chick limb bud through interaction with FGF8, an apical ectodermal factor. Development *124*, 2235-2244.

Ohuchi, H., Shibusawa, M., Nakagawa, T., Ohata, T., Yoshioka, H., Hirai, Y., Nohno, T., Noji, S., and Kondo, N. (1997). A chick wingless mutation causes abnormality in maintenance of Fgf8 expression in the wing apical ridge, resulting in loss of the

dorsoventral boundary. Mech Dev *62*, 3-13.

Ohuchi, H., Yoshioka, H., Tanaka, A., Kawakami, Y., Nohno, T., and Noji, S. (1994). Involvement of androgen-induced growth factor (FGF-8) gene in mouse embryogenesis and morphogenesis. Biochem Biophys Res Commun *204*, 882-888.
Okada, Y., Nonaka, S., Tanaka, Y., Saijoh, Y., Hamada, H., and Hirokawa, N. (1999). Abnormal nodal flow precedes situs inversus in iv and inv mice. Mol Cell *4*, 459-468.

Pachnis, V., Mankoo, B., and Costantini, F. (1993). Expression of the c-ret proto-oncogene during mouse embryogenesis. Development *119*, 1005-1017.

Piedra, M.E., Icardo, J.M., Albajar, M., Rodriguez-Rey, J.C., and Ros, M.A. (1998). Pitx2 participates in the late phase of the pathway controlling left-right asymmetry. Cell *94*, 319-324.

Pomikal, C., and Streicher, J. (2010). 4D-analysis of early pelvic girdle development in the mouse (Mus musculus). J Morphol *271*, 116-126.

Rallis, C., Bruneau, B.G., Del Buono, J., Seidman, C.E., Seidman, J.G., Nissim, S., Tabin, C.J., and Logan, M.P. (2003). Tbx5 is required for forelimb bud formation and continued outgrowth. Development *130*, 2741-2751.

Rallis, C., Del Buono, J., and Logan, M.P. (2005). Tbx3 can alter limb position along the rostrocaudal axis of the developing embryo. Development *132*, 1961-1970.

Reik, W., and Walter, J. (2001). Genomic imprinting: parental influence on the genome. Nat Rev Genet *2*, 21-32.

Riddle, R.D., Johnson, R.L., Laufer, E., and Tabin, C. (1993). Sonic hedgehog mediates the polarizing activity of the ZPA. Cell *75*, 1401-1416.

Rodriguez-Esteban, C., Tsukui, T., Yonei, S., Magallon, J., Tamura, K., and Izpisua Belmonte, J.C. (1999). The T-box genes Tbx4 and Tbx5 regulate limb outgrowth and identity. Nature *398*, 814-818.

Rohmann, E., Brunner, H.G., Kayserili, H., Uyguner, O., Nurnberg, G., Lew, E.D., Dobbie, A., Eswarakumar, V.P., Uzumcu, A., Ulubil-Emeroglu, M., et al. (2006). Mutations in different components of FGF signaling in LADD syndrome. Nat Genet *38*, 414-417.

Rybak, M., Kozlowski, K., Kleczkowska, A., Lewandowska, J., Sokolowski, J., and Soltysik-Wilk, E. (1971). Holt-Oram syndrome associated with ectromelia and chromosomal aberrations. Am J Dis Child *121*, 490-495.

Sandell, L.L., Sanderson, B.W., Moiseyev, G., Johnson, T., Mushegian, A., Young, K., Rey, J.P., Ma, J.X., Staehling-Hampton, K., and Trainor, P.A. (2007). RDH10 is essential for synthesis of embryonic retinoic acid and is required for limb, craniofacial, and organ development. Genes Dev *21*, 1113-1124.

Saunders, J.W., Jr. (1948). The proximo-distal sequence of origin of the parts of the chick wing and the role of the ectoderm. J Exp Zool *108*, 363-403.

Saunders, J.W.a.G., M. T. (1968). Ectodermal-mesenchymal interactions in the origin of limb symmetry. Epithelial-mesenchymal Interactions, 78-97.

Schreiner, C.M., Scott, W.J., Jr., Supp, D.M., and Potter, S.S. (1993). Correlation of forelimb malformation asymmetries with visceral organ situs in the transgenic mouse insertional mutation, legless. Dev Biol *158*, 560-562.

Scott, J.E., and Taor, W.S. (1979). The "small patella" syndrome. J Bone Joint Surg Br *61-B*, 172-175.

Sekine, K., Ohuchi, H., Fujiwara, M., Yamasaki, M., Yoshizawa, T., Sato, T., Yagishita, N., Matsui, D., Koga, Y., Itoh, N., et al. (1999). Fgf10 is essential for limb and lung formation. Nat Genet *21*, 138-141.

Shapiro, M.D., Bell, M.A., and Kingsley, D.M. (2006). Parallel genetic origins of pelvic reduction in vertebrates. Proc Natl Acad Sci U S A *103*, 13753-13758.

Shapiro, M.D., Marks, M.E., Peichel, C.L., Blackman, B.K., Nereng, K.S., Jonsson, B., Schluter, D., and Kingsley, D.M. (2004). Genetic and developmental basis of evolutionary pelvic reduction in threespine sticklebacks. Nature *428*, 717-723.

Shiang, E.L., and Holmes, L.B. (1977). The lacrimo-auriculo-dento-digital syndrome. Pediatrics *59*, 927-930.

Shih, H.P., Gross, M.K., and Kioussi, C. (2007). Expression pattern of the homeodomain transcription factor Pitx2 during muscle development. Gene Expr Patterns *7*, 441-451.

Smith, A.T., Sack, G.H., Jr., and Taylor, G.J. (1979). Holt-Oram syndrome. J Pediatr *95*, 538-543.

Solomin, L., Johansson, C.B., Zetterstrom, R.H., Bissonnette, R.P., Heyman, R.A., Olson, L., Lendahl, U., Frisen, J., and Perlmann, T. (1998). Retinoid-X receptor signalling in the developing spinal cord. Nature *395*, 398-402.

Sparago, A., Cerrato, F., Vernucci, M., Ferrero, G.B., Silengo, M.C., and Riccio, A. (2004). Microdeletions in the human H19 DMR result in loss of IGF2 imprinting and Beckwith-Wiedemann syndrome. Nat Genet *36*, 958-960.

Stephens, T.D., and McNulty, T.R. (1981). Evidence for a metameric pattern in the development of the chick humerus. J Embryol Exp Morphol *61*, 191-205.

Stratford, T., Horton, C., and Maden, M. (1996). Retinoic acid is required for the initiation of outgrowth in the chick limb bud. Curr Biol *6*, 1124-1133.

Summerbell, D. (1974). A quantitative analysis of the effect of excision of the AER from the chick limb-bud. J Embryol Exp Morphol *32*, 651-660.

Summerbell, D., and Wolpert, L. (1973). Precision of development in chick limb morphogenesis. Nature *244*, 228-230.

Surka, W.S., Kohlhase, J., Neunert, C.E., Schneider, D.S., and Proud, V.K. (2001). Unique family with Townes-Brocks syndrome, SALL1 mutation, and cardiac defects. Am J Med Genet *102*, 250-257.

Sweeney, R.M., and Watterson, R.L. (1969). Rib development in chick embryos analyzed by means of tantalum foil blocks. Am J Anat *126*, 127-149.

Szeto, D.P., Rodriguez-Esteban, C., Ryan, A.K., O'Connell, S.M., Liu, F., Kioussi, C., Gleiberman, A.S., Izpisua-Belmonte, J.C., and Rosenfeld, M.G. (1999). Role of the Bicoid-related homeodomain factor Pitx1 in specifying hindlimb morphogenesis and pituitary development. Genes Dev *13*, 484-494.

Tabin, C.J., and Vogan, K.J. (2003). A two-cilia model for vertebrate left-right axis specification. Genes Dev *17*, 1-6.

Tanaka, Y., Okada, Y., and Hirokawa, N. (2005). FGF-induced vesicular release of Sonic hedgehog and retinoic acid in leftward nodal flow is critical for left-right determination. Nature *435*, 172-177.

Thompson, E., Pembrey, M., and Graham, J.M. (1985). Phenotypic variation in LADD syndrome. J Med Genet *22*, 382-385.

Townes, P.L., and Brocks, E.R. (1972). Hereditary syndrome of imperforate anus with hand, foot, and ear anomalies. J Pediatr *81*, 321-326.

Varlet, I., Collignon, J., Norris, D.P., and Robertson, E.J. (1997). Nodal signaling and axis formation in the mouse. Cold Spring Harb Symp Quant Biol *62*, 105-113.

Veltmaat, J.M., Relaix, F., Le, L.T., Kratochwil, K., Sala, F.G., van Veelen, W., Rice, R., Spencer-Dene, B., Mailleux, A.A., Rice, D.P., et al. (2006). Gli3-mediated somitic Fgf10 expression gradients are required for the induction and patterning of mammary epithelium along the embryonic axes. Development *133*, 2325-2335.

Vermot, J., Gallego Llamas, J., Fraulob, V., Niederreither, K., Chambon, P., and Dolle, P. (2005). Retinoic acid controls the bilateral symmetry of somite formation in the mouse embryo. Science *308*, 563-566.

Vermot, J., and Pourquie, O. (2005). Retinoic acid coordinates somitogenesis and left-right patterning in vertebrate embryos. Nature *435*, 215-220.

Vilhais-Neto, G.C., Maruhashi, M., Smith, K.T., Vasseur-Cognet, M., Peterson, A.S., Workman, J.L., and Pourquie, O. (2010). Rere controls retinoic acid signalling and somite bilateral symmetry. Nature *463*, 953-957.

Walpole, I.R., and Hockey, A. (1982). Syndrome of imperforate anus, abnormalities of hands and feet, satyr ears, and sensorineural deafness. J Pediatr *100*, 250-252.

Wiedemann, H.R., and Drescher, J. (1986). LADD syndrome: report of new cases and review of the clinical spectrum. Eur J Pediatr *144*, 579-582.

Wilkie, A.O. (1996). Fibroblast growth factor receptor mutations and craniosynostosis:

three receptors, five syndromes. Indian J Pediatr *63*, 351-356.

Wu, H.K., Weksberg, R., Minden, M.D., and Squire, J.A. (1997). Loss of imprinting of human insulin-like growth factor II gene, IGF2, in acute myeloid leukemia. Biochem Biophys Res Commun *231*, 466-472.

Xu, X., Weinstein, M., Li, C., Naski, M., Cohen, R.I., Ornitz, D.M., Leder, P., and Deng, C. (1998). Fibroblast growth factor receptor 2 (FGFR2)-mediated reciprocal regulation loop between FGF8 and FGF10 is essential for limb induction. Development *125*, 753-765.

Yamamoto, M., Mine, N., Mochida, K., Sakai, Y., Saijoh, Y., Meno, C., and Hamada, H. (2003). Nodal signaling induces the midline barrier by activating Nodal expression in the lateral plate. Development *130*, 1795-1804.

Yang, J., Hu, D., Xia, J., Yang, Y., Ying, B., Hu, J., and Zhou, X. (2000). Three novel TBX5 mutations in Chinese patients with Holt-Oram syndrome. Am J Med Genet *92*, 237-240.

Yokoyama, T., Copeland, N.G., Jenkins, N.A., Montgomery, C.A., Elder, F.F., and Overbeek, P.A. (1993). Reversal of left-right asymmetry: a situs inversus mutation. Science *260*, 679-682.

Yonei-Tamura, S., Endo, T., Yajima, H., Ohuchi, H., Ide, H., and Tamura, K. (1999). FGF7 and FGF10 directly induce the apical ectodermal ridge in chick embryos. Dev Biol *211*, 133-143.

Zhou, X., Sasaki, H., Lowe, L., Hogan, B.L., and Kuehn, M.R. (1993). Nodal is a novel TGF-beta-like gene expressed in the mouse node during gastrulation. Nature *361*, 543-547.

Zuniga, A., Haramis, A.P., McMahon, A.P., and Zeller, R. (1999). Signal relay by BMP antagonism controls the SHH/FGF4 feedback loop in vertebrate limb buds. Nature *401*, 598-602.